

FLUXNET-CH4: a global, multi-ecosystem datasetand analysis of methane seasonalityfrom freshwater wetlands

Sara Helen Knox, Ma Carmelita R Alberto, Jaclyn Hatala Matthes, Camilo Rey Sanchez, Guan Xhuan Wong, Kyle B Delwiche, Sara Helen Knox, Avni Malhotra, Etienne Fluet-Chouinard, Gavin Mcnicol, et al.

▶ **To cite this version:**

Sara Helen Knox, Ma Carmelita R Alberto, Jaclyn Hatala Matthes, Camilo Rey Sanchez, Guan Xhuan Wong, et al.. FLUXNET-CH4: a global, multi-ecosystem datasetand analysis of methane seasonalityfrom freshwater wetlands. Earth System Science Data, 2021, 13 (7), pp.3607-3689. 10.5194/essd-13-3607-2021 . insu-03335685

HAL Id: insu-03335685
https://insu.hal.science/insu-03335685

Submitted on 6 Sep 2021

HAL is a multi-disciplinary open access archive for the deposit and dissemination of scientific research documents, whether they are published or not. The documents may come from teaching and research institutions in France or abroad, or from public or private research centers.

L'archive ouverte pluridisciplinaire **HAL**, est destinée au dépôt et à la diffusion de documents scientifiques de niveau recherche, publiés ou non, émanant des établissements d'enseignement et de recherche français ou étrangers, des laboratoires publics ou privés.



Distributed under a Creative Commons Attribution 4.0 International License

Earth Syst. Sci. Data, 13, 3607–3689, 2021
https://doi.org/10.5194/essd-13-3607-2021
© Author(s) 2021. This work is distributed under
the Creative Commons Attribution 4.0 License.

Open Access Earth System Science Data

FLUXNET-CH_4: a global, multi-ecosystem dataset and analysis of methane seasonality from freshwater wetlands

Kyle B. Delwiche[1], Sara Helen Knox[2], Avni Malhotra[1], Etienne Fluet-Chouinard[1], Gavin McNicol[1], Sarah Feron[1,3], Zutao Ouyang[1], Dario Papale[4,5], Carlo Trotta[5], Eleonora Canfora[5], You-Wei Cheah[6], Danielle Christianson[6], Ma. Carmelita R. Alberto[7], Pavel Alekseychik[8], Mika Aurela[9], Dennis Baldocchi[10], Sheel Bansal[11], David P. Billesbach[12], Gil Bohrer[13], Rosvel Bracho[14], Nina Buchmann[15], David I. Campbell[16], Gerardo Celis[17], Jiquan Chen[18], Weinan Chen[19], Housen Chu[20], Higo J. Dalmagro[21], Sigrid Dengel[6], Ankur R. Desai[22], Matteo Detto[23], Han Dolman[24], Elke Eichelmann[25], Eugenie Euskirchen[26], Daniela Famulari[27], Kathrin Fuchs[28], Mathias Goeckede[29], Sébastien Gogo[30], Mangaliso J. Gondwe[31], Jordan P. Goodrich[16], Pia Gottschalk[32], Scott L. Graham[33], Martin Heimann[29], Manuel Helbig[34,35], Carole Helfter[36], Kyle S. Hemes[1,37], Takashi Hirano[38], David Hollinger[39], Lukas Hörtnagl[15], Hiroki Iwata[40], Adrien Jacotot[30], Gerald Jurasinski[41], Minseok Kang[42], Kuno Kasak[43], John King[44], Janina Klatt[45], Franziska Koebsch[41], Ken W. Krauss[46], Derrick Y. F. Lai[47], Annalea Lohila[9,48], Ivan Mammarella[48], Luca Belelli Marchesini[50], Giovanni Manca[49], Jaclyn Hatala Matthes[51], Trofim Maximov[52], Lutz Merbold[53], Bhaskar Mitra[54], Timothy H. Morin[55], Eiko Nemitz[36], Mats B. Nilsson[56], Shuli Niu[19], Walter C. Oechel[57], Patricia Y. Oikawa[58], Keisuke Ono[59], Matthias Peichl[56], Olli Peltola[9], Michele L. Reba[60], Andrew D. Richardson[61,62], William Riley[6], Benjamin R. K. Runkle[63], Youngryel Ryu[64], Torsten Sachs[32], Ayaka Sakabe[65], Camilo Rey Sanchez[10], Edward A. Schuur[66], Karina V. R. Schäfer[67], Oliver Sonnentag[68], Jed P. Sparks[69], Ellen Stuart-Haëntjens[70], Cove Sturtevant[71], Ryan C. Sullivan[72], Daphne J. Szutu[10], Jonathan E. Thom[73], Margaret S. Torn[6], Eeva-Stiina Tuittila[74], Jessica Turner[75], Masahito Ueyama[76], Alex C. Valach[10], Rodrigo Vargas[77], Andrej Varlagin[78], Alma Vazquez-Lule[77], Joseph G. Verfaillie[10], Timo Vesala[48,79], George L. Vourlitis[80], Eric J. Ward[46], Christian Wille[32], Georg Wohlfahrt[81], Guan Xhuan Wong[82], Zhen Zhang[83], Donatella Zona[57,84], Lisamarie Windham-Myers[85], Benjamin Poulter[86], and Robert B. Jackson[1,37,87]

[1]Department of Earth System Science, Stanford University, Stanford, California, USA
[2]Department of Geography, The University of British Columbia, Vancouver, British Columbia, Canada
[3]Department of Physics, University of Santiago de Chile, Santiago, Chile
[4]Dipartimento per la Innovazione nei Sistemi Biologici, Agroalimentari e Forestali, Università degli Studi della Tuscia, Largo dell'Università, Viterbo, Italy
[5]Euro-Mediterranean Center on Climate Change CMCC, Lecce, Italy
[6]Earth and Environmental Sciences Area, Lawrence Berkeley National Lab, Berkeley, California, USA
[7]International Rice Research Institute, Los Baños, Laguna, Philippines
[8]Natural Resources Institute Finland (LUKE), Helsinki, Finland
[9]Finnish Meteorological Institute, P.O. Box 501, 00101 Helsinki, Finland
[10]Department of Environmental Science, Policy and Management, University of California, Berkeley, CA, USA
[11]Northern Prairie Wildlife Research Center, US Geological Survey, 8711 37th St Southeast, Jamestown, ND 58401, USA
[12]Department of Biological Systems Engineering, University of Nebraska-Lincoln, Lincoln, NE 68583, USA
[13]Department of Civil, Environmental and Geodetic Engineering, Ohio State University, Columbus, OH, USA
[14]School of Forest Resources and Conservation, University of Florida, Gainesville, FL 32611, USA
[15]Department of Environmental Systems Science, Institute of Agricultural Sciences, ETH Zurich, 8092 Zurich, Switzerland

Published by Copernicus Publications.

[16]School of Science, University of Waikato, Hamilton, New Zealand
[17]Agronomy Department, University of Florida, Gainesville, FL 32601, USA
[18]Department of Geography, Environment, and Spatial Sciences, Michigan State University, East Lansing, MI 48823, USA
[19]Institute of Geographic Sciences and Natural Resources Research, Chinese Academy of Sciences, Beijing 100101, PR China
[20]Climate and Ecosystem Sciences Division, Lawrence Berkeley National Lab, Berkeley, CA 94702, USA
[21]Environmental Sciences Graduate Program, University of Cuiabá, Cuiabá, Mato Grosso, Brazil
[22]Department of Atmospheric and Oceanic Sciences, University of Wisconsin-Madison, Madison, WI 53706, USA
[23]Department of Ecology and Evolutionary Biology, Princeton University, Princeton, NJ, USA
[24]Department of Earth Sciences, Vrije Universiteit, Amsterdam, the Netherlands
[25]School of Biology and Environmental Science, University College Dublin, Dublin, Ireland
[26]Institute of Arctic Biology, University of Alaska Fairbanks, Fairbanks, AK, USA
[27]CNR – Institute for Agricultural and Forestry Systems in the Mediterranean, Piazzale Enrico Fermi, 1 Portici, Napoli, Italy
[28]Institute of Meteorology and Climate Research – Atmospheric Environmental Research, Karlsruhe Institute of Technology (KIT Campus Alpin), 82467 Garmisch-Partenkirchen, Germany
[29]Max Planck Institute for Biogeochemistry, Jena, Germany
[30]ISTO, Université d'Orléans, CNRS, BRGM, UMR 7327, 45071, Orléans, France
[31]Okavango Research Institute, University of Botswana, Maun, Botswana
[32]GFZ German Research Centre for Geosciences, Telegrafenberg, 14473 Potsdam, Germany
[33]Manaaki Whenua – Landcare Research, Lincoln, New Zealand
[34]Département de géographie, Université de Montréal, Montréal, QC H2V 0B3, Canada
[35]Department of Physics and Atmospheric Science, Dalhousie University, Halifax, NS B2Y 1P3, Canada
[36]UK Centre for Ecology and Hydrology, Edinburgh, UK
[37]Woods Institute for the Environment, Stanford University, Stanford, California
[38]Research Faculty of Agriculture, Hokkaido University, Sapporo, Japan
[39]Northern Research Station, USDA Forest Service, Durham, NH 03824, USA
[40]Department of Environmental Science, Faculty of Science, Shinshu University, Matsumoto, Japan
[41]Landscape Ecology, University of Rostock, Rostock, Germany
[42]National Center for AgroMeteorology, Seoul, South Korea
[43]Department of Geography, University of Tartu, Vanemuise st 46, Tartu, 51410, Estonia
[44]Department of Forestry and Environmental Resources, North Carolina State University, Raleigh, NC, USA
[45]Chair of Vegetation Ecology, Institute of Ecology and Landscape, University of Applied Sciences Weihenstephan-Triesdorf, Am Hofgarten 1, 85354 Freising, Germany
[46]Wetland and Aquatic Research Center, US Geological Survey, Lafayette, LA, USA
[47]Department of Geography and Resource Management, The Chinese University of Hong Kong, Shatin, New Territories, Hong Kong SAR, China
[48]Institute for Atmospheric and Earth System Research/Physics, Faculty of Science, University of Helsinki, Helsinki, Finland
[49]Joint Research Centre (JRC), European Commission, Ispra, Italy
[50]Department of Sustainable Agro-Ecosystems and Bioresources, Research and Innovation Centre, Fondazione Edmund Mach, San Michele all'Adige, Italy
[51]Department of Biological Sciences, Wellesley College, Wellesley, MA 02481, USA
[52]Institute for Biological Problems of the Cryolithozone, RAS, Yakutsk, Russia
[53]International Livestock Research Institute (ILRI), Mazingira Centre, Old Naivasha Road, P.O. Box 30709, 00100 Nairobi, Kenya
[54]School of Informatics, Computing and Cyber Systems, Northern Arizona University, Flagstaff, AZ, USA
[55]Environmental Resources Engineering, SUNY College of Environmental Science and Forestry, Syracuse, NY, USA
[56]Department of Forest Ecology and Management, Swedish University of Agricultural Sciences, 901 83 Umeå, Sweden

[57]Department of Biology, San Diego State University, San Diego, CA 92182, USA
[58]Department of Earth and Environmental Sciences, Cal State East Bay, Hayward, CA 94542, USA
[59]National Agriculture and Food Research Organization, Tsukuba, Japan
[60]USDA-ARS Delta Water Management Research Unit, Jonesboro, Arkansas 72401, USA
[61]School of Informatics, Computing and Cyber Systems, Northern Arizona University, Flagstaff, AZ 86011, USA
[62]Center for Ecosystem Science and Society, Northern Arizona University, Flagstaff, AZ 86011, USA
[63]Department of Biological and Agricultural Engineering, University of Arkansas, Fayetteville, AR 72701, USA
[64]Department of Landscape Architecture and Rural Systems Engineering, Seoul National University, Seoul, South Korea
[65]Hakubi Center, Kyoto University, Kyoto, Japan
[66]Department of Biological Sciences, Northern Arizona University, Flagstaff, AZ, USA
[67]Department of Earth and Environmental Science, Rutgers University Newark, NJ, USA
[68]Département de géographie, Université de Montréal, Montréal, QC H2V 0B3, Canada
[69]Department of Ecology and Evolution, Cornell, Ithaca, NY, USA
[70]California Water Science Center, US Geological Survey, 6000 J Street, Placer Hall, Sacramento, CA 95819, USA
[71]National Ecological Observatory Network, Battelle, 1685 38th St Ste 100, Boulder, Colorado 80301, USA
[72]Environmental Science Division, Argonne National Laboratory, Lemont, IL, USA
[73]Space Sciences and Engineering Center, University of Wisconsin-Madison, Madison, WI 53706, USA
[74]School of Forest Sciences, University of Eastern Finland, Joesnuu, Finland
[75]Freshwater and Marine Science, University of Wisconsin-Madison, Madison, WI 53706, USA
[76]Graduate School of Life and Environmental Sciences, Osaka Prefecture University, Osaka, Japan
[77]Department of Plant and Soil Sciences, University of Delaware, Newark, DE, USA
[78]A.N. Severtsov Institute of Ecology and Evolution, Russian Academy of Sciences, Moscow, Russia
[79]Yugra State University, 628012, Khanty-Mansiysk, Russia
[80]Biological Sciences Department, California State University San Marcos, San Marcos, CA, USA
[81]Department of Ecology, University of Innsbruck, Sternwartestr. 15, 6020 Innsbruck, Austria
[82]Sarawak Tropical Peat Research Institute, Sarawak, Malaysia
[83]Department of Geographical Sciences, University of Maryland, College Park, MD 20740, USA
[84]Department of Animal and Plant Sciences, University of Sheffield, Western Bank, Sheffield, S10 2TN, United Kingdom
[85]Water Mission Area, US Geological Survey, 345 Middlefield Road, Menlo Park, CA 94025, USA
[86]Biospheric Sciences Laboratory, NASA Goddard Space Flight Center, Greenbelt, Maryland, USA
[87]Precourt Institute for Energy, Stanford University, Stanford, California, USA

Correspondence: Kyle B. Delwiche (delwiche@stanford.edu)

Received: 15 October 2020 – Discussion started: 18 January 2021
Revised: 27 April 2021 – Accepted: 28 April 2021 – Published: 29 July 2021

Abstract. Methane (CH_4) emissions from natural landscapes constitute roughly half of global CH_4 contributions to the atmosphere, yet large uncertainties remain in the absolute magnitude and the seasonality of emission quantities and drivers. Eddy covariance (EC) measurements of CH_4 flux are ideal for constraining ecosystem-scale CH_4 emissions due to quasi-continuous and high-temporal-resolution CH_4 flux measurements, coincident carbon dioxide, water, and energy flux measurements, lack of ecosystem disturbance, and increased availability of datasets over the last decade. Here, we (1) describe the newly published dataset, FLUXNET-CH_4 Version 1.0, the first open-source global dataset of CH_4 EC measurements (available at https://fluxnet.org/data/fluxnet-ch4-community-product/, last access: 7 April 2021). FLUXNET-CH_4 includes half-hourly and daily gap-filled and non-gap-filled aggregated CH_4 fluxes and meteorological data from 79 sites globally: 42 freshwater wetlands, 6 brackish and saline wetlands, 7 formerly drained ecosystems, 7 rice paddy sites, 2 lakes, and 15 uplands. Then, we (2) evaluate FLUXNET-CH_4 representativeness for freshwater wetland coverage globally because the majority of sites in FLUXNET-CH_4 Version 1.0 are freshwater wetlands which are a substantial source of total atmospheric CH_4 emissions; and (3) we provide the first global estimates of the seasonal variability and seasonality predictors of freshwater wetland CH_4 fluxes. Our representativeness analysis

suggests that the freshwater wetland sites in the dataset cover global wetland bioclimatic attributes (encompassing energy, moisture, and vegetation-related parameters) in arctic, boreal, and temperate regions but only sparsely cover humid tropical regions. Seasonality metrics of wetland CH_4 emissions vary considerably across latitudinal bands. In freshwater wetlands (except those between 20° S to 20° N) the spring onset of elevated CH_4 emissions starts 3 d earlier, and the CH_4 emission season lasts 4 d longer, for each degree Celsius increase in mean annual air temperature. On average, the spring onset of increasing CH_4 emissions lags behind soil warming by 1 month, with very few sites experiencing increased CH_4 emissions prior to the onset of soil warming. In contrast, roughly half of these sites experience the spring onset of rising CH_4 emissions prior to the spring increase in gross primary productivity (GPP). The timing of peak summer CH_4 emissions does not correlate with the timing for either peak summer temperature or peak GPP. Our results provide seasonality parameters for CH_4 modeling and highlight seasonality metrics that cannot be predicted by temperature or GPP (i.e., seasonality of CH_4 peak). FLUXNET-CH_4 is a powerful new resource for diagnosing and understanding the role of terrestrial ecosystems and climate drivers in the global CH_4 cycle, and future additions of sites in tropical ecosystems and site years of data collection will provide added value to this database. All seasonality parameters are available at https://doi.org/10.5281/zenodo.4672601 (Delwiche et al., 2021). Additionally, raw FLUXNET-CH_4 data used to extract seasonality parameters can be downloaded from https://fluxnet.org/data/fluxnet-ch4-community-product/ (last access: 7 April 2021), and a complete list of the 79 individual site data DOIs is provided in Table 2 of this paper.

1 Introduction

Methane (CH_4) has a global warming potential that is 28 times larger than carbon dioxide (CO_2) on a 100-year timescale (Myhre et al., 2013), and its atmospheric concentration has increased by > 1000 ppb since 1800 (Etheridge et al., 1998). While atmospheric CH_4 concentrations are substantially lower than those of CO_2, CH_4 has contributed 20 %–25 % as much radiative forcing as CO_2 since 1750 (Etminan et al., 2016). Despite its importance to global climate change, natural CH_4 sources and sinks remain poorly constrained and with uncertain attribution to the various biogenic and anthropogenic sources (Saunois et al., 2016, 2020). Bottom-up and top-down estimates differ by 154 Tg yr^{-1} (745 versus 591 Tg yr^{-1}, respectively); much of this difference arises from natural sources (Saunois et al., 2020). Vegetated wetlands and inland water bodies account for most natural CH_4 emissions, as well as the majority of uncertainty in bottom-up emission estimates (Saunois et al., 2016). Better diagnosis and prediction of terrestrial CH_4 sources to the atmosphere requires high frequency and continuous measurements of CH_4 exchange across a continuum of time (hours to years) and space (meters to kilometers) scales.

Tower-based eddy covariance (EC) measurements providing ecosystem-scale CH_4 fluxes at high temporal resolution across years are coupled with measurements of key CH_4 drivers such as temperature, water, and recent substrate input (inferred from CO_2 flux) and thus help constrain bottom-up CH_4 budgets and improve CH_4 predictions. Although EC towers began measuring CO_2 fluxes in the late 1970s (Desjardins, 1974; Anderson et al., 1984), and some towers began measuring CH_4 in the 1990s (Verma et al., 1992), most CH_4 flux EC measurements began within the last decade (2010s). Given that many EC CH_4 sites are relatively new, the flux community has only recently compiled them for global synthesis efforts (e.g., Chang et al., 2021) and is still working to standardize CH_4 flux measurements and establish gap-filling protocols (Nemitz et al., 2018; Knox et al., 2019). Furthermore, the growth of EC networks for CH_4 fluxes has sometimes taken place in a relatively ad hoc fashion, often at sites that were already measuring CO_2 fluxes or where higher CH_4 fluxes were expected, potentially introducing bias. The representativeness and spatial distribution of CO_2 flux tower networks have been assessed to evaluate their ability to upscale fluxes regionally (Hargrove et al., 2003; Hoffman et al., 2013; Papale et al., 2015; Villarreal et al., 2018, 2019) and globally (Jung et al., 2009, 2020). However, a relatively sparse coverage of CH_4 flux towers prompts the question of how well the current observation network provides a sufficient sampling of global or ecosystem-specific bioclimatic conditions.

Broad-scale wetland CH_4 seasonality estimates, such as when fluxes increase, peak, and decrease and the predictors of seasonality, remain relatively unconstrained across wetlands globally. These key seasonality metrics vary considerably across high-emitting systems such as wetlands and other aquatic systems (Desjardins, 1974; Dise, 1992; Melloh and Crill, 1996; Wik et al., 2013; Zona et al., 2016; Treat et al., 2018). The few continuous CH_4 flux datasets across representative site years make it difficult to establish trends in seasonal dynamics, though monthly or annually aggregated estimates of CH_4 fluxes from different seasons do exist for high latitudes (Zona et al., 2016; Treat et al., 2018). Seasonal variability in freshwater wetland CH_4 fluxes is expected to be driven by changes in air (TA) and soil temperature (ST), soil moisture (including water table dynamics), and recent carbon

substrate availability, which influence the rates of CH_4 production and consumption (Lai, 2009; Bridgham et al., 2013; Dean et al., 2018). Temperature has widely been found to strongly affect CH_4 flux (Chu et al., 2014; Yvon-Durocher et al., 2014; Sturtevant et al., 2016), but the relationship is complex (Chang et al., 2020) and varies seasonally (Koebsch et al., 2015; Helbig et al., 2017). CH_4 flux is also driven by inundation depth since anoxic conditions are typically necessary for methanogenesis (Lai, 2009; Bridgham et al., 2013), though CH_4 production under bulk-oxic conditions has been observed (Angle et al., 2017). Substrate availability influences CH_4 production potential and is linked with gross primary productivity (GPP) because recent photosynthate fuels methanogenesis, though this relationship can vary by ecosystem type, plant functional type, and biome (Megonigal et al., 1999; Chanton et al., 2008; Hatala et al., 2012; Lai et al., 2014; Malhotra and Roulet, 2015; Sturtevant et al., 2016). In process models, the seasonality of CH_4 emissions from wetlands globally is primarily constrained by inundation (Poulter et al., 2017) with secondary within-wetland influences from temperature and availability of carbon (C) substrates (Melton et al., 2013; Castro-Morales et al., 2018). Bottom-up and top-down global CH_4 estimates continue to disagree on total CH_4 flux magnitudes and seasonality, including the timing of annual peak emissions (Spahni et al., 2011; Saunois et al., 2020). Thus, the variability in and predictors of wetland CH_4 seasonality globally remain a knowledge gap that high-frequency and long-term EC data can help fill.

Here, we first describe version 1.0 of the FLUXNET-CH_4 dataset (available at https://fluxnet.org/data/fluxnet-ch4-community-product/, last access: 7 April 2021). Version 1.0 of the dataset expands and formalizes the publication of data scattered among regional flux networks as described previously in Knox et al. (2019). FLUXNET-CH_4 includes half-hourly and daily gap-filled and non-gap-filled aggregated CH_4 fluxes and meteorological data from 79 sites globally: 42 freshwater wetlands, 6 brackish and saline wetlands, 7 formerly drained ecosystems, 7 rice paddy sites, 2 lakes, and 15 upland ecosystems. FLUXNET-CH_4 includes an additional two wetland sites (RU-Vrk and SE-St1), but they are not available under the CC BY 4.0 data policy and thus are excluded from this analysis. Since the majority of sites in FLUXNET-CH_4 Version 1.0 (hereafter referred to solely as "FLUXNET-CH_4") are freshwater wetlands, which are a substantial source of total atmospheric CH_4 emissions, we use the subset of data from freshwater wetlands to evaluate the representativeness of freshwater wetland coverage in the FLUXNET-CH_4 dataset relative to wetlands globally, and we provide the first assessment of global variability in and predictors of freshwater wetland CH_4 flux seasonality. We quantify a suite of CH_4 seasonality metrics and evaluate temperature and GPP (a proxy for recent substrate input) as predictors of seasonality across four latitudinal bands (northern, temperate, subtropical, and tropical). Due to a lack of high-temporal-resolution water table data at all sites, our analyses are unable to evaluate the critical role of water table on CH_4 seasonality. Here we provide parameters for better understanding and modeling seasonal variability in freshwater wetland CH_4 fluxes and generate new hypotheses and data resources for future syntheses.

2 Methods

2.1 FLUXNET-CH_4 dataset

2.1.1 History and data description

The FLUXNET-CH_4 dataset was initiated by the Global Carbon Project (GCP) in 2017 to better constrain the global CH_4 budget (https://www.globalcarbonproject.org/methanebudget/index.htm, last access: 6 July 2021). Beginning with a kick-off meeting in May 2018 in Washington DC, hosted by Stanford University, we coordinated with the AmeriFlux Management Project, the European Ecosystem Fluxes Database, and the Integrated Carbon Observation System Ecosystem Thematic Centre (ICOS-ETC) to avoid duplication of efforts as most sites are part of different regional networks (albeit with different data products). We collected and standardized data for FLUXNET-CH_4 with assistance from the regional flux networks, AmeriFlux's "Year of Methane", FLUXNET, the EU's Readiness of ICOS for Necessities of Integrated Global Observations (RINGO) project, and a US Geological Survey Powell Center working group. FLUXNET-CH_4 is a community-led project, so while we developed it with assistance from FLUXNET, we do not necessarily use standard FLUXNET data variables, formats, or methods.

FLUXNET-CH_4 includes gap-filled half-hourly CH_4 fluxes and meteorological variables. Gaps in meteorological variables (TA – air temperature; SW_IN – incoming shortwave radiation; LW_IN – incoming longwave radiation; VPD – vapor pressure deficient; PA – pressure; P – precipitation; WS – wind speed) were filled with the ERA-Interim (ERA-I) reanalysis product (Vuichard and Papale, 2015). We used the REddyProc package (Wutzler et al., 2018) to filter flux values with low friction velocity (u_*) based on relating nighttime u_* to fill gaps in CO_2, latent heat, and sensible heat fluxes and to partition net CO_2 fluxes into gross primary production (GPP) and ecosystem respiration (RECO) using both the daytime (Lasslop et al., 2010) and nighttime (Reichstein et al., 2005) approaches. Data gaps of CH_4 flux were filled using artificial neural network (ANN) methods first described in Knox et al. (2015, 2019) and summarized here in Sect. 2.1.2. Gap-filled data for gaps exceeding 2 months are provided and flagged for quality. Please see Table B1 for variable description and units, as well as quality flag information. For the seasonality analysis in this paper we excluded data from gaps exceeding 2 months, and we encourage future users of FLUXNET-CH_4 to critically evaluate gap-filled

values from long data gaps before including them in analyses (Dengel et al., 2013; Kim et al., 2020).

In addition to half-hourly data, the FLUXNET-CH_4 Version 1.0 release also contains a full set of daily mean values for all parameters except wind direction and precipitation. Daily precipitation is included as the daily sum of the half-hourly data, and daily average wind direction is not included.

2.1.2 Gap-filling methods and uncertainty estimates

As described in Knox et al. (2015, 2019), the ANN routine used to gap-fill the CH_4 data was optimized for generalizability and representativeness. To avoid biasing the ANN toward environmental conditions with typically better data coverage (e.g., summertime and daytime measurements), the explanatory data were divided into a maximum of 15 clusters using a *k*-means clustering algorithm. Data used to train, test, and validate the ANN were proportionally sampled from these clusters. For generalizability, the simplest ANN architecture with good performance ($< 5\,\%$ gain in model accuracy for additional increases in architecture complexity) was selected for 20 extractions of the training, test, and validation data. Within each extraction, each tested ANN architecture was reinitialized 10 times, and the initialization with the lowest root-mean-square error was selected to avoid local minima. The median of the 20 predictions was used to fill each gap. A standard set of variables available across all sites was used to gap-fill CH_4 fluxes (Dengel et al., 2013), which included the previously mentioned meteorological variables TA, SW_IN, WS, and PA and sine and cosine functions to represent seasonality. These meteorological variables were selected for their relevance to CH_4 exchange and were gap-filled using the ERA-I reanalysis data. Other variables related to CH_4 flux (e.g., water table depth, WTD, and soil temperature, TS) were not included as explanatory variables as they were not available across all sites or had large gaps that could not be filled using the ERA-I reanalysis data (Knox et al., 2019). The ANN gap-filling was performed using MATLAB (Mathworks 2018a, version 9.4.0).

While the median of the 20 predictions was used to fill each gap, the spread of the predictions was used to provide a measure of uncertainty resulting from the ANN gap-filling procedure. Specifically, the combined annual gap-filling and random uncertainty was calculated from the variance of the cumulative sums of the 20 ANN predictions (Knox et al., 2015; Anderson et al., 2016; Oikawa et al., 2017). The (non-cumulative) variance of the 20 ANN predictions was also used to provide gap-filling uncertainty for each half-hourly gap-filled value. While this output is useful for data–model comparisons, it cannot be used to estimate cumulative annual gap-filling error because gap-filling error is not random, which is why the cumulative sums of the 20 ANN predictions are used to estimate annual gap-filling error.

Random errors in EC fluxes follow a double exponential (Laplace) distribution with the standard deviation varying with flux magnitude (Richardson et al., 2006, 2012). For half-hourly CH_4 flux measurements, random error was estimated using the residuals of the median ANN predictions, providing a conservative "upper limit" estimate of the random flux uncertainty (Moffat et al., 2007; Richardson et al., 2008). The annual cumulative uncertainty at 95 % confidence was estimated by adding the cumulative gap-filling and random measurement uncertainties in quadrature (Richardson and Hollinger, 2007; Anderson et al., 2016). Annual uncertainties in CH_4 flux for individual site years are provided in Table B2. Throughout this paper, we include uncertainties on individual site years when discussing single years of data. In sites with multiple years of data, we report the standard deviation of the multiple years.

2.1.3 Dataset structure and site metadata

FLUXNET-CH_4 contains two comma-separated data files per site at half-hourly and daily resolutions which are available for download at https://fluxnet.org/data/fluxnet-ch4-community-product/ (last access: 7 April 2021), along with a file containing select site metadata. Each site has a unique FLUXNET-CH_4 DOI. All data from the 79 sites used in this analysis are available under CC BY 4.0 (https://creativecommons.org/licenses/by/4.0/, last access: 6 July 2021) copyright license (FLUXNET-CH_4 has an additional two sites available under the FLUXNET Tier 2 license (https://fluxnet.org/data/data-policy/, last access: 6 July 2021), though these sites are not included in our analysis).

Metadata (Table B3) include site coordinates, ecosystem classification based on site literature, presence/absence and dominance for specific vegetation types, and DOI link, as well as calculated data such as annual and quarterly CH_4 flux values. FLUXNET-CH_4 Version 1.0 sites were classified based on site-specific literature as fen, bog, swamp, marsh, salt marsh, lake, mangrove, rice paddy field, wet tundra, upland, or drained ecosystems that previously could have been wetlands, seasonally flooded pastures, or agricultural areas. To the extent possible, we followed classification systems of previous wetland CH_4 syntheses (Olefeldt et al., 2013; Turetsky et al., 2014; Treat et al., 2018). Drained systems are former wetlands that have subsequently been drained but may maintain a relatively shallow water table, which can contribute to occasional methane emissions, although we do not have specific water table depth information at all drained sites. Upland ecosystems are further divided into alpine meadows, grasslands, needleleaf forests, mixed forest, crops, tundra, and urban. Freshwater wetland classifications follow hydrological definitions of bog (ombrotrophic), fen (minerotrophic), wet tundra, marshes, and swamps and were designated as per the primary literature on the site. For all sites, vegetation was classified for the presence or absence of brown mosses (all species from the division Bryophyta except those in the class Sphagnopsida), *Sphagnum* mosses

(any species from class Sphagnopsida), ericaceous shrubs, trees (of any height), and aerenchymatous species (mostly order Poales but includes exceptions). These categories closely follow Treat et al. (2018) except that aerenchymatous species had to be expanded beyond Cyperaceae to incorporate wetlands globally. Presence/absence of vegetation groups was designated based on species lists in primary literature from the site. Out of the vegetation groups present, the dominant (most abundant) group is also reported and is based on information provided by lead site investigators.

In addition to the variable description table (Table B1) and the site metadata (Table B3), we provide several more tables to complement our analysis. Table B4 includes the climatic data used in the representativeness analysis. Table B5 provides seasonality parameters for CH_4 flux, air temperature, soil temperature (from the probe closest to the ground surface), and GPP. For sites with multiple soil temperature probes, the full set of soil temperature parameters are in Table B6. Table B7 contains the soil temperature probe depths. Table B2 contains the annual CH_4 flux and uncertainty. All Appendix B tables are also available at https://doi.org/10.5281/zenodo.4672601 (Delwiche et al., 2021).

2.1.4 Annual CH_4 fluxes

Annual CH_4 fluxes were calculated from gap-filled data for site years with data gaps shorter than 2 consecutive months or for sites above 20° N where >2-month data gaps occurred outside of the highest CH_4-emission months of 1 May through 31 October. Since we did not sum gap-filled values for >2 month-gaps during the winter, annual sums from these years will be an underestimate since winter fluxes can be important (Zona et al., 2016; Treat et al., 2018). Several sites had less than 1 year of data, and we report gap-filled CH_4 flux annual sums for sites with between 6 months and 1 year of data (BW-Gum = 228 d, CH-Oe2 = 200 d, JP-Swl = 210 d, and US-EDN = 182 d). While these sums will be an underestimate of annual CH_4 flux since they do not span a full year (and we therefore do not use them in the seasonality analysis), their relative magnitude can still be informative. For example, site JP-SWL is a lake site, and even with less than 1 year of data the summed CH_4 flux of 66 g C m^{-2} is relatively high (Taoka et al., 2020). In addition to sites with short time series, the annual CH_4 sum for site ID-Pag represents 365 d spanning June 2016 to June 2017.

2.1.5 Subset analysis on freshwater wetland CH_4 flux

In addition to the FLUXNET-CH_4-wide description of site class distributions and annual CH_4 fluxes, we also include a subset analysis on freshwater wetlands given that it is the dominant ecosystem type in our dataset and an important global CH_4 source (Saunois et al., 2016). First, we analyze freshwater wetland representativeness and subsequently the seasonality of their CH_4 emissions. Freshwater wetlands included in the seasonality and representativeness analysis are indicated in Table B3, column "IN_SEASONALITY_ANALYSIS".

2.2 Wetland representativeness

2.2.1 Principal component analysis

To compare the FLUXNET-CH_4 site distribution to the global wetland distribution, we evaluated their representativeness in the entire global wetland cover along four bioclimatic gradients. Only freshwater wetland sites were included in this analysis. Coastal sites were excluded because salinity, an important control on CH_4 production, could not be evaluated across the tower network due to a lack of global gridded salinity data (Bartlett et al., 1987; Poffenbarger et al., 2011). The four bioclimatic variables used were mean annual air temperature (MAT), latent heat flux (LE), enhanced vegetation index (EVI), and simple ratio water index (SRWI; data sources in Table B4). We use EVI because it is a more direct measurement than GPP from global gridded products and is considered a reasonable proxy for GPP (Sims et al., 2006). Together, these environmental variables account for, or are, proxies for key controls of CH_4 production, oxidation at the surface, and transport (Bridgham et al., 2013). We use a principal components analysis (PCA) to visualize the site distribution across the four environmental drivers at once. For this analysis, we consider the annual average bioclimatic conditions over 2003–2015. In the PCA output, we evaluate the coverage of the 42 freshwater sites over 0.25° grid cells containing >5 % wetland mean cover in Wetland Area and Dynamics for Methane Modeling (WAD2M; Zhang et al., 2020, 2021) for the same time period.

2.2.2 Global dissimilarity and constituency analysis

To further identify geographical gaps in the coverage of the FLUXNET-CH_4 Version 1.0 network, we quantified the dissimilarity of global wetlands from the tower network, using a similar approach to that taken for CO_2 flux towers (Meyer and Pebesma, 2020). We calculated the 4-dimensional Euclidean distance from the four bioclimatic variables between every point at the land surface to every tower location at the FLUXNET-CH_4 network. We then divided these distances by the average distance between towers to produce a dissimilarity index. Dissimilarity scores <1 represent areas whose nearest tower is closer than the average distance among towers, while areas with scores >1 are more distant. Lastly, we identified the importance of an individual tower in the network by estimating the geographical area to which it is most analogous in bioclimate space. We divided the world's land surface according to closest towers in bioclimatic space. The area to which each tower is nearest is defined as the tower's constituency.

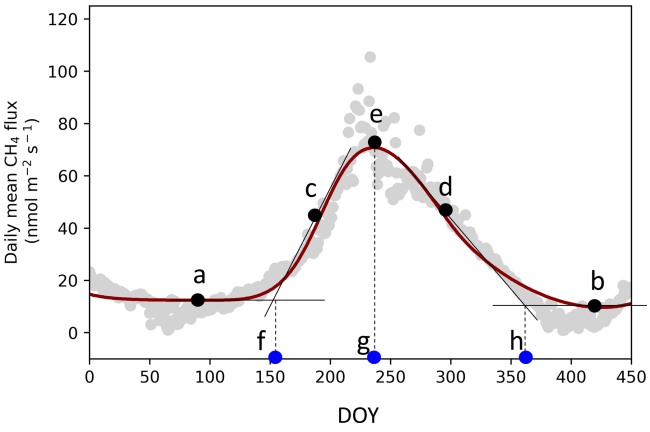


Figure 1. TIMESAT parameter description. **(a, b)** Base values (TIMESAT reports the average of these two values), **(c, d)** slopes of seasonal curves (lines drawn between 20 % and 80 % of the amplitude), **(e)** peak value, and day of year (DOY) for the start **(f)**, peak **(g)**, and end **(h)** of the elevated methane (CH_4) emission season. Data points are the mean daily gap-filled CH_4 fluxes from site JP-Bby in 2015.

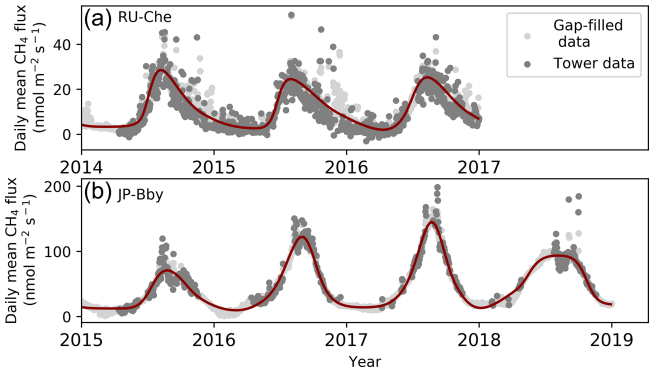


Figure 2. Examples of TIMESAT fits for two FLUXNET-CH_4 sites, **(a)** RU-Che and **(b)** JP-Bby. Methane (CH_4) flux data showing daily average flux tower data, with several high outliers excluded to improve the plot (dark gray), gap-filled values (light gray), and TIMESAT-fitted curve (dark red line) for sites JP-Bby and RU-Che. TIMESAT captures the size and shape of peaks (note different scale on y axes). CH_4 = methane.

2.3 Wetland CH_4 seasonality

To examine freshwater wetland CH_4 seasonality across the global range of sites in FLUXNET-CH_4, we extracted seasonality parameters for CH_4, temperature, and GPP using TIMESAT, a software package designed to analyze seasonality of environmental systems (Jönsson and Eklundh, 2002, 2004; Eklundh and Jönsson, 2015). TIMESAT calculates several seasonality parameters, including baseline flux, peak flux, and the slope of spring flux increase and fall decrease (Fig. 1). We also calculate parameters such as amplitude (peak flux minus baseline, which is the average of spring and fall baselines; "e" − (("a" + "b")/2) in Fig. 1) and relative peak timing (("g" − "f")/("h" − "f") in Fig. 1). TIMESAT uses a double-logistic fitting function to create a series of localized fits centered on data minima and maxima. Localized fits are determined by minimizing a merit function with the Levenberg–Marquardt method (Madsen et al., 2004; Nielsen, 1999). These localized fits are then merged using a global function to create a smooth fit over the full time interval. To fit CH_4 time series in TIMESAT, we used gap-filled data after removing gaps exceeding 2 months. We do not report TIMESAT parameters when large gaps occur during the spring CH_4 emissions' increase, peak, or fall decrease.

We estimate "start of elevated emission season" when CH_4 emissions begin to increase in the spring ("f" in Fig. 1), and "end of elevated emission season" when the period of elevated CH_4 flux ends in the fall ("h" in Fig. 1), as the intercept between the TIMESAT fitted baseline parameter and shoulder-season slope (similar to Gu et al., 2009). To extract seasonality parameters with TIMESAT, sites need a sufficiently pronounced seasonality, a sufficiently long time period, and minimal data gaps (we note that while TIMESAT is capable of fitting two peaks per year, all the freshwater wetland sites have a single annual peak). We excluded site years in restored wetlands when wetlands were still under construction. Of the 42 freshwater wetland sites in FLUXNET-CH_4 Version 1.0, 36 had sufficient data series to extract seasonality parameters. These 36 wetlands had 141 site years of data in total, which we fit with the double-logistic fitting method which followed site data well (representative examples in Fig. 2). For extratropical sites in the Southern Hemisphere, we shifted all data by 182 d so that maximum solar insolation seasonality would be congruent across the globe.

We also used TIMESAT to extract seasonality metrics for GPP, partitioned using the daytime-based approach (Lasslop et al., 2010) (GPP_DT), air temperature (TA), and soil temperature (TS_1, TS_2, etc). For sites where winter soil temperatures fall significantly below 0 °C, TIMESAT fits a soil temperature "start of elevated season" date to periods when the soil is still frozen. In order for TIMESAT to define the soil temperature seasonality within the thawed season, we converted all negative soil temperatures to zero (simply removing these values results in too many missing values for TIMESAT to fit). Many sites have more than one soil temperature probe, so we extracted separate seasonality metrics from each individual probe (although we used the metrics from the shallowest temperature probe in our analysis). Table B4 contain the TIMESAT seasonality parameters used in the seasonality analysis. We did not include water table depth in the seasonality analysis because many sites either lack water table depth measurements or have sparse data.

We regressed the CH_4 seasonality parameters from TIMESAT against annual temperature, annual water table depth, and TIMESAT seasonality parameters for air temperature, soil temperature, and GPP (proxy for recent carbon input available as substrate) using linear mixed-effect modeling

with the *lmer* command (with site as a random effect) from the R (R Core Team, 2018, version 3.6.2) package lmerTest (Kuznetsova et al., 2017). For these regressions we present the marginal R^2 outputs from *lmer*, which represent the variance explained only by the fixed effects. Mixed-effect modeling was necessary to account for the non-independence between measurements taken at the same site during different years (Zona et al., 2016; Treat et al., 2018). We also compared how seasonality metrics varied across latitudinal bands by dividing sites into northern (> 60° N), temperate (between 40 and 60° N), subtropical (absolute value between 20 and 40° N latitude, with site NZ-KOP being the only Southern Hemisphere site), and tropical (absolute value below 20° N). Site-year totals for the northern, temperate, subtropical, and tropical bands were $n = 57$, 36, 39, and 9, respectively. We used the Kruskal–Wallis test to establish whether groups (either across quarters or across latitudes) were from similar distributions and the post hoc multiple comparison "Dwass, Steel, Critchlow, and Fligner" procedure for intergroup comparisons. Kruskal–Wallis and post hoc tests were implemented in Python Version 3.7.4, using stats from scipy for Kruskal–Wallis and posthoc_dscf from scikit_posthocs.

We also compared quarterly CH_4 flux sums by dividing data into quarterly periods: January–February–March (JFM), April–May–June (AMJ), July–August–September (JAS), and October–November–December (OND). For the sake of simplicity, we chose to compare quarterly periods rather than site-specific growing/non-growing season periods so that all time periods would be the same length. Quarterly sums were computed from the gap-filled CH_4 fluxes when the longest continuous data gap within the quarter did not exceed 30 d, leading to site-year counts of 67, 92, 95, and 72 for JFM, AMJ, JAS, and OND, respectively. We compared quarterly CH_4 fluxes across latitudinal bands both for the total CH_4 flux and for the quarterly percentage of the annual CH_4 flux. Quarterly statistics were also conducted with the Kruskal–Wallis test and the post hoc multiple comparison "Dwass, Steel, Critchlow, and Fligner" procedure implemented in Python. Quarterly values are provided in Table B3, and the sum of mean quarterly CH_4 flux does not always equal mean annual CH_4 flux because some quarters either do not have data or have data gaps that exceed 30 d.

3 Results and discussion

3.1 FLUXNET-CH_4 dataset

3.1.1 Dataset description

Version 1.0 of the FLUXNET-CH_4 dataset contains 79 unique sites, 293 total site years of data, and 201 site years with sufficient data to estimate annual CH_4 emissions. A synthesis paper, published prior to the public data release of FLUXNET-CH_4 Version 1.0, had 60 unique sites and 139 site years with annual CH_4 emission estimates (Knox et al., 2019). Freshwater wetlands make up the majority of sites ($n = 42$), and the dataset also includes five salt marshes and one mangrove wetland. Notable additions to FLUXNET-CH_4 from the previous unpublished dataset used in Knox et al. (2019) include six tropical sites (between 20° S and 20° N), including one site in South America, two sites in southern Africa, and three sites in Southeast Asia. The 15 upland sites include six needleleaf forests, three crop sites (excluding rice), two alpine meadows, one grassland, one mixed forest, one tundra, and one urban site. The drained sites represent former wetlands that have been artificially drained for use as grasslands ($n = 3$) or croplands ($n = 3$). FLUXNET-CH_4 sites span the globe, though they are concentrated in North America and Europe (Fig. 3). Table B3 includes characteristics of all sites in the dataset.

Sites represent a range of ecosystem types, latitudes, median fluxes, and seasonality patterns (Table 1). Across all FLUXNET-CH_4 sites (including non-wetland sites), mean average annual CH_4 flux is positively skewed with a median flux of 9.5 g C m^{-2} yr^{-1}, a mean flux of 16.9 g C m^{-2} yr^{-1}, and numerous annual CH_4 fluxes exceeding 60 g C m^{-2} yr^{-1}. Marshes and swamps have the highest median flux, and upland, salt marsh, and tundra sites have the lowest (Fig. 4). Lake emissions are highly variable due to one high-flux lake site (JP-SWL). Flux data at many sites show strong seasonality in CH_4 emissions, but data coverage is also lower outside the growing season (Table 1). Data coverage is lowest during the JFM quarter (on average 20 % of half-hourly time periods contain flux data), reflecting the predominance of Northern Hemisphere sites and the practical difficulties in maintaining EC tower sites during colder winter months (Table 1). Bogs, fens, and marshes have pronounced seasonality, with fluxes being highest in the AMJ and JAS quarters. In contrast, CH_4 fluxes from uplands, drained sites, and salt marshes are more uniform and low year-round.

3.1.2 Freshwater wetland CH_4 characteristics

The FLUXNET-CH_4 Version 1.0 dataset contains 42 freshwater wetlands that span 37° S to 69° N, including bogs, fens, wet tundra, marshes, and swamps, and a range of annual CH_4 emission rates (Fig. 4). The majority of freshwater wetlands in our dataset emit 0–20 g C m^{-2} yr^{-1}, with 10 emitting 20–60 g C m^{-2} yr^{-1}, and one more than 60 g C m^{-2} yr^{-1}. Differences in annual CH_4 flux among wetland types is partially driven by temperature (which is often linked to site type), with mean annual air temperature explaining 51 % of the variance between sites (Fig. 5, exponential relationship). The global relationship between annual methane emissions and temperature can be described using a Q_{10} relationship where $Q_{10} = R2/R1^{((T2-T1)/10)}$, with $R2$ and $R1$ being the CH_4 emission rates at temperatures $T2$ and $T1$, respectively (temperature in °C). The Q_{10} based on Fig. 5 data is 2.57. We also note that annual CH_4 flux from individual biomes may have different relationships with temperature, as previ-

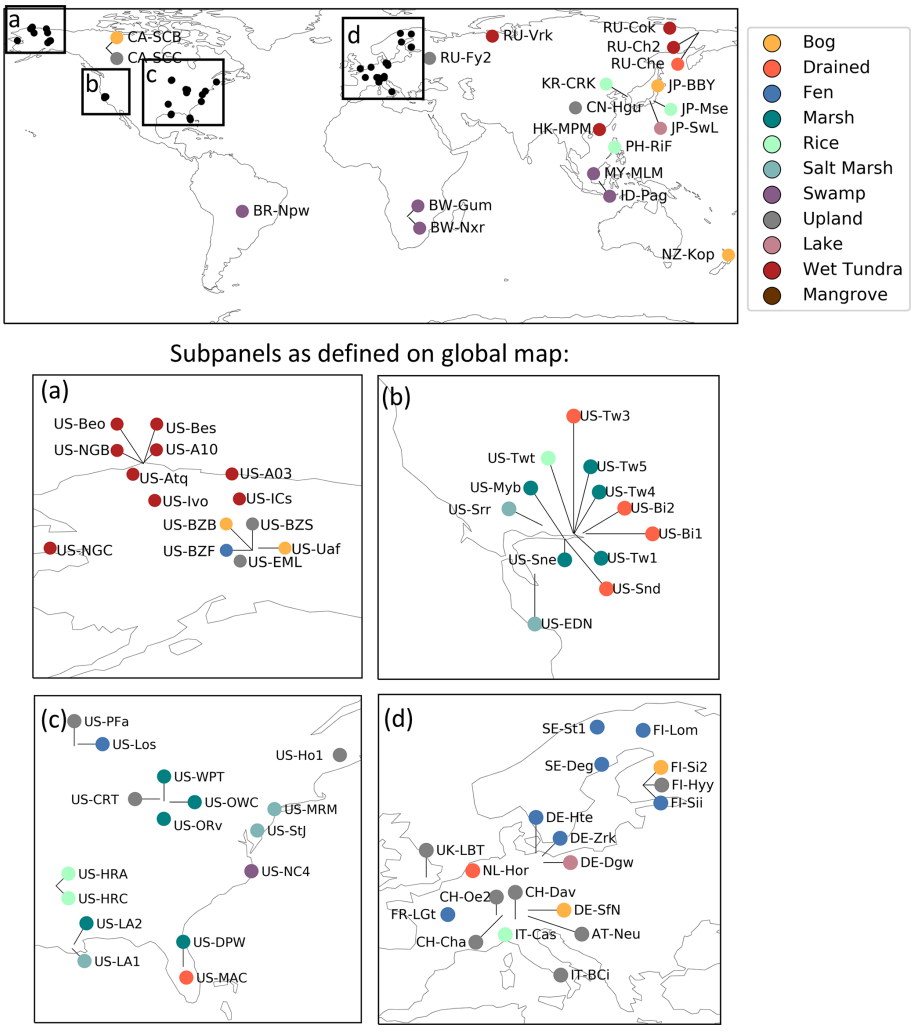


Figure 3. Global map of FLUXNET-CH$_4$ Version 1.0 site locations colored by site type. Panels **(a)**–**(d)** show sites that were too closely located to distinguish in the global map.

ous work has shown biome-specific trends in CH$_4$ flux with environmental drivers (Abdalla et al., 2016). However, there currently are not enough data points in each biome category to compare relationships between mean annual CH$_4$ flux and temperature. Annual CH$_4$ flux is not correlated with mean annual water table depth in FLUXNET-CH$_4$, unlike in Knox et al. (2019), which used a subset of the FLUXNET-CH$_4$ sites in which CH$_4$ flux was correlated with water table depth only for sites with water table below ground for 90 % of measured days ($r^2 = 0.31$, $p < 0.05$, $n = 27$ site years). Freshwater wetland seasonality is further described in Sect. 3.3.

3.1.3 Upland, rice, and urban CH$_4$ characteristics

Upland agricultural sites are characterized by a lack of seasonal pattern in CH$_4$ emissions, relatively low flux, and sometimes negative daily flux (i.e., CH$_4$ uptake) averages. All of the upland non-agricultural sites in FLUXNET-CH$_4$ Version 1.0 are net (albeit weak) CH$_4$ sources except for the needleleaf forest site US-Ho1, which has a mean annual CH$_4$ flux of $-0.1 \pm 0.1\,\mathrm{g\,C\,m^{-2}\,yr^{-1}}$ (see Table B3 for site acronyms and metadata). The average agricultural site emissions are $1.3 \pm 0.8\,\mathrm{g\,C\,m^{-2}\,yr^{-1}}$, and non-agricultural site emissions are $1.6 \pm 1.2\,\mathrm{g\,C\,m^{-2}\,yr^{-1}}$ across sites.

Rice sites ($n = 7$) have average annual emissions across all sites of $16.7 \pm 7.7\,\mathrm{g\,C\,m^{-2}\,yr^{-1}}$ and are characterized by strong seasonal patterns, with either one or more CH$_4$ emission peaks per year depending on the number of rice seasons and field water management. One peak is typically observed during the reproductive period for the continuously flooded sites with one rice season (i.e., US-HRC, JP-MSE) (Iwata et al., 2018; Runkle et al., 2019; Hwang et al., 2020). For sites with only one rice season but with single or multiple drainage and re-flooding periods, a secondary peak may appear before the reproductive peak (i.e., KR-CRK, IT-Cas, and US-HRA; Meijide et al., 2011; Runkle et al., 2019; Hwang et al., 2020).

Table 1. Summary table of sites grouped by ecosystem class reporting annual mean flux (Ann_Flux) and standard deviation from interannual variability (Ann_Flux_SD), site years of data, percent data cover per quarter, and median (med.) flux across site class. JFM signifies January–February–March, AMJ April–May–June, JAS July–August–September, and OND October–November–December.

	No. of sites	No. of site years	Ann_Flux ($g C m^{-2} yr^{-1}$)	Ann_Flux_SD ($g C m^{-2} yr^{-1}$)	JFM cover -age (%)	AMJ cover -age (%)	JAS cover -age (%)	OND cover -age (%)	JFM flux (med.)	AMJ flux (med.)	JAS flux (med.)	OND flux (med.)
Salt marsh	5	10	2.9	4.7	7	42	50	37	1.5	1.7	2.1	1.6
Wet tundra	11	39	3.8	1.8	8	28	40	18	0.4	2.6	8.1	3.2
Upland	15	47	4.0	10.5	23	35	39	28	1.2	0.5	1.4	0.8
Drained	7	20	6.3	7.1	22	39	39	29	4.6	3.6	5.1	3.6
Bog	7	32	10.5	6.4	8	27	37	18	7.2	11.0	24.8	9.5
Mangrove	1	3	11.1	0.5	46	28	30	41	3.2	7.2	22.5	14.1
Rice	7	20	14.4	8.8	16	37	45	27	3.2	11.9	43.1	4.2
Fen	8	40	20.5	16.0	29	43	40	30	2.8	14.2	26.0	6.4
Swamp	6	15	26.4	19.9	24	34	29	19	14.7	24.9	31.0	24.4
Lake	2	4	28.2	33.4	15	13	27	36	0.2	47.6	90.2	40.3
Marsh	10	42	40.8	20.7	22	43	53	30	13.5	55.0	85.8	36.1

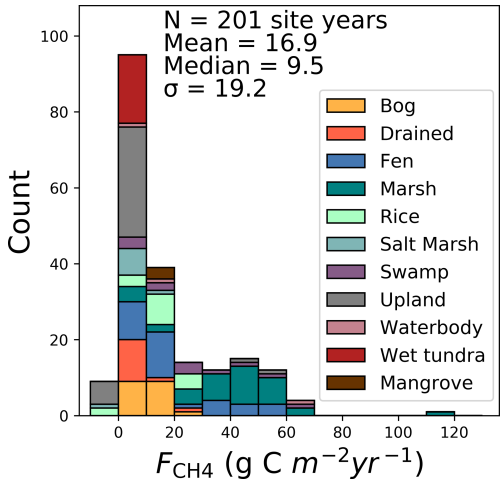


Figure 4. Histogram of annual methane fluxes (F_{CH_4}, $g C m^{-2} yr^{-1}$) grouped by site type.

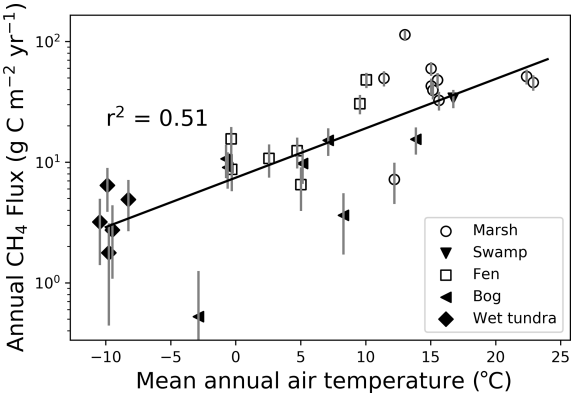


Figure 5. Relationship between mean annual wetland methane (CH_4) flux ($g C m^{-2} yr^{-1}$, logarithmic scale) and mean annual air temperature (°C) for each freshwater wetland site, with wetland type indicated by symbol. Markers represent individual site means, with vertical error bars representing the standard deviation of interannual variability.

Two reproductive peaks appear for sites with two rice seasons (i.e., PH-RiF), and each reproductive peak may be accompanied by a secondary peak due to drainage events (Alberto et al., 2015). Even sites with one continuously flooded rice season may experience a second peak if the field is flooded during the fallow season to provide habitat for migrating birds (e.g., US-Twt; Knox et al., 2016).

The dataset has 1 year of urban data from site UK-LBT in London, England. UK-LBT observes CH_4 fluxes from a 190 m tall communications tower in the center of London and has a mean annual CH_4 flux of $46.5 \pm 5.6 g C m^{-2} yr^{-1}$. This flux is more than twice as high as the mean annual CH_4 flux across all FLUXNET-CH_4 sites, $16.9 g C m^{-2} yr^{-1}$. The London site has higher CH_4 emissions in the winter com-

pared to summer, which is attributed to a seasonal increase in natural gas usage (Helfter et al., 2016.)

3.1.4 Saltwater and mangrove wetland CH_4 characteristics

Three of the five saltwater wetlands in FLUXNET-CH_4 (US-Edn, US-MRM, and US-Srr) have a very low mean annual CH_4 flux (see Table B2 for individual site-year CH_4 flux sums and associated uncertainty) and minimal seasonality. Two other FLUXNET-CH_4 saltwater sites (US-La1 and US-StJ) have significantly higher fluxes, with annual sums of 12.6 ± 0.6 and $9.6 \pm 1.0\,g\,C\,m^{-2}\,yr^{-1}$, respectively, while the mangrove site HK-MPM has annual mean fluxes of $11.1 \pm 0.5\,g\,C\,m^{-2}\,yr^{-1}$. This range of CH_4 fluxes across different saltwater ecosystems could be valuable for exploring the effect of salinity and different biogeochemical pathways of CH_4 production, oxidation, and transport of CH_4 (Bartlett et al., 1987; Poffenbarger et al., 2011). Saltwater wetlands along the coast have unique CH_4 dynamics attributable to the presence of abundant electron acceptors, most importantly sulfates which inhibit methanogenesis (Pattnaik et al., 2000; Mishra et al., 2003; Weston et al., 2006) but at low concentrations can have no effect (Chambers et al., 2011) or even increase methanogenesis (Weston et al., 2011). In fact, estuarine wetlands with moderate salinity can still be significant sources of CH_4 (Liu et al., 2020). Even under sulfate-rich conditions, high CH_4 production can be found via methylotrophic methanogenesis (Dalcin Martins et al., 2017; Seyfferth et al., 2020,) or because the processes of sulfate reduction and methanogenesis are spatially separated (Koebsch et al., 2019). Consequently, representing the biophysical drivers of ecosystem-scale CH_4 fluxes in non-freshwater wetlands is challenging and may represent a combination of competing or confounding effects (Vazquez-Lule and Vargas, 2021).

3.2 Freshwater wetland representativeness

We evaluated the representativeness of freshwater wetland sites in the FLUXNET-CH_4 Version 1.0 dataset against wetlands globally, based on bioclimatic conditions of our sites. When evaluating bioclimatic variables individually, the distribution of freshwater wetlands across the network was significantly different from the global distribution (alpha > 0.05; two-tailed Kolmogorov–Smirnov tests; see Table B4). We exclude wetlands classified as "salt marsh" in this representativeness analysis and the seasonality analysis below because of the unique CH_4 flux dynamics in saltwater ecosystems (as discussed in Sect. 3.1.4), though we note that some of the coastal wetlands included in the freshwater analysis periodically experience brackish water (i.e., US-Myb, US-Sne).

When considering the four bioclimatic variables, MAT, LE, EVI, and SRWI in a PCA, we found that our tower network generally samples the bioclimatic conditions of global wetland cover, but some noticeable gaps remain (Fig. 6). Three clusters of the world's wetland-dense regions are identified but are not equally sampled by the network. A cluster of low-temperature wetlands is sampled by a large number of high-latitude sites. The other two wetland clusters are not as well sampled: a high-temperature and LE cluster is represented only by two towers (ID-Pag and MY-MLM), while drier and temperate and subtropical wetlands including large swathes of the Sahel in Africa only have a site in Botswana (BW-Npw) as their closest analog tower.

Evaluating the bioclimatic dissimilarity of global wetlands to the FLUXNET-CH_4 network shows the least captured regions are in the tropics (Fig. 7a). Sparse coverage in the tropics also means that the few existing towers occupy a critical place in the network, particularly as tropical wetlands are the largest CH_4 emitters (Bloom et al., 2017; Poulter et al., 2017). Highly dissimilar wetlands are limited in extent and distributed across all latitudes, but the average dissimilarity is higher in north temperate (55 to 65°) and tropical (−5 to 5°) latitudes (Fig. 7b). To evaluate the importance of individual towers in the network, we estimated the geographical area to which it is most analogous in bioclimate space (Fig. 7c). We found that some towers have disproportionately large constituencies (i.e., wetland areas that share the same closest bioclimatic analog tower). Towers in Indonesia (ID-Pag), Brazilian Pantanal (BR-Npw), and Botswana floodplains (BW-Nxr) represent the closest climate analog for much of the tropics (678 000, 300 000, and 284 000 km^2, respectively), while CA-SCB represents a vast swath (291 000 km^2) of boreal and arctic regions (Fig. 7d).

Our assessment of wetland CH_4 tower coverage determines the ability of our dataset to represent global wetland distributions and highlights some clear representation gaps in the network, particularly in tropical and humid regions. Other geographic regions such India, China, and Australia, where towers exist but are not included in the current network, should be prioritized when expanding the network even though they are not among the most distant areas to the current network. Similar representativeness assessments have been developed for CO_2 tower networks to identify gaps and priorities for expansion (Jung et al., 2009). To improve the geographic coverage of the network for representing global-scale fluxes, locations for new tower sites can be targeted to cover bio-climatically distant areas from the current network (Villarreal et al., 2019). Candidate regions for expansion that are both high CH_4 emitting (Saunois et al., 2020) and located in under-sampled climates are the following: African Sahel, Amazon Basin, Congo Basin, and Southeast Asia. Climatic conditions over boreal and arctic biomes are generally better represented (primarily at lower elevations), but there is scope to expand the network in wetland-dense regions like the Hudson Bay Lowlands and North Siberian Lowlands. Moreover, establishing sites in other ecosystem types, especially lakes and reservoirs (see Deemer et al., 2016; Bastviken et al., 2011; Matthews et al.,

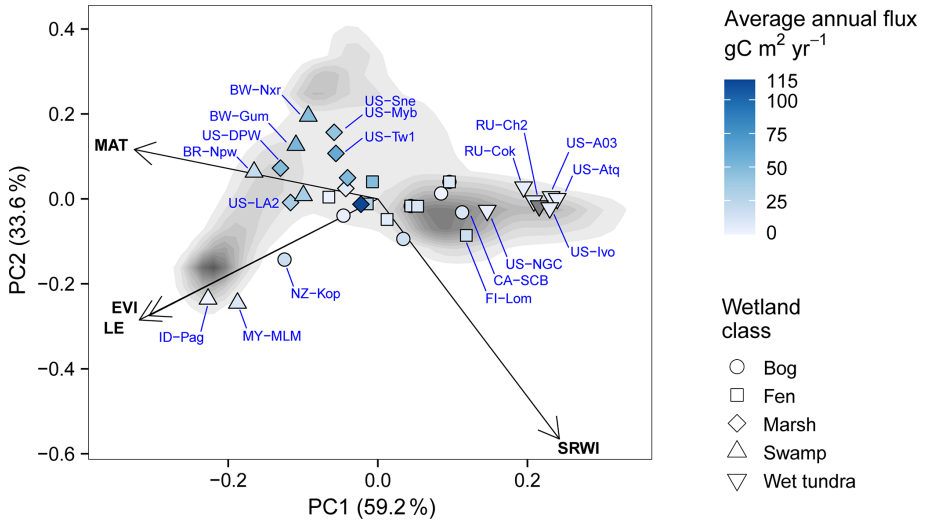


Figure 6. Principal component analysis displaying the distribution of freshwater wetland sites (points) along the two main principal components together accounting for 91.9 % of variance. Tower sites are represented as points with shapes indicating their wetland type and color shade representing the annual methane (CH_4) flux (gray points represent sites for which < 6 months of flux data were available to estimate annual budget). Sites codes are labeled in blue text for selected sites deviating from average conditions. Loading variables are represented by the arrows: mean annual temperature (MAT), simple ratio water index (SRWI), latent heat flux (LE), and enhanced vegetation index (EVI). The background shades of gray are a qualitative representation of the density of global wetland pixels and their distribution in the PCA climate space, with darker color representing higher densities (excluding Greenland and Antarctica). Only grid cells with > 5 % average wetland fraction according to the WAD2M over 2000–2018 are included (Zhang et al., 2020).

2020) in most climatic zones would help capture CH_4 fluxes from these ecosystems.

Understanding the representativeness of the network is essential when inferring general patterns of flux magnitude, seasonality, and drivers from the tower data (Villarreal et al., 2018). We produced a first-order representativeness of average bioclimatic conditions, but temporal representativeness (across seasons, climate anomalies, and extreme events) is particularly needed given the episodic nature of CH_4 fluxes (Chu et al., 2017; Mahecha et al., 2017; Göckede et al., 2019).

Assessing representation of wetland CH_4 sites is complicated by the fact that wetlands occupy only a fraction of most landscapes (except wetland-dense regions such as North Siberian Lowlands, Hudson Bay Lowlands, Congo Basin, etc.) and that not all relevant factors affecting CH_4 production and consumption could be considered in our analysis. For instance, our assessment of representation did not consider wetland types as such maps are limited by the inherent difficulties in remotely sensing wetland features (Gallant, 2015). The attribution of representativeness is further complicated by the fact that many EC tower locations are subject to small-scale variability within the field of view, or footprint, of the sensor. Consequently, the individual time steps within EC flux time series may represent a mixture of different wetland types or different fractions of wetland contribution to the total CH_4 flux, varying with wind direction, atmospheric stability, or season (Chu et al., 2021). This further complicates upscaling efforts. Additionally, this representativeness analysis did not apply weights to the drivers to reflect their varying influence on CH_4 flux. Such weights can be included in future versions as they are generated by a cross-validated machine learning approach (Jung et al., 2020). Future efforts could include the dissimilarity index from this analysis as a metric of extrapolation in a CH_4 flux upscaling effort.

3.3 Freshwater wetland flux seasonality

3.3.1 Seasonal flux comparisons by latitudinal bands

CH_4 flux and seasonality varied substantially across latitudinal bands (northern, temperate, subtropical, and tropical) (Fig. 8). Annual CH_4 fluxes for temperate, and subtropical sites were significantly higher than for northern sites (8.7 ± 5.0, 29.7 ± 25.2, 40.1 ± 14.6, and 24.5 ± 20.7 g C m^{-2} yr^{-1} for northern, temperate, subtropical, and tropical, respectively, and $p < 0.0001$ using Kruskal–Wallis and post hoc comparisons; Fig. 8a), and tropical sites were similar to all other latitudinal bands likely because of their small sample size. The ratio of seasonal amplitude to peak flux provides a measure of the relative seasonal increase in emissions compared with baseline, in which a ratio of 0 indicates no seasonal change in amplitude, a ratio of 1 indicates the off-season flux is zero, and values over 1 mean the off-season baseline CH_4 fluxes were negative (i.e., uptake). Average amplitude to peak flux ratios were similar across all latitudinal bands (0.9 ± 0.1, 0.9 ± 0.1, 0.9 ± 0.1,

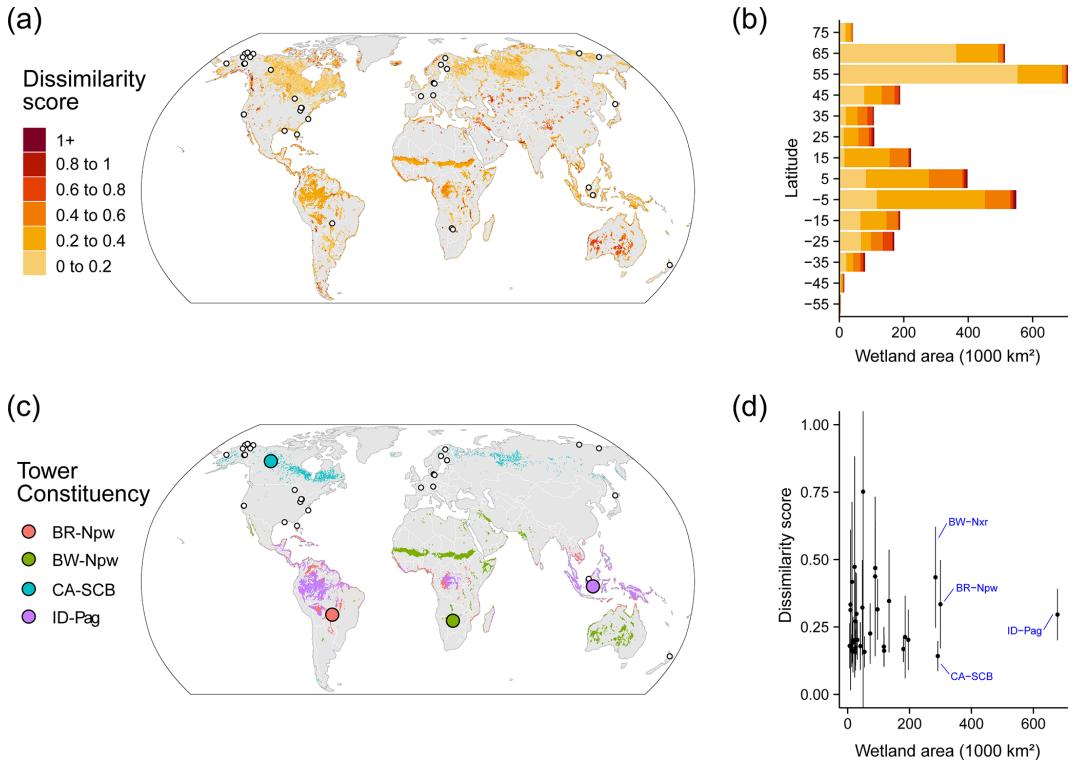


Figure 7. **(a)** Distance in bioclimatic space between global land surface and the FLUXNET-CH_4 Version 1.0 tower network (gray areas indicate no mapped wetlands). The Euclidean distance was computed on the four bioclimatic variables and was then standardized by the average distance within the network. Most of the land surface has a dissimilarity score lower than 1, meaning these areas are closer than the average tower distance (lower dissimilarity score means a similar bioclimate to that represented by towers in the network). However, this pattern reflects more the sparsity of the tower network than a similarity of the land surface to the network. Areas with $< 5\,\%$ coverage by wetlands were excluded to focus on wetland-dense regions. **(b)** Latitudinal distribution of dissimilarity score, **(c)** map of the four largest tower constituencies, and **(d)** scatterplot of wetland area in each tower constituency plotted against the average dissimilarity score (point) and $\pm$ standard deviation (error bar).

and 1.0 ± 0.7 for northern, temperate, subtropical, and tropical, respectively; Fig. 8b). The spring increase in CH_4 emissions began later in northern sites compared with temperate and subtropical sites (end of May versus April, respectively, and $p = 0.001$; Fig. 8c), while tropical sites vary widely in elevated emission season start date. Northern sites also had shorter elevated CH_4 flux season lengths (138 ± 24 d) compared to temperate sites (162 ± 32 d), and both were shorter than subtropical sites (209 ± 43 d; $p < 0.0001$; Fig. 8e). On average, CH_4 flux peaked earlier for temperate sites compared to northern ($p = 0.008$) and subtropical sites ($p = 0.02$; middle to late July compared with early August; Fig. 8f), while tropical sites again vary widely. Given their unique seasonality and low number of site years ($n = 9$), tropical systems are discussed separately in Sect. 3.3.3 and are not included in the comparisons in the remainder of this section. While our results on CH_4 seasonality corroborate expected trends for these latitudinal bands, they provide some of the first estimates of CH_4 seasonality parameters and ranges across a global distribution of sites.

We found that latitudinal groups showed strong differences in absolute CH_4 flux across quarters and narrower differences in percentage of annual CH_4 flux (Fig. 9a versus 9b). Thus, the AMJ quarter had a similar relative contribution to the annual CH_4 flux across latitudes regardless of the absolute annual CH_4 flux. CH_4 fluxes (Fig. 9a) were highest during JAS for northern, temperate, and subtropical sites and highest in AMJ and JAS for temperate sites ($p < 0.01$). Though CH_4 fluxes in northern sites are most commonly measured during warm summer months (Sachs et al., 2010; Parmentier et al., 2011), fluxes in JFM and OND (50 % of the yearly duration) on average make up $18.1 \pm 3.6\,\%$, $15.3 \pm 0.1\,\%$, and $31.2 \pm 0.1\,\%$ (northern, temperate, and subtropical, respectively) of annual emissions. This pattern indicates that a substantial fraction of annual CH_4 fluxes occur during cooler months. The contribution of non-growing season CH_4 emissions to annual CH_4 fluxes has previously been described for arctic and boreal regions (Zona et al., 2016; Treat et al., 2018), and our analysis suggests comparable contributions in temperate and subtropical systems for the same quarterly periods.

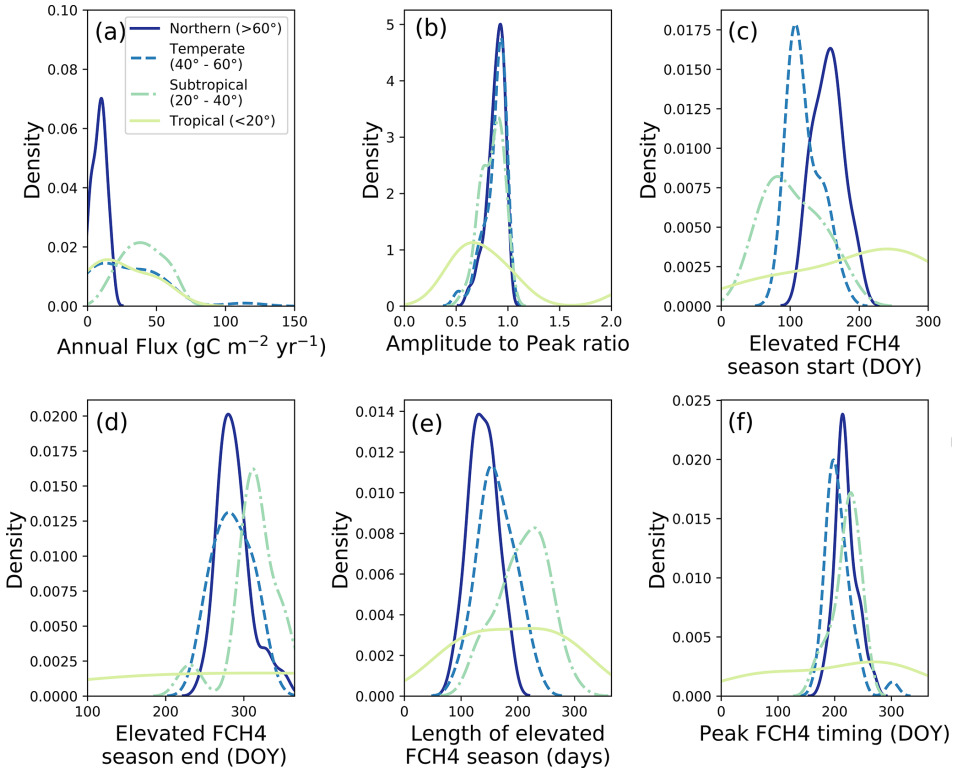


Figure 8. **(a)** Annual methane (CH_4) flux (g C m^{-2} yr^{-1}), **(b)** ratio of seasonal amplitude to seasonal peak, where values of 0 indicate uniform annual CH_4 flux, values of 1 indicate zero off-season fluxes, and values exceeding 1 indicate negative off-season fluxes, **(c)** CH_4 flux (FCH_4) elevated emission season start by day of year (DOY), **(d)** FCH4 elevated emission season end by DOY, **(e)** length of elevated CH_4 flux season (days), and **(f)** DOY of peak FCH_4. Northern (dark blue, solid line), temperate (blue, dashed line), sub-tropical (green, dot-dash line), and tropical (light green, solid line) wetlands plotted using the kernel density function. Each panel has lines that represent latitudinal bands as follows: northern ($> 60°$), temperate (between 40 and 60°), subtropical (between 20 and 40°), and tropical ($< 20°$), though the site-year totals vary between these groups ($n = 57$, $n = 36$, $n = 39$, and $n = 9$ respectively). All total CH_4 flux values and elevated season start values are positive, and the apparent continuation of the data distribution into negative values is an artifact of the kernel density function. Southern Hemisphere sites below 20° S were shifted by 182 d to make summer the middle of the year for comparability with Northern Hemisphere sites.

3.3.2 Predictors of CH_4 flux phenology

The start of the elevated CH_4 flux season, and how long the elevated flux season lasts, correlated strongly with mean annual air temperature (Fig. 10; $p < 0.0001$ for each). Methane flux began to increase roughly 2 months earlier in the warmest systems (mean annual temperature $> 20\,°C$) compared to the coldest (mean annual temperature near $-10\,°C$), though several of the warmer sites had high variability. Our data suggest that the CH_4 season started 2.8 ± 0.5 d earlier for every degree Celsius increase in mean annual temperature (Fig. 10a). In contrast, the end of the CH_4 emission season was not correlated with mean annual temperature, but a positive trend existed despite high variability at the warmest and coldest sites (Fig. 10b). The high variability seen in the end of the CH_4 season at northern sites is important to note and would likely be better resolved by incorporating other seasonality or phenological characteristics, such as moisture, active layer depth, and plant community composition (e.g., Kittler et al., 2017). Plants with aerenchymatous tissue, for example, influence the timing of plant-mediated CH_4 flux and are a key source of uncertainty when predicting CH_4 seasonality for northern wetlands (Xu et al., 2016; Kwon et al., 2017). Despite the relative lack of trend with season end date, the season length was still positively correlated with mean annual temperature, with the warmest sites having roughly 3 more months of seasonally elevated CH_4 emissions than the coldest sites (Fig. 10c). CH_4 season length increased 3.6 ± 0.6 d for every degree Celsius increase in mean annual temperature (note that these relationships are correlations, and we cannot disentangle causality with this analysis). Temperature is highly correlated with other parameters (i.e., radiation, days of snow cover, etc.), so CH_4 flux is also likely to correlate with other environmental parameters.

Although the spring onset of increasing CH_4 emissions correlated with mean annual air temperature, on average it lagged behind the spring increase in the shallowest soil temperatures by 31 ± 40 d (Fig. 11; lag is significantly different

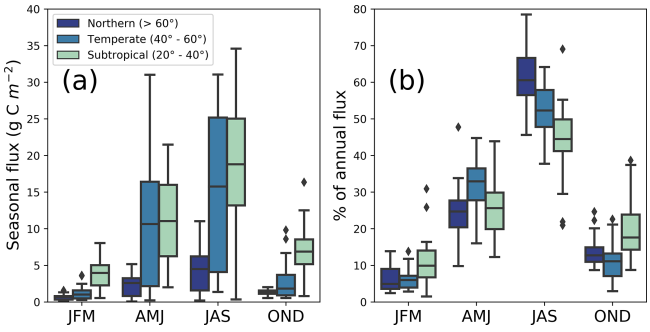


Figure 9. **(a)** Quarterly contribution to total annual CH_4 flux (in g C m^{-2}) and **(b)** percentage of annual CH_4 flux. Sites were divided into northern (> 60° N), temperate (40–60° N), and subtropical (20–40° N). Quarters with continuous data gaps exceeding 30 d were excluded. We used the following quarterly periods: January–February–March (JFM), April–May–June (AMJ), July–August–September (JAS), and October–November–December (OND). Tropical sites are discussed separately in Sect. 3.3.3 because of their unique seasonality and low number of sites.

than zero, and $p < 0.001$), with very few instances of CH_4 emissions beginning before seasonal soil temperatures increase (and by 20 ± 50 d for the deepest temperature probes). In contrast, for roughly half of the sites, CH_4 emission increased prior to seasonal GPP (a proxy for fresh substrate availability) increases. This suggests that the initiation of increased CH_4 fluxes at the beginning of the season was not limited by availability of substrate derived from recent photosynthates. Additionally, the onset of CH_4 fluxes tended to occur closer to the onset of soil temperature increase for cooler temperature sites (sites with later start dates tend to be cooler; Fig. 11a). This result is likely attributable to the direct influence of increased temperature on microbial processes (Chadburn et al., 2020), as well as the indirect influences of snowmelt, both via release of CH_4 from the snowpack and a higher water table leading to more CH_4 production (Hargreaves et al., 2001; Tagesson et al., 2012; Mastepanov et al., 2013; Helbig et al., 2017). These observed trends hold for the entire temperature or GPP range of freshwater wetland sites but are not necessarily applicable within individual latitudinal bands.

In contrast with the CH_4 season start timing, the timing of the CH_4 peak did not correlate with the timing of either the soil temperature peak or the GPP peak (Fig. A1). For 63 % of the sites, the average timing of peak CH_4 emissions lagged behind the soil temperature peak, and at 83 % of the sites average peak CH_4 lagged behind peak GPP (Fig. A1). Although there was no simple relationship between absolute CH_4 peak timing and the environmental drivers we investigated, there was a correlation ($p = 0.0005$) between the relative timing of peak CH_4 compared to season onset (calculated as described in Sect. 2.3) and mean annual air temperature (Fig. 12a). For cooler sites, the peak of seasonal CH_4 emissions occurred closer to the onset of the CH_4 emission season than the end of the season, resulting in an asymmetrical seasonal CH_4 flux shape that is illustrated in Fig. 2a. Soil temperature also peaked earlier in the season for cooler wetlands, though the relationship is not as pronounced ($p = 0.009$; Fig. 12b). In contrast, GPP peaked later in the season for cooler wetlands ($p = 0.009$, Fig. 12c). Previous work on Arctic sites (sites US-Ivo, US-Beo, US-Atq, US-Bes, and RU-CH2) highlighted the asymmetrical annual CH_4 peak, with higher fall emissions being attributed to the "zero curtain" period when soil below the surface remains thawed for an extended period of time due to snow insulation (Zona et al., 2016; Kittler et al., 2017). Furthermore, soils can stay above the "zero curtain" range for an extended time into the fall and winter (Helbig et al., 2017), which may also be caused by snow insulation. The rapid onset of emissions in the spring following snowmelt could be attributed to the release of accumulated CH_4 (Friborg et al., 1997), and other high latitude sites have seen similarly sharp increases in CH_4 emissions at snowmelt (Dise, 1992; Windsor, 1992). However, not all studies in high latitudes have observed asymmetrical CH_4 emission peaks, pointing to the inherent complexity of these ecosystems (Rinne et al., 2007; Tagesson et al., 2012).

3.3.3 Uniqueness of tropical wetlands

Tropical wetlands typically do not experience the large swings in temperature and GPP that contribute to CH_4 flux seasonality in temperate and northern sites. Indeed, the relatively constant high temperatures and high GPP in tropical ecosystems may lead to the lower ratio between seasonal amplitude and peak CH_4 flux compared with temperate and northern sites (Fig. 8b). Tropical flux sites have historically been under-studied, leading to a lack of synthesized information about these ecosystems. FLUXNET-CH_4 has five tropical wetland sites (latitudes between 20° S and 20° N) and one tropical rice site, representing 13 site years of data. These sites are especially insightful as they provide the first estimates of CH_4 fluxes from large, tropical, seasonal floodplain systems.

We found a broad range of annual CH_4 fluxes across tropical sites in FLUXNET-CH_4 Version 1.0. Annual CH_4 flux emissions from two Southeast Asian flooded peat forests were relatively low, 0.01 ± 0.1 and 9.5 ± 0.6 g C m^{-2} yr^{-1} for ID-PAG and MY-MLM, respectively, which is consistent with annual CH_4 fluxes measured at another peat forest in Indonesia (Deshmukh et al., 2020). In contrast, mean annual CH_4 flux for a seasonally flooded swamp in the Brazilian Pantanal region (BR-NPW) was over twice as high as MY-MLM, at 19.2 ± 2.5 g C m^{-2} yr^{-1}. Similarly high annual CH_4 fluxes were observed at the two Botswana swamp sites in the Okavango Delta (51.7 ± 10.6 and 47.3 ± 3.7 g C m^{-2} yr^{-1} for BW-GUM and BW-NXR, respectively), one of which is seasonally inundated and sur-

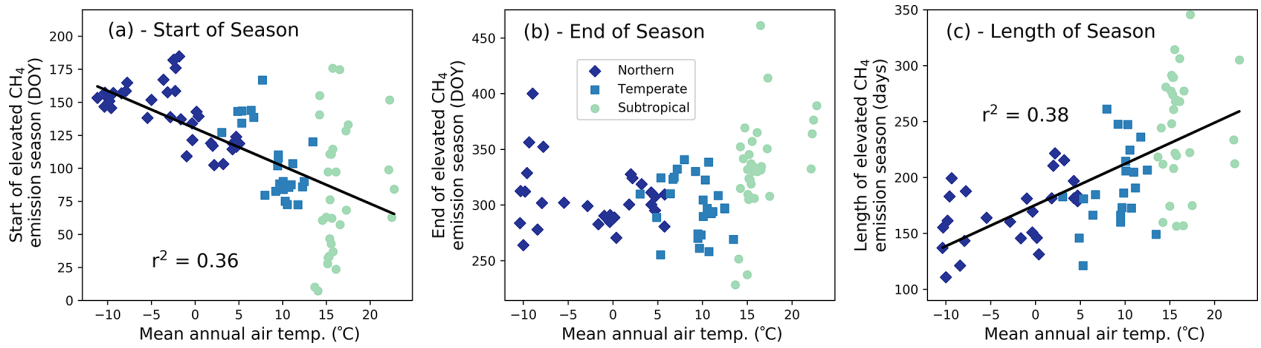


Figure 10. The **(a)** start of the elevated methane (CH_4) emission season (y =-2.8x + 130, with "x" in °C and "y" in day of year, DOY), **(b)** the end of the elevated emission season in DOY, and **(c)** the length of the emission season with mean annual site air temperature ($y = 3.6x + 176.6$, with "x" in °C and "y" in days). Each point represents a site year of data, and all reported r^2 values are significant to $p < 0.0001$. Tropical sites are discussed separately in Sect. 3.3.3.

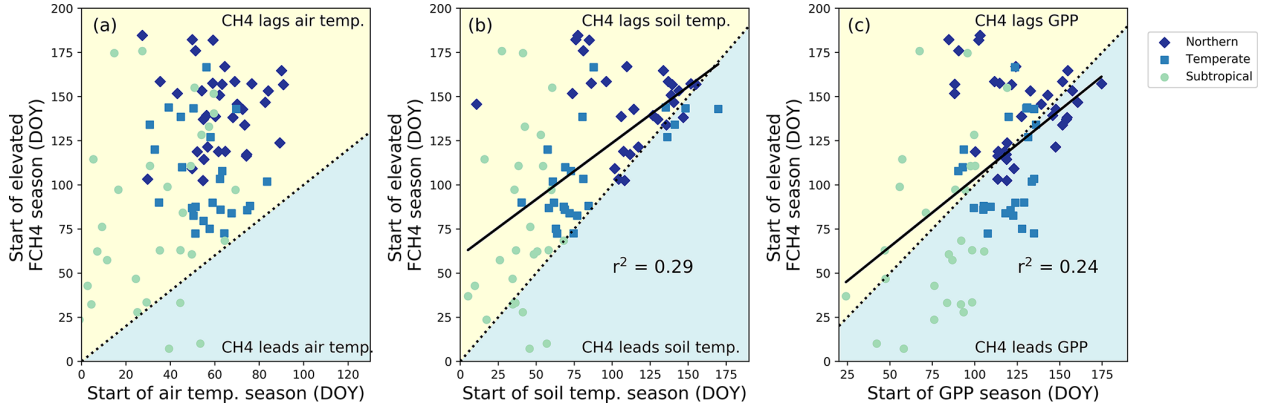


Figure 11. Relationship between the onset of the methane (CH_4) emission season to **(a)** the beginning of the air warming by day of year (DOY), **(b)** soil warming at the shallowest probe depth per site by DOY, and **(c)** gross primary productivity (GPP) increase for the subset of sites with soil temperature data by DOY. Each point represents a site year of data. Dashed lines represent a 1 : 1 relationship, and solid lines are significant ($p < 0.05$) regression fits. On average, the CH_4 emission season lags behind the soil temperature increase by 31 ± 40 d and is more synchronous with GPP.

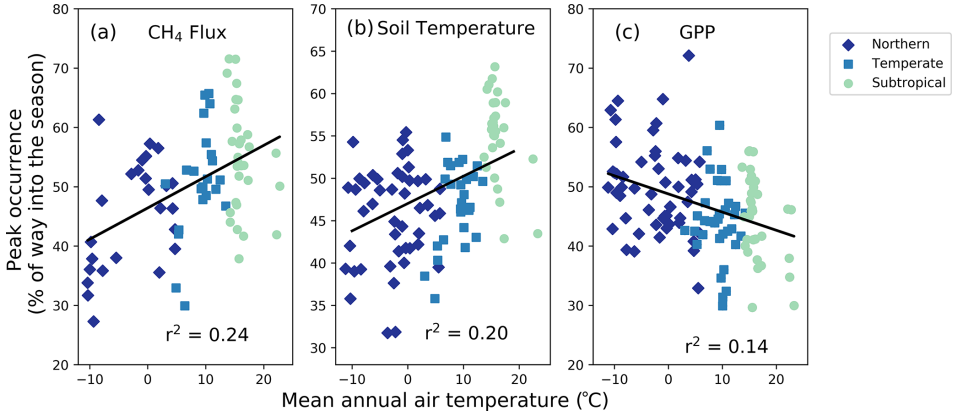


Figure 12. Site-year peak methane (CH_4) emissions **(a)** and peak soil temperature **(b)** occur earlier in the season for sites with lower mean annual temperatures. **(c)** Gross primary productivity (GPP) tends to peak earlier in the season for warmer sites, though the trend is weak. All r^2 values are significant at $p < 0.001$. Each point represents a site year of data.

Table 2. Site identification (SITE_ID), data DOI, and DOI reference for each FLUXNET-CH_4 site.

SITE_ID	DOI	DOI_REFERENCE
AT-Neu	https://doi.org/10.18140/FLX/1669365	Wohlfahrt (2020)
BR-Npw	https://doi.org/10.18140/FLX/1669368	Vourlitis et al. (2020)
BW-Gum	https://doi.org/10.18140/FLX/1669370	Helfter (2020a)
BW-Nxr	https://doi.org/10.18140/FLX/1669518	Helfter (2020b)
CA-SCB	https://doi.org/10.18140/FLX/1669613	Sonnentag and Helbig (2020a)
CA-SCC	https://doi.org/10.18140/FLX/1669628	Sonnentag and Helbig (2020b)
CH-Cha	https://doi.org/10.18140/FLX/1669629	Merbold et al. (2020a)
CH-Dav	https://doi.org/10.18140/FLX/1669630	Merbold et al. (2020b)
CH-Oe2	https://doi.org/10.18140/FLX/1669631	Maier et al. (2020)
CN-Hgu	https://doi.org/10.18140/FLX/1669632	Niu and Chen (2020)
DE-Dgw	https://doi.org/10.18140/FLX/1669633	Sachs and Wille (2020a)
DE-Hte	https://doi.org/10.18140/FLX/1669634	Koebsch and Jurasinski (2020)
DE-SfN	https://doi.org/10.18140/FLX/1669635	Schmid and Klatt (2020)
DE-Zrk	https://doi.org/10.18140/FLX/1669636	Sachs and Wille (2020b)
FI-Hyy	https://doi.org/10.18140/FLX/1669637	Mammarella et al. (2020)
FI-Lom	https://doi.org/10.18140/FLX/1669638	Lohila et al. (2020)
FI-Si2	https://doi.org/10.18140/FLX/1669639	Vesala et al. (2020a)
FI-Sii	https://doi.org/10.18140/FLX/1669640	Vesala et al. (2020b)
FR-LGt	https://doi.org/10.18140/FLX/1669641	Jacotot et al. (2020)
HK-MPM	https://doi.org/10.18140/FLX/1669642	Lai (2020)
ID-Pag	https://doi.org/10.18140/FLX/1669643	Sakabe et al. (2020)
IT-BCi	https://doi.org/10.18140/FLX/1669644	Famulari (2020)
IT-Cas	https://doi.org/10.18140/FLX/1669645	Manca and Goded (2020)
JP-BBY	https://doi.org/10.18140/FLX/1669646	Ueyama et al. (2020)
JP-Mse	https://doi.org/10.18140/FLX/1669647	Iwata (2020a)
JP-SwL	https://doi.org/10.18140/FLX/1669648	Iwata (2020b)
KR-CRK	https://doi.org/10.18140/FLX/1669649	Ryu et al. (2020)
MY-MLM	https://doi.org/10.18140/FLX/1669650	Wong et al. (2020)
NL-Hor	https://doi.org/10.18140/FLX/1669651	Dolman et al. (2020a)
NZ-Kop	https://doi.org/10.18140/FLX/1669652	Campbell and Goodrich (2020)
PH-RiF	https://doi.org/10.18140/FLX/1669653	Alberto and Wassmann (2020)
RU-Ch2	https://doi.org/10.18140/FLX/1669654	Goeckede (2020)
RU-Che	https://doi.org/10.18140/FLX/1669655	Merbold (2020)
RU-Cok	https://doi.org/10.18140/FLX/1669656	Dolman et al. (2020b)
RU-Fy2	https://doi.org/10.18140/FLX/1669657	Varlagin (2020)
SE-Deg	https://doi.org/10.18140/FLX/1669659	Nilsson and Peichl (2020)
UK-LBT	https://doi.org/10.18140/FLX/1670207	Helfter (2020c)
US-A03	https://doi.org/10.18140/FLX/1669661	Billesbach and Sullivan (2020a)
US-A10	https://doi.org/10.18140/FLX/1669662	Billesbach and Sullivan (2020b)
US-Atq	https://doi.org/10.18140/FLX/1669663	Zona and Oechel (2020a)
US-Beo	https://doi.org/10.18140/FLX/1669664	Zona and Oechel (2020b)
US-Bes	https://doi.org/10.18140/FLX/1669665	Zona and Oechel (2020c)
US-Bi1	https://doi.org/10.18140/FLX/1669666	Rey-Sanchez et al. (2020a)
US-Bi2	https://doi.org/10.18140/FLX/1669667	Rey-Sanchez et al. (2020b)
US-BZB	https://doi.org/10.18140/FLX/1669668	Euskirchen and Edgar (2020a)
US-BZF	https://doi.org/10.18140/FLX/1669669	Euskirchen and Edgar (2020b)
US-BZS	https://doi.org/10.18140/FLX/1669670	Euskirchen and Edgar (2020c)
US-CRT	https://doi.org/10.18140/FLX/1669671	Chen and Chu (2020a)
US-DPW	https://doi.org/10.18140/FLX/1669672	Hinkle and Bracho (2020)
US-EDN	https://doi.org/10.18140/FLX/1669673	Oikawa (2020)
US-EML	https://doi.org/10.18140/FLX/1669674	Schuur (2020)
US-Ho1	https://doi.org/10.18140/FLX/1669675	Richardson and Hollinger (2020)
US-HRA	https://doi.org/10.18140/FLX/1669676	Runkle et al. (2020)
US-HRC	https://doi.org/10.18140/FLX/1669677	Reba et al. (2020)
US-ICs	https://doi.org/10.18140/FLX/1669678	Euskirchen et al. (2020)

Table 2. Continued.

SITE_ID	DOI	DOI_REFERENCE
US-Ivo	https://doi.org/10.18140/FLX/1669679	Zona and Oechel (2020d)
US-LA1	https://doi.org/10.18140/FLX/1669680	Holm et al. (2020a)
US-LA2	https://doi.org/10.18140/FLX/1669681	Holm et al. (2020b)
US-Los	https://doi.org/10.18140/FLX/1669682	Desai (2020a)
US-MAC	https://doi.org/10.18140/FLX/1669683	Sparks (2020)
US-MRM	https://doi.org/10.18140/FLX/1669684	Schäfer (2020)
US-Myb	https://doi.org/10.18140/FLX/1669685	Matthes et al. (2020)
US-NC4	https://doi.org/10.18140/FLX/1669686	Noormets et al. (2020)
US-NGB	https://doi.org/10.18140/FLX/1669687	Torn and Dengel (2020a)
US-NGC	https://doi.org/10.18140/FLX/1669688	Torn and Dengel (2020b)
US-ORv	https://doi.org/10.18140/FLX/1669689	Bohrer and Morin (2020)
US-OWC	https://doi.org/10.18140/FLX/1669690	Bohrer et al. (2020)
US-PFa	https://doi.org/10.18140/FLX/1669691	Desai (2020b)
US-Snd	https://doi.org/10.18140/FLX/1669692	Detto et al. (2020)
US-Sne	https://doi.org/10.18140/FLX/1669693	Shortt et al. (2020)
US-Srr	https://doi.org/10.18140/FLX/1669694	Windham-Myers et al. (2020)
US-StJ	https://doi.org/10.18140/FLX/1669695	Vazquez-Lule and Vargas (2020)
US-Tw1	https://doi.org/10.18140/FLX/1669696	Valach et al. (2020a)
US-Tw3	https://doi.org/10.18140/FLX/1669697	Chamberlain et al. (2020)
US-Tw4	https://doi.org/10.18140/FLX/1669698	Eichelmann et al. (2020)
US-Tw5	https://doi.org/10.18140/FLX/1669699	Valach et al. (2020b)
US-Twt	https://doi.org/10.18140/FLX/1669700	Knox et al. (2020)
US-Uaf	https://doi.org/10.18140/FLX/1669701	Iwata et al. (2020)
US-WPT	https://doi.org/10.18140/FLX/1669702	Chen and Chu (2020b)

rounded by grassland (BW-NXR) and the other a permanently flooded lagoon covered in a floating papyrus mat (BW-GUM). The relatively low fluxes found at the two Southeast Asian peat forest sites indicate that these ecosystems may be smaller CH_4 sources than expected given their location in the humid tropics. Even the higher-emitting tropical sites in Brazil and Botswana are still well within the range of annual CH_4 flux typical in cooler latitudes (Fig. 1).

In addition to having highly variable CH_4 flux magnitudes, the tropical sites differ from each other in their seasonality. CH_4 flux hit a minimum around July for two sites (BW-GUM, latitude 18.965° S, and MY-MLM, latitude 1.46° N), while CH_4 flux increased through July and the subsequent months for the other Botswana site, BW-NXR (latitude 19.548° S). Site ID-Pag (latitude 2.32° S) had minimal seasonality, whereas the flooded forest site in Brazil (BR-NPW, latitude 16.49° S) had near-zero fluxes from approximately July to January and consistently high fluxes for the remainder of the year. The rice site PH-RiF (latitude 14.14° N) had two annual CH_4 flux peaks, which is consistent with some other rice sites and likely reflects management practices. Baseline CH_4 flux values also differed, with the two Botswana sites having the highest off-season fluxes (29 and 133 nmol m^{-2} s^{-1} for BW-NXR and BW-GUM, respectively, estimated by TIMESAT), MY-MLM having an intermediate baseline CH_4 flux (16 nmol m^{-2} s^{-1}, estimated by TIMESAT), and the remainder of the sites having essentially zero flux at baseline. While more tropical wetland data will be needed to extract broad-scale conclusions about these ecosystems, the six tropical sites in FLUXNET-CH_4 provide an important starting point for synthesis studies and highlight tropical wetland CH_4 variability.

4 Data availability

Half-hourly and daily aggregations are available for download at https://fluxnet.org/data/fluxnet-ch4-community-product/ (for citations, please cite this study), along with a table containing site metadata compiled from Table B3. Variable descriptions and units are provided in Table B1 and at https://fluxnet.org/data/fluxnet-ch4-community-product/ (last access: 7 April 2021). Each site has a unique FLUXNET-CH_4 DOI as listed in Table B3. All site data used in this analysis are available under the CC BY 4.0 (https://creativecommons.org/licenses/by/4.0/, last access: 6 July 2021) copyright policy (two additional sites in FLUXNET-CH_4 are available under the more restrictive Tier 2 data policy, https://fluxnet.org/data/data-policy/ (last access: 6 July 2021); these sites are not used in our analysis). The individual site DOIs are provided below in Table 2. All seasonality parameters used in these analyses are available at https://doi.org/10.5281/zenodo.4672601 (Delwiche et al., 2021).

5 Conclusions

The breadth and scope of CH_4 flux data in the FLUXNET-CH_4 dataset make it possible to study the global patterns of CH_4 fluxes, particularly for global freshwater wetlands which release a substantial fraction of atmospheric CH_4. To help data users understand seasonal patterns within the dataset, we provide the first global estimates of CH_4 flux patterns and predictors in CH_4 seasonality using freshwater wetland data. In the seasonality analysis, we find that, on average, the seasonal increase in CH_4 emissions begins about 3 months earlier and lasts about 4 months longer at the warmest sites compared with the coolest sites. We also find that the beginning of the CH_4 emission season lags behind the beginning of seasonal soil warming by approximately 1 month with almost no instances of CH_4 emissions increasing before temperature increases. Additionally, roughly half the sites have CH_4 emissions increasing prior to GPP increase, highlighting the importance of substrate versus temperature limitations on wetland CH_4 emissions. Furthermore, relative to warmer climates, wetland CH_4 emissions in cooler climates increase faster in the warming season and decrease slower in the cooling season. This phenomenon has previously been noted on a regional scale, and we show that it persists at the global scale. Constraining the seasonality of CH_4 fluxes on a global scale can help improve the accuracy of global wetland models.

FLUXNET-CH_4 is an important new resource for the research community, but critical data gaps and opportunities remain. The current FLUXNET-CH_4 dataset is biased towards sites in boreal and temperate regions, which influence the relationships presented in our analyses. Tropical ecosystems are estimated to account for 64 % of potential natural CH_4 emissions ($< 30°$ N; Saunois et al., 2020) but only account for 13 % of the FLUXNET-CH_4 sites in the dataset. Unsurprisingly, tropical sites in our network do not represent the range of bioclimatic wetland conditions present in the tropics. Therefore, while maintaining flux towers in tropical ecosystems is challenging, it is necessary to further constrain the global CH_4 cycle. Coastal wetlands are also poorly represented in FLUXNET-CH_4 even though there is evidence of substantial CH_4 emissions from these ecosystems, and so better representation across salinity gradients is warranted. Lastly, the average time series for FLUXNET-CH_4 Version 1.0 is relatively short, only 3.7 site years on average compared with 7.2 for CO_2 sites in FLUXNET (Pastorello et al., 2020). Adding additional site years of data from existing sites, as a complement to adding new sites, will increase the community's ability to explain interannual variability in CH_4 emissions and seasonality. Nevertheless, FLUXNET-CH_4 is an important and unprecedented resource with which to diagnose and understand drivers of the global CH_4 cycle.

Appendix A

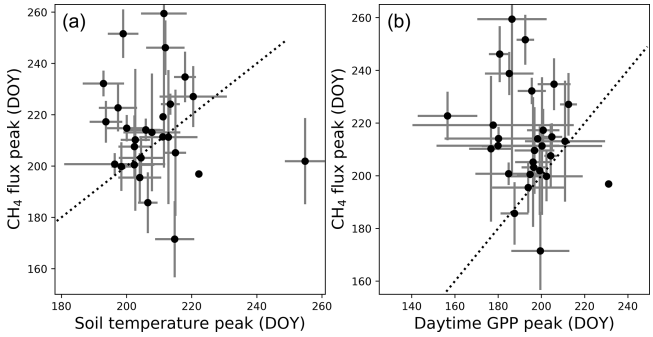


Figure A1. Peak methane (CH_4) flux timing versus peak gross primary productivity (GPP) timing **(a)** and peak soil temperature timing by day of year **(b)**. Points represent site average, and error bars represent standard deviations. Dotted line represents 1 : 1 relationship.

Appendix B: FLUXNET-CH_4 data variables

This web page describes data variables and file formatting for the FLUXNET-CH_4 Community Product.

B1 Data variable: base names

Base names indicate fundamental quantities that are either measured or calculated/derived. They can also indicate quantified quality information.

B2 Data variable: qualifiers

Qualifiers are suffixes appended to variable base names that provide additional information about the variable. For example, the _DT qualifier in the variable label GPP_DT indicates that gross primary production (GPP) has been partitioned using the flux partitioning method from Lasslop et al. (2010).

Multiple qualifiers can be added, and they must follow the order in which they are presented here.

B2.1 Qualifiers: general

General qualifiers indicate additional information about a variable.

- _F: variable has been gap-filled by the FLUXNET-CH_4 team. Gaps in meteorological variables, including air temperature (TA), incoming shortwave (SW_IN) and longwave (LW_IN) radiation, vapor pressure deficit (VPD), pressure (PA), precipitation (P), and wind speed (WS), were filled with ERA-Interim (ERA-I) reanalysis data (Vuichard and Papale, 2015). Other variables were filled using the multidimensional scaling (MDS) approach in REddyProc (see Delwiche et al., 2021, for more details).
- _DT: variable is acquired using the flux partitioning method from Lasslop et al. (2010), with values estimated by fitting the light-response curve.
- _NT: variable is acquired using the flux partitioning method from Reichstein et al. (2005), with values estimated from nighttime data and extrapolated to daytime.
- _RANDUNC: random uncertainty is introduced from several different sources including errors associated with the flux measurement system (gas analyzer, sonic anemometer, data acquisition system, flux calculations), errors associated with turbulent transport, and statistical errors relating to the location and activity of the sites of flux exchange ("footprint heterogeneity") (Hollinger and Richardson, 2005).
- _ANNOPTLM: gap-filled variable uses an artificial neural net routine from Matlab with the Levenberg–Marquardt algorithm as the training function and parameters optimized across runs (more detail in Knox et al., 2016, 2019).
- _UNC: uncertainty is introduced from ANNOPTLM gap-filling routine, as described in Knox et al. (2016, 2019).
- _QC: this reports quality checks on FCH4 gap-filled data (_ANNOPTLM) based on length of data gap: 1 signifies data gap shorter than 2 months, and 3 signifies data gap exceeding 2 months which could lead to poor-quality gap-filled data.

B2.2 Qualifiers: positional *(_V)*

Positional qualifiers are used to indicate relative positions of observations at the site. For FLUXNET-CH_4, positional qualifiers are used to distinguish soil temperature probes for sites with more than one probe. Probe depths for each positional qualifier per site are included in the metadata file included with data download and also in Table B7 of Delwiche et al. (2021). For sites where the original database file release in AmeriFlux, AsiaFlux, or EuroFlux contains multiple probes at the same _V depth, we average values and report only the average for each _V position. The one exception to this is site US-UAF where the original positional qualifier from the data we downloaded from AmeriFlux had different depths for the same qualifier. We still averaged the probe data, so _V qualifiers from US-UAF represent an average of more than one depth.

B3 Missing data

Missing data are reported using −9999. Data for all days in a leap year are reported.

Table B1. Data variable names, descriptions, and units.

Variable	Description	Units
TIMEKEEPING		
TIMESTAMP_START	ISO time stamp start of averaging period, used in half-hourly data	YYYYMMDDHHMM
TIMESTAMP_END	ISO time stamp end of averaging period, used in half-hourly data	YYYYMMDDHHMM
TIMESTAMP	ISO time stamp used in daily aggregation files	YYYYMMDD
MET_RAD		
SW_IN	Shortwave radiation, incoming	$W\,m^{-2}$
SW_OUT	Shortwave radiation, outgoing	$W\,m^{-2}$
LW_IN	Longwave radiation, incoming	$W\,m^{-2}$
LW_OUT	Longwave radiation, outgoing	$W\,m^{-2}$
PPFD_IN	Photosynthetic photon flux density, incoming	$\mu mol\,photon\,m^{-2}\,s^{-1}$
PPFD_OUT	Photosynthetic photon flux density, outgoing	$\mu mol\,photon\,m^{-2}\,s^{-1}$
NETRAD	Net radiation	$W\,m^{-2}$
MET_WIND		
USTAR	Friction velocity	$m\,s^{-1}$
WD	Wind direction	Decimal degrees
WS	Wind speed	$m\,s^{-1}$
HEAT		
H	Sensible heat turbulent flux (with storage term if provided by site principal investigator)	$W\,m^{-2}$
LE	Latent heat turbulent flux (with storage term if provided by site principal investigator)	$W\,m^{-2}$
G	Soil heat flux	$W\,m^{-2}$
MET_ATM		
PA	Atmospheric pressure	kPa
TA	Air temperature	°C
VPD	Vapor pressure deficit	hPa
RH	Relative humidity, range 0–100	%
MET_PRECIP		
P	Precipitation	mm
PRODUCTS		
NEE	Net ecosystem exchange	$\mu mol\,CO_2\,m^{-2}\,s^{-1}$
GPP	Gross primary productivity	$\mu mol\,CO_2\,m^{-2}\,s^{-1}$
RECO	Ecosystem respiration	$\mu mol\,CO_2\,m^{-2}\,s^{-1}$
GASES		
FCH4	Methane (CH_4) turbulent flux (no storage correction)	$nmol\,CH_4\,m^{-2}\,s^{-1}$
MET_SOIL		
TS	Soil temperature	°C
WTD	Water table depth (negative values indicate below the surface)	m

Table B2. Annual methane flux sum and uncertainty, annual mean soil temperature, and annual mean water table depth. Column headers are explained after the table.

	SITE_ID	Year	Ann_Flux_g_C_m−2	Ann_Flux_Uncertainty_g_C_m−2	Mean_Soil_Temp_C	Mean_Water_Table_Depth_m
1	AT-Neu	2010	0.38	0.03	8.65	NaN
2	AT-Neu	2011	0.25	0.02	8.61	NaN
3	AT-Neu	2012	NaN	NaN	9.39	NaN
4	BR-Npw	2013	NaN	NaN	NaN	NaN
5	BR-Npw	2014	NaN	NaN	25.95	NaN
6	BR-Npw	2015	20.95	1.18	26.2	−0.47
7	BR-Npw	2016	17.48	1.14	25.31	−0.41
8	BW-Gum	2018	51.73	10.59	NaN	NaN
9	BW-Nxr	2018	47.32	3.70	NaN	NaN
10	CA-SCB	2014	10.42	0.66	9.6	−0.15
11	CA-SCB	2015	NaN	NaN	5.58	−0.1
12	CA-SCB	2016	12.12	0.31	5.38	−0.15
13	CA-SCB	2017	9.48	0.27	6.32	−0.21
14	CA-SCC	2013	NaN	NaN	7.2	NaN
15	CA-SCC	2014	4.94	0.12	4.38	NaN
16	CA-SCC	2015	6.76	0.15	3.15	NaN
17	CA-SCC	2016	6.76	0.12	NaN	NaN
18	CH-Cha	2012	2.13	0.38	11.88	NaN
19	CH-Cha	2013	2.30	0.36	10.89	NaN
20	CH-Cha	2014	3.46	0.40	12.2	NaN
21	CH-Cha	2015	3.93	0.68	11.93	NaN
22	CH-Cha	2016	NaN	NaN	12.28	NaN
23	CH-Dav	2016	1.21	0.40	4.33	NaN
24	CH-Dav	2017	NaN	NaN	4.41	NaN
25	CH-Oe2	2018	0.29	0.13	12.32	NaN
26	CN-Hgu	2015	NaN	NaN	NaN	NaN
27	CN-Hgu	2016	0.81	0.16	7.26	NaN
28	CN-Hgu	2017	0.82	0.45	7.66	NaN
29	DE-Dgw	2015	NaN	NaN	NaN	NaN
30	DE-Dgw	2016	7.51	0.22	NaN	NaN
31	DE-Dgw	2017	10.42	0.16	NaN	NaN
32	DE-Dgw	2018	NaN	NaN	NaN	NaN
33	DE-Hte	2011	59.85	6.39	NaN	−0.41
34	DE-Hte	2012	36.83	3.46	NaN	−0.21
35	DE-Hte	2013	49.72	2.34	NaN	−0.25
36	DE-Hte	2014	NaN	NaN	13.26	−0.19
37	DE-Hte	2015	51.37	1.75	10.78	−0.26
38	DE-Hte	2016	50.77	2.09	9.8	−0.25
39	DE-Hte	2017	46.61	1.40	10.39	−0.4
40	DE-Hte	2018	41.62	2.52	6.12	−0.22
41	DE-SfN	2012	NaN	NaN	NaN	−0.08
42	DE-SfN	2013	3.62	0.93	10.32	−0.05
43	DE-SfN	2014	NaN	NaN	8.16	NaN
44	DE-Zrk	2013	NaN	NaN	13.03	NaN
45	DE-Zrk	2014	NaN	NaN	11.67	NaN
46	DE-Zrk	2015	30.76	1.00	10.85	NaN
47	DE-Zrk	2016	31.14	1.23	11.28	0.12
48	DE-Zrk	2017	29.10	0.87	10.84	0.31
49	DE-Zrk	2018	31.10	1.20	10.54	0.25
50	FI-Hyy	2016	NaN	NaN	5.41	NaN
51	FI-Lom	2006	13.77	0.76	4.47	0
52	FI-Lom	2007	17.22	0.25	4.33	0.04
53	FI-Lom	2008	15.52	0.22	3.79	0.06
54	FI-Lom	2009	17.63	0.27	3.98	0.02
55	FI-Lom	2010	13.78	0.29	3.71	0.03
56	FI-Si2	2012	9.27	1.17	9.4	0.06
57	FI-Si2	2013	10.22	1.17	10.47	0.13
58	FI-Si2	2014	NaN	NaN	7.7	0.1
59	FI-Si2	2015	NaN	NaN	8.18	0.09
60	FI-Si2	2016	NaN	NaN	7.67	0.09
61	FI-Sii	2013	14.58	0.32	6.45	0.04
62	FI-Sii	2014	12.93	0.78	6.42	0.03

Table B2. Continued.

	SITE_ID	Year	Ann_Flux_g_C_m−2	Ann_Flux_Uncertainty_g_C_m−2	Mean_Soil_Temp_C	Mean_Water_Table_Depth_m
63	FI-Sii	2015	NaN	NaN	6.92	−0.02
64	FI-Sii	2016	16.56	0.68	5.87	−0.01
65	FI-Sii	2017	8.63	0.23	8.4	0.06
66	FI-Sii	2018	9.46	1.10	6.68	0.11
67	FR-LGt	2017	NaN	NaN	10.45	−0.24
68	FR-LGt	2018	2.45	0.60	10.87	−0.22
69	HK-MPM	2016	11.62	0.61	25.06	−0.61
70	HK-MPM	2017	10.60	0.30	23.14	−0.64
71	HK-MPM	2018	11.04	0.59	NaN	−0.8
72	ID-Pag*	2016	0.09	0.07	NaN	NaN
73	ID-Pag*	2017	0.09	0.09	NaN	NaN
74	IT-BCi	2017	NaN	NaN	17.16	NaN
75	IT-BCi	2018	NaN	NaN	17.36	NaN
76	IT-Cas	2009	25.44	1.46	9.62	NaN
77	IT-Cas	2010	17.80	1.26	12.37	NaN
78	JP-BBY	2015	9.53	0.29	10.12	0
79	JP-BBY	2016	16.42	0.45	10.02	0
80	JP-BBY	2017	19.61	0.65	9.33	−0.03
81	JP-BBY	2018	NaN	NaN	9.79	−0.04
82	JP-Mse	2012	9.50	1.97	14.52	0.03
83	JP-SwL	2016	66.68	4.29	NaN	1.91
84	KR-CRK	2015	NaN	NaN	14.41	0.02
85	KR-CRK	2016	29.12	0.91	12.48	0.03
86	KR-CRK	2017	25.84	0.86	13.94	0.02
87	KR-CRK	2018	28.82	1.15	11.32	0.02
88	MY-MLM	2014	9.55	0.59	26.8	−0.09
89	MY-MLM	2015	NaN	NaN	26.9	−0.01
90	NL-Hor	2007	NaN	NaN	12.4	NaN
91	NL-Hor	2008	NaN	NaN	10.37	NaN
92	NL-Hor	2009	NaN	NaN	11.61	NaN
93	NK-Kop	2012	23.98	1.38	12.17	−0.08
94	NK-Kop	2013	15.33	0.43	12.68	−0.13
95	NK-Kop	2014	15.67	0.39	12.38	−0.11
96	NK-Kop	2015	14.37	2.66	12.46	−0.1
97	PH-RiF	2012	NaN	NaN	27.78	NaN
98	PH-RiF	2013	12.41	0.99	28.17	NaN
99	PH-RiF	2014	NaN	NaN	27.47	NaN
100	RU-Ch2	2014	6.99	0.14	−4.21	NaN
101	RU-Ch2	2015	5.86	0.14	−4.87	NaN
102	RU-Ch2	2016	NaN	NaN	−2.88	NaN
103	RU-Che	2014	3.84	0.14	−3.31	NaN
104	RU-Che	2015	4.19	0.22	−3.28	NaN
105	RU-Che	2016	4.24	0.19	−1.65	NaN
106	RU-Cok	2008	NaN	NaN	NaN	NaN
107	RU-Cok	2009	NaN	NaN	NaN	NaN
108	RU-Cok	2010	NaN	NaN	NaN	NaN
109	RU-Cok	2011	NaN	NaN	NaN	NaN
110	RU-Cok	2012	NaN	NaN	−0.46	NaN
111	RU-Cok	2013	NaN	NaN	−5.73	NaN
112	RU-Cok	2014	NaN	NaN	−4.82	NaN
113	RU-Cok	2015	4.45	0.15	−4.4	NaN
114	RU-Cok	2016	NaN	NaN	−11.1	NaN
115	RU-Fy2	2015	NaN	NaN	9.83	NaN
116	RU-Fy2	2016	2.69	0.59	6.88	0.68
117	RU-Fy2	2017	2.17	0.52	6.1	0.19
118	RU-Fy2	2018	5.66	1.37	6.48	0.79
119	SE-Deg	2014	11.24	1.98	5.02	−0.02
120	SE-Deg	2015	11.11	0.08	5.04	0.02
121	SE-Deg	2016	11.19	0.15	5.19	−0.01
122	SE-Deg	2017	NaN	NaN	4.19	0
123	SE-Deg	2018	9.42	0.09	5.49	−0.03
124	UK-LBT	2011	NaN	NaN	NaN	NaN
125	UK-LBT	2012	NaN	NaN	NaN	NaN

Table B2. Continued.

	SITE_ID	Year	Ann_Flux_g_C_m−2	Ann_Flux_Uncertainty_g_C_m−2	Mean_Soil_Temp_C	Mean_Water_Table_Depth_m
126	UK-LBT	2013	50.50	0.97	NaN	NaN
127	UK-LBT	2014	42.57	2.25	NaN	NaN
128	US-A03	2015	NaN	NaN	−6.65	NaN
129	US-A03	2016	NaN	NaN	−6.14	NaN
130	US-A03	2017	7.26	2.58	−4.48	NaN
131	US-A03	2018	4.35	0.62	−4.93	NaN
132	US-A10	2012	NaN	NaN	NaN	NaN
133	US-A10	2013	NaN	NaN	NaN	NaN
134	US-A10	2014	NaN	NaN	NaN	NaN
135	US-A10	2015	NaN	NaN	NaN	NaN
136	US-A10	2016	NaN	NaN	NaN	NaN
137	US-A10	2017	NaN	NaN	NaN	NaN
138	US-A10	2018	NaN	NaN	NaN	NaN
139	US-Atq	2013	NaN	NaN	−5.65	NaN
140	US-Atq	2014	1.80	0.19	−4.48	NaN
141	US-Atq	2015	1.75	0.11	−0.43	NaN
142	US-Atq	2016	1.75	0.00	NaN	NaN
143	US-Beo	2013	NaN	NaN	−2.67	NaN
144	US-Beo	2014	2.74	0.05	−4.95	NaN
145	US-Bes	2013	NaN	NaN	−6.01	NaN
146	US-Bes	2014	3.32	0.04	−5.69	NaN
147	US-Bes	2015	3.06	0.54	−6.24	NaN
148	US-Bi1	2016	NaN	NaN	15.62	NaN
149	US-Bi1	2017	NaN	NaN	17.17	NaN
150	US-Bi1	2018	0.69	0.29	16.82	NaN
151	US-Bi2	2017	0.86	0.20	20.42	NaN
152	US-Bi2	2018	1.69	0.29	17.12	NaN
153	US-BZB	2014	8.02	4.61	4.03	NaN
154	US-BZB	2015	7.52	0.82	3.9	NaN
155	US-BZB	2016	11.61	2.25	4.89	NaN
156	US-BZF	2014	6.61	0.63	4.32	NaN
157	US-BZF	2015	10.82	0.90	3.99	NaN
158	US-BZF	2016	NaN	NaN	5.93	NaN
159	US-BZS	2015	0.68	0.68	0.48	NaN
160	US-BZS	2016	0.89	0.27	0.67	NaN
161	US-CRT	2011	2.21	0.15	11.49	−0.92
162	US-CRT	2012	2.21	0.11	12.38	−1.45
163	US-DPW	2013	NaN	NaN	NaN	NaN
164	US-DPW	2014	58.91	0.69	NaN	NaN
165	US-DPW	2015	NaN	NaN	NaN	NaN
166	US-DPW	2016	43.60	1.29	NaN	NaN
167	US-DPW	2017	43.60	0.06	NaN	NaN
168	US-EDN	2018	−0.04	0.06	NaN	NaN
169	US-EML	2015	NaN	NaN	5.71	NaN
170	US-EML	2016	1.04	0.08	3.07	NaN
171	US-EML	2017	0.36	0.27	3.8	NaN
172	US-EML	2018	0.36	0.07	NaN	NaN
173	US-Ho1	2012	NaN	NaN	NaN	−0.43
174	US-Ho1	2013	−0.05	0.02	NaN	−0.33
175	US-Ho1	2014	−0.04	0.02	NaN	−0.38
176	US-Ho1	2015	−0.16	0.01	NaN	−0.48
177	US-Ho1	2016	−0.22	0.01	NaN	−0.57
178	US-Ho1	2017	−0.24	0.01	NaN	−0.56
179	US-Ho1	2018	−0.24	0.01	NaN	NaN
180	US-HRA	2017	−0.24	0.56	NaN	NaN
181	US-HRC	2017	−0.24	0.81	NaN	NaN
182	US-ICs	2014	NaN	NaN	−1.55	NaN
183	US-ICs	2015	NaN	NaN	−0.62	NaN
184	US-ICs	2016	NaN	NaN	−1.48	NaN
185	US-Ivo	2013	NaN	NaN	3.19	NaN
186	US-Ivo	2014	5.05	0.22	0.02	NaN
187	US-Ivo	2015	3.89	0.27	0.47	NaN

Table B2. Continued.

	SITE_ID	Year	Ann_Flux_g_C_m−2	Ann_Flux_Uncertainty_g_C_m−2	Mean_Soil_Temp_C	Mean_Water_Table_Depth_m
188	US-Ivo	2016	5.77	0.55	−1.01	NaN
189	US-LA1	2011	NaN	NaN	18.92	NaN
190	US-LA1	2012	12.68	0.63	24.23	NaN
191	US-LA2	2011	12.68	0.19	NaN	NaN
192	US-LA2	2012	48.42	1.57	23.09	NaN
193	US-LA2	2013	43.34	1.32	23.19	NaN
194	US-Los	2014	6.66	1.48	8.3	−0.06
195	US-Los	2015	5.51	0.40	5.65	−0.1
196	US-Los	2016	8.67	0.35	6.3	−0.07
197	US-Los	2017	6.00	0.33	5.5	−0.09
198	US-Los	2018	5.71	0.37	4.29	−0.19
199	US-MAC	2013	5.71	2.68	NaN	NaN
200	US-MAC	2014	26.37	1.69	23.18	−0.71
201	US-MAC	2015	15.40	0.85	23.29	−0.55
202	US-MRM	2012	0.30	0.19	11.16	NaN
203	US-MRM	2013	0.37	0.14	8.99	NaN
204	US-Myb	2010	NaN	NaN	NaN	0.95
205	US-Myb	2011	33.83	0.72	17.18	1.23
206	US-Myb	2012	64.20	0.58	16.25	1.12
207	US-Myb	2013	59.81	0.92	15.7	1.19
208	US-Myb	2014	58.97	0.68	11.27	1.24
209	US-Myb	2015	60.85	0.55	NaN	1.3
210	US-Myb	2016	45.72	0.48	NaN	1.22
211	US-Myb	2017	30.32	0.84	18.5	1.35
212	US-Myb	2018	29.33	0.55	17.05	1.19
213	US-NC4	2012	38.28	1.70	17.12	NaN
214	US-NC4	2013	18.60	3.88	NaN	NaN
215	US-NC4	2014	26.98	0.60	18.02	NaN
216	US-NC4	2015	23.37	2.30	16.27	NaN
217	US-NC4	2016	62.20	2.78	16.35	NaN
218	US-NGB	2012	NaN	NaN	NaN	NaN
219	US-NGB	2013	NaN	NaN	NaN	NaN
220	US-NGB	2014	NaN	NaN	NaN	NaN
221	US-NGB	2015	NaN	NaN	NaN	NaN
222	US-NGB	2016	NaN	NaN	NaN	NaN
223	US-NGB	2017	2.31	0.11	NaN	NaN
224	US-NGB	2018	2.52	0.22	NaN	NaN
225	US-NGC	2017	2.52	0.06	NaN	NaN
226	US-NGC	2018	2.52	0.05	NaN	NaN
227	US-ORv	2011	3.53	0.54	16.64	NaN
228	US-ORv	2012	9.11	0.45	14.23	NaN
229	US-ORv	2013	7.70	0.41	13.19	NaN
230	US-ORv	2014	8.46	0.26	12	NaN
231	US-ORv	2015	NaN	NaN	13.36	NaN
232	US-OWC	2015	NaN	NaN	22.11	0.9
233	US-OWC	2016	113.99	3.25	21.19	0.54
234	US-PFa	2010	NaN	NaN	NaN	NaN
235	US-PFa	2011	0.34	0.05	NaN	NaN
236	US-PFa	2012	0.30	0.04	NaN	NaN
237	US-PFa	2013	0.31	0.05	NaN	NaN
238	US-PFa	2014	NaN	NaN	NaN	NaN
239	US-PFa	2015	0.63	0.03	NaN	NaN
240	US-PFa	2016	0.85	0.02	NaN	NaN
241	US-PFa	2017	0.80	0.06	NaN	NaN
242	US-PFa	2018	NaN	NaN	NaN	NaN
243	US-Snd	2010	NaN	NaN	16.85	NaN
244	US-Snd	2011	NaN	NaN	14.96	NaN
245	US-Snd	2012	6.34	0.25	16.06	NaN
246	US-Snd	2013	6.04	0.48	16.59	−0.65
247	US-Snd	2014	3.23	0.36	17.52	−0.78
248	US-Snd	2015	3.23	0.21	NaN	NaN
249	US-Sne	2016	NaN	NaN	17.85	−0.2

Table B2. Continued.

	SITE_ID	Year	Ann_Flux_g_C_m−2	Ann_Flux_Uncertainty_g_C_m−2	Mean_Soil_Temp_C	Mean_Water_Table_Depth_m
250	US-Sne	2017	45.96	0.40	17.05	0.16
251	US-Sne	2018	39.63	0.66	16.83	0.09
252	US-Srr	2014	0.71	0.10	NaN	NaN
253	US-Srr	2015	0.88	0.11	NaN	NaN
254	US-Srr	2016	0.86	0.10	16.3	−0.18
255	US-Srr	2017	0.86	0.11	NaN	NaN
256	US-StJ	2016	9.55	1.04	11.66	−0.26
257	US-Tw1	2011	26.09	2.70	14.01	NaN
258	US-Tw1	2012	NaN	NaN	11.58	0.24
259	US-Tw1	2013	33.93	1.78	11.92	0.25
260	US-Tw1	2014	49.60	1.67	13.14	0.25
261	US-Tw1	2015	54.80	2.58	12.79	0.33
262	US-Tw1	2016	45.93	1.90	12.91	0.41
263	US-Tw1	2017	38.66	2.09	12.53	0.38
264	US-Tw1	2018	27.60	1.64	12.1	0.24
265	US-Tw3	2013	NaN	NaN	19.63	NaN
266	US-Tw3	2014	NaN	NaN	17.91	NaN
267	US-Tw4	2013	NaN	NaN	NaN	NaN
268	US-Tw4	2014	16.26	0.39	NaN	0.48
269	US-Tw4	2015	27.61	0.43	17.2	0.36
270	US-Tw4	2016	33.49	0.37	14.8	0.18
271	US-Tw4	2017	47.95	0.58	13.78	0.07
272	US-Tw4	2018	37.41	0.48	13.02	0.08
273	US-Tw5	2018	59.72	1.15	16.67	0.69
274	US-Twt	2009	NaN	NaN	17.66	−0.01
275	US-Twt	2010	9.87	1.15	15.67	−0.18
276	US-Twt	2011	12.32	4.92	14.95	−0.11
277	US-Twt	2012	8.12	0.51	16.05	−0.04
278	US-Twt	2013	12.64	0.48	15.98	−0.11
279	US-Twt	2014	17.02	0.97	17.44	−0.09
280	US-Twt	2015	14.43	0.38	17.04	−0.14
281	US-Twt	2016	11.07	0.59	16.44	−0.29
282	US-Twt	2017	11.07	0.31	NaN	NaN
283	US-Uaf	2011	0.32	0.04	−2.14	−0.17
284	US-Uaf	2012	NaN	NaN	−2.43	−0.18
285	US-Uaf	2013	NaN	NaN	−1.15	−0.18
286	US-Uaf	2014	NaN	NaN	−1.18	−0.13
287	US-Uaf	2015	NaN	NaN	−0.49	−0.12
288	US-Uaf	2016	0.68	0.05	−0.05	−0.1
289	US-Uaf	2017	0.58	0.06	1.09	−0.13
290	US-Uaf	2018	NaN	NaN	0.87	−0.13
291	US-WPT	2011	41.05	1.57	17.22	0.43
292	US-WPT	2012	54.96	1.71	14.27	0.28
293	US-WPT	2013	52.76	1.29	12.89	0.44

* Data from ID-Pag spans 365 d from June 2016 to June 2017. Annual methane flux for each year is the sum of these 365 d, with uncertainty being calculated separately for each year.

Column	Description
SITE_ID	Site identification code as assigned by regional flux data network
Year	Data year
Ann_Flux_g_C_m−2	Total annual methane flux ($g\,C\,m^{-2}$)
Ann_Flux_Uncertainty_g_C_m−2	Gap-filling and random uncertainty associated with annual flux ($g\,C\,m^{-2}$)
Mean_Soil_Temp_C	Annual mean soil temperature (degree C). For sites with multiple probes, we use the probe closest to the surface.
Mean_Water_Table_Depth_m	Annual mean water table depth (m)

Table B3. Metadata and select data for FLUXNET-CH_4 sites.

(a)	SITE _ID	SITE _NAME	SITE _PERSONNEL	COUNTRY	LAT	LON	DATA _DOI	YEAR _START	YEAR _END	UTC _OFFSET	ORIGINAL_DATA _SOURCE
1	AT-Neu	Neustift	Georg Wohlfahrt	Austria	47.117	11.318	https://doi.org/10.18140/FLX/1669365	2010	2012	1	EuroFlux
2	BR-Npw	Northern Pantanal Wetland	George Vourlitis	Brazil	−16.498	−56.412	https://doi.org/10.18140/FLX/1669368	2013	2016	−4	AmeriFlux
3	BW-Gum	Guma	Carole Helfter	Botswana	−18.965	22.371	https://doi.org/10.18140/FLX/1669370	2018	2018	2	EuroFlux
4	BW-Nxr	Nxaraga	Carole Helfter	Botswana	−19.548	23.179	https://doi.org/10.18140/FLX/1669518	2018	2018	2	EuroFlux
5	CA-SCB	Scotty Creek Bog	Oliver Sonnentag, Manuel Helbig	Canada	61.309	−121.298	https://doi.org/10.18140/FLX/1669613	2014	2017	−7	AmeriFlux
6	CA-SCC	Scotty Creek Landscape	Oliver Sonnentag, Manuel Helbig	Canada	61.308	−121.299	https://doi.org/10.18140/FLX/1669628	2013	2016	−7	AmeriFlux
7	CH−Cha	Chamau	Nina Buchmann	Switzerland	47.210	8.410	https://doi.org/10.18140/FLX/1669629	2012	2016	1	EuroFlux
8	CH−Dav	Davos	Nina Buchmann	Switzerland	46.815	9.856	https://doi.org/10.18140/FLX/1669630	2016	2017	1	EuroFlux
9	CH−Oe2	Oensingen crop	Nina Buchmann	Switzerland	47.286	7.734	https://doi.org/10.18140/FLX/1669631	2018	2018	1	EuroFlux
10	CN-Hgu	Hongyuan	Shuli Niu, Weinan Chen	China	32.845	102.590	https://doi.org/10.18140/FLX/1669632	2015	2017	8	EuroFlux
11	DE-Dgw	Dagowsee	Torsten Sachs	Germany	53.151	13.054	https://doi.org/10.18140/FLX/1669633	2015	2018	1	EuroFlux
12	DE-Hte	Huetelmoor	Gerald Jurasinski	Germany	54.210	12.176	https://doi.org/10.18140/FLX/1669634	2011	2018	1	EuroFlux
13	DE-SfN	Schechenfilz Nord	Hans Peter Schmid	Germany	47.806	11.328	https://doi.org/10.18140/FLX/1669635	2012	2014	1	EuroFlux
14	DE-Zrk	Zarnekow	Torsten Sachs	Germany	53.876	12.889	https://doi.org/10.18140/FLX/1669636	2013	2018	1	EuroFlux
15	FI-Hyy	Hyytiala	Timo Vesala, Ivan Mammarella	Finland	61.847	24.295	https://doi.org/10.18140/FLX/1669637	2016	2016	2	EuroFlux
16	FI-Lom	Lompolojankka	Annalea Lohila	Finland	67.997	24.209	https://doi.org/10.18140/FLX/1669638	2006	2010	2	EuroFlux
17	FI-Si2	Siikaneva−2 Bog	Timo Vesala, Ivan Mammarella, Eeva-Stiina Tuittila	Finland	61.837	24.197	https://doi.org/10.18140/FLX/1669639	2012	2016	2	EuroFlux
18	FI-Sii	Siikaneva	Timo Vesala, Ivan Mammarella, Eeva-Stiina Tuittila	Finland	61.833	24.193	https://doi.org/10.18140/FLX/1669640	2013	2018	2	EuroFlux
19	FR-LGt	La Guette	Adrien Jacotot, Sébastien Gogo, Fatima Laggoun-Défarge, Laurent Perdereau	France	47.323	2.284	https://doi.org/10.18140/FLX/1669641	2017	2018	1	EuroFlux
20	HK-MPM	Mai Po Mangrove	Derrick Lai, Jiangong Liu	Hong Kong	22.498	114.029	https://doi.org/10.18140/FLX/1669642	2016	2018	8	EuroFlux
21	ID-Pag	Palangkaraya undrained forest	Takashi Hirano	Indonesia	−2.320	113.900	https://doi.org/10.18140/FLX/1669643	2016	2017	7	EuroFlux
22	IT-BCi	Borgo Cioffi	Vincenzo Magliulo	Italy	40.524	14.957	https://doi.org/10.18140/FLX/1669644	2017	2018	1	EuroFlux
23	IT-Cas	Castellaro	Giovanni Manca, Ignacio Goded, Carsten Gruening, Ana Meijide	Italy	45.070	8.718	https://doi.org/10.18140/FLX/1669645	2009	2010	1	EuroFlux
24	JP-BBY	Bibai bog	Masahito Ueyama	Japan	43.323	141.811	https://doi.org/10.18140/FLX/1669646	2015	2018	9	AsiaFlux
25	JP-Mse	Mase rice paddy field	Akira Miyata	Japan	36.054	140.027	https://doi.org/10.18140/FLX/1669647	2012	2012	9	AsiaFlux
26	JP-SwL	Suwa Lake	Hiroki Iwata	Japan	36.047	138.108	https://doi.org/10.18140/FLX/1669648	2016	2016	9	AsiaFlux
27	KR-CRK	Cheorwon Rice paddy	Youngryel Ryu, Minseok Kang	Korea	38.201	127.251	https://doi.org/10.18140/FLX/1669649	2015	2018	9	AsiaFlux
28	MY-MLM	Maludam National Park	Angela C. I. Tang, Guan Xhuan Wong, Lulie Melling	Malaysia	1.454	111.149	https://doi.org/10.18140/FLX/1669650	2014	2015	8	AsiaFlux
29	NL-Hor	Horstermeer	Han Dolman	Netherlands	52.240	5.071	https://doi.org/10.18140/FLX/1669651	2007	2009	1	EuroFlux
30	NZ-Kop	Kopuatai	Dave Campbell	New Zealand	−37.388	175.554	https://doi.org/10.18140/FLX/1669652	2012	2015	13	OzFlux
31	PH-RiF	Philippines Rice Institute flooded	Ma. Carmelita Alberto	Philippines	14.141	121.265	https://doi.org/10.18140/FLX/1669653	2012	2014	8	EuroFlux
32	RU-Ch2	Chersky reference	Matthias Goeckede	Russia	68.617	161.351	https://doi.org/10.18140/FLX/1669654	2014	2016	11	EuroFlux
33	RU-Che	Cherski	Matthias Goeckede	Russia	68.613	161.341	https://doi.org/10.18140/FLX/1669655	2014	2016	11	EuroFlux
34	RU-Cok	Chokurdakh	Han Dolman	Russia	70.829	147.494	https://doi.org/10.18140/FLX/1669656	2008	2016	11	EuroFlux
35	RU-Fy2	Fyodorovskoye dry spruce	Andrej Varlagin	Russia	56.448	32.902	https://doi.org/10.18140/FLX/1669657	2015	2018	3	EuroFlux
36	SE-Deg	Degero	Matthias Peichl, Mats Nilsson	Sweden	64.182	19.557	https://doi.org/10.18140/FLX/1669659	2014	2018	1	EuroFlux
37	UK-LBT	London_BT	Carole Helfter	UK	51.522	−0.139	https://doi.org/10.18140/FLX/1670207	2011	2014	0	EuroFlux
38	US-A03	ARM−AMF3−Oliktok	Ryan Sullivan, David Cook, David Billesbach	USA	70.495	−149.882	https://doi.org/10.18140/FLX/1669661	2015	2018	−9	AmeriFlux
39	US-A10	ARM−NSA−Barrow	Ryan Sullivan, David Cook, David Billesbach	USA	71.324	−156.615	https://doi.org/10.18140/FLX/1669662	2012	2018	−9	AmeriFlux
40	US-Atq	Atqasuk	Donatella Zona	USA	70.470	−157.409	https://doi.org/10.18140/FLX/1669663	2013	2016	−9	AmeriFlux
41	US-Beo	Barrow Environmental Observatory (BEO) tower	Donatella Zona	USA	71.281	−156.612	https://doi.org/10.18140/FLX/1669664	2013	2014	−8	AmeriFlux
42	US-Bes	Barrow-Bes (Biocomplexity Experiment South tower)	Donatella Zona	USA	71.281	−156.597	https://doi.org/10.18140/FLX/1669665	2013	2015	−8	AmeriFlux
43	US-Bi1	Bouldin Island Alfalfa	Dennis Baldocchi	USA	38.099	−121.499	https://doi.org/10.18140/FLX/1669666	2016	2018	−8	AmeriFlux
44	US-Bi2	Bouldin Island corn	Dennis Baldocchi	USA	38.109	−121.535	https://doi.org/10.18140/FLX/1669667	2017	2018	−8	AmeriFlux
45	US-BZB	Bonanza Creek Thermokarst Bog	Eugenie Euskirchen	USA	64.696	−148.321	https://doi.org/10.18140/FLX/1669668	2014	2016	−9	AmeriFlux
46	US-BZF	Bonanza Creek Rich Fen	Eugenie Euskirchen	USA	64.704	−148.313	https://doi.org/10.18140/FLX/1669669	2014	2016	−9	AmeriFlux
47	US-BZS	Bonanza Creek Black Spruce	Eugenie Euskirchen	USA	64.696	−148.324	https://doi.org/10.18140/FLX/1669670	2015	2016	−9	AmeriFlux
48	US-CRT	Curtice Walter−Berger cropland	Jiquen Chen, Housen Chu	USA	41.628	−83.347	https://doi.org/10.18140/FLX/1669671	2011	2012	−5	AmeriFlux
49	US-DPW	Disney Wilderness Preserve Wetland	Charles Ross Hinkle, Rosvel Bracho, Scott Graham, Brian Benscoter	USA	28.052	−81.436	https://doi.org/10.18140/FLX/1669672	2013	2017	−5	AmeriFlux

Table B3. Continued.

	SITE _ID	SITE _NAME	SITE _PERSONNEL	COUNTRY	LAT	LON	DATA _DOI	YEAR _START	YEAR _END	UTC _OFFSET	ORIGINAL_DATA _SOURCE
50	US-EDN	Eden Landing Ecological Reserve	Patty Oikawa	USA	37.616	−122.114	https://doi.org/10.18140/FLX/1669673	2018	2018	−8	AmeriFlux
51	US-EML	Eight Mile Lake Permafrost thaw gradient, Healy Alaska	Ted Schuur	USA	63.878	−149.254	https://doi.org/10.18140/FLX/1669674	2015	2018	−9	AmeriFlux
52	US-Ho1	Howland Forest (main tower)	Andrew Richardson, David Hollinger	USA	45.204	−68.740	https://doi.org/10.18140/FLX/1669675	2012	2018	−5	AmeriFlux
53	US-HRA	Humnoke Farm Rice Field – Field A	Benjamin Runkle	USA	34.585	−91.752	https://doi.org/10.18140/FLX/1669676	2017	2017	−6	AmeriFlux
54	US-HRC	Humnoke Farm Rice Field – Field C	Benjamin Runkle	USA	34.589	−91.752	https://doi.org/10.18140/FLX/1669677	2017	2017	−6	AmeriFlux
55	US-ICs	Imnavait Creek Watershed Wet Sedge Tundra	Eugenie Euskirchen	USA	68.606	−149.311	https://doi.org/10.18140/FLX/1669678	2014	2016	−9	AmeriFlux
56	US-Ivo	Ivotuk	Donatella Zona	USA	68.487	−155.750	https://doi.org/10.18140/FLX/1669679	2013	2016	−9	AmeriFlux
57	US-LA1	Pointe-aux-Chenes Brackish Marsh	Ken Krauss	USA	29.501	−90.445	https://doi.org/10.18140/FLX/1669680	2011	2012	−6	AmeriFlux
58	US-LA2	Salvador WMA Freshwater Marsh	Ken Krauss	USA	29.859	−90.287	https://doi.org/10.18140/FLX/1669681	2011	2013	−6	AmeriFlux
59	US-Los	Lost Creek	Ankur Desai	USA	46.083	−89.979	https://doi.org/10.18140/FLX/1669682	2014	2018	−6	AmeriFlux
60	US-MAC	MacArthur Agro-Ecology	Jed Sparks, Sam Chamberlain	USA	27.163	−81.187	https://doi.org/10.18140/FLX/1669683	2013	2015	−5	AmeriFlux
61	US-MRM	Marsh Resource Meadowlands Mitigation Bank	Karina Schäfer	USA	40.816	−74.044	https://doi.org/10.18140/FLX/1669684	2012	2013	5	AmeriFlux
62	US-Myb	Mayberry Wetland	Dennis Baldocchi	USA	38.050	−121.765	https://doi.org/10.18140/FLX/1669685	2010	2018	−8	AmeriFlux
63	US-NC4	NC_AlligatorRiver	Asko Noormets	USA	35.788	−75.904	https://doi.org/10.18140/FLX/1669686	2012	2016	−5	AmeriFlux
64	US-NGB	NGEE Arctic Barrow	Margaret Torn	USA	71.280	−156.609	https://doi.org/10.18140/FLX/1669687	2012	2018	−9	AmeriFlux
65	US-NGC	NGEE Arctic Council	Margaret Torn	USA	64.861	−163.701	https://doi.org/10.18140/FLX/1669688	2017	2018	−9	AmeriFlux
66	US-ORv	Olentangy River Wetland Research Park	Gil Bohrer	USA	40.020	−83.018	https://doi.org/10.18140/FLX/1669689	2011	2015	−5	AmeriFlux
67	US-OWC	Old Woman Creek	Gil Bohrer	USA	41.380	−82.512	https://doi.org/10.18140/FLX/1669690	2015	2016	−5	AmeriFlux
68	US-PFa	Park Falls/WLEF	Ankur Desai	USA	45.946	−90.272	https://doi.org/10.18140/FLX/1669691	2010	2018	−6	AmeriFlux
69	US-Snd	Sherman Island	Dennis Baldocchi	USA	38.037	−121.754	https://doi.org/10.18140/FLX/1669692	2010	2015	−8	Ameriflux
70	US-Sne	Sherman Island Restored Wetland	Dennis Baldocchi	USA	38.037	−121.755	https://doi.org/10.18140/FLX/1669693	2016	2018	−8	AmeriFlux
71	US-Srr	Suisun marsh – Rush Ranch	Lisamarie Windham-Myers	USA	38.201	−122.026	https://doi.org/10.18140/FLX/1669694	2014	2017	−8	AmeriFlux
72	US-StJ	St Jones Reserve	Rodrigo Vargas	USA	39.088	−75.437	https://doi.org/10.18140/FLX/1669695	2016	2016	−5	AmeriFlux
73	US-Tw1	Twitchell Wetland West Pond	Dennis Baldocchi	USA	38.107	−121.647	https://doi.org/10.18140/FLX/1669696	2011	2018	−8	AmeriFlux
74	US-Tw3	Twitchell Alfalfa	Dennis Baldocchi	USA	38.116	−121.647	https://doi.org/10.18140/FLX/1669697	2013	2014	−8	AmeriFlux
75	US-Tw4	Twitchell East End Wetland	Dennis Baldocchi	USA	38.103	−121.641	https://doi.org/10.18140/FLX/1669698	2013	2018	−8	AmeriFlux
76	US-Tw5	East Pond Wetland	Dennis Baldocchi	USA	38.107	−121.643	https://doi.org/10.18140/FLX/1669699	2018	2018	−8	AmeriFlux
77	US-Twt	Twitchell Island	Dennis Baldocchi	USA	38.109	−121.653	https://doi.org/10.18140/FLX/1669700	2009	2017	−8	AmeriFlux
78	US-Uaf	University of Alaska, Fairbanks	Masahito Ueyama	USA	64.866	−147.856	https://doi.org/10.18140/FLX/1669701	2011	2018	−9	AmeriFlux
79	US-WPT	Winous Point North Marsh	Jiquen Chen, Housen Chu	USA	41.465	−82.996	https://doi.org/10.18140/FLX/1669702	2011	2013	−5	AmeriFlux

https://doi.org/10.5194/essd-13-3607-2021

Table B3. Continued.

(b)	SITE _ID	SITE _CLASSIFICATION	UPLAND _CLASS	IGBP	KOP−PEN	MEAN_ANNUAL_TEMP _C_WORLDCLIM	MEAN_ANNUAL_PRECIP _MM_WORLDCLIM	MOSS _BROWN	MOSS _SPHAGNUM	AERENCHYMATOUS	ERI _SHRUB	TREE	DOM _VEG	IN_SEASONALITY _ANALYSIS
1	AT-Neu	Upland	Alpine meadow	GRA	Dfb	7.0	1029	0	0	1	0	0	aerenchymatous	0
2	BR-Npw	Swamp		WSA	Aw	25.2	1318	0	0	1	0	1	tree	0
3	BW-Gum	Swamp		WET	Bsh	23.1	459	0	0	1	0	1	aerenchymatous	0
4	BW-Nxr	Swamp		GRA	Bsh	23.5	433	0	0	1	0	1	aerenchymatous	0
5	CA-SCB	Bog		WET	Dfc	−2.8	414	0	1	1	1	0	moss_sphagnum	1
6	CA-SCC	Upland	Needleleaf forest	ENF	Dfc	−2.9	414	0	1	0	1	1	tree	0
7	CH−Cha	Upland	Grassland	GRA	Cfb	9.6	1194	0	0	1	0	0	aerenchymatous	0
8	CH−Dav	Upland	Needleleaf forest	ENF	ET	3.8	1053	1	0	0	1	1	tree	0
9	CH−Oe2	Upland	Crop − wheat	CRO	Cfb	9.1	1122	0	0	1	0	0	aerenchymatous	0
10	CN-Hgu	Upland	Alpine meadow	GRA	Cwc	2.8	702	0	0	1	0	0	aerenchymatous	0
11	DE-Dgw	Lake		WAT	Cfb	8.3	567	0	0	0	0	0	no vegetation	0
12	DE-Hte	Fen		WET	Dfb	8.5	584	0	0	1	0	0	aerenchymatous	1
13	DE-SfN	Bog		WET	Cfb	8.3	1123	0	1	1	1	1	tree	1
14	DE-Zrk	Fen		WET	Dfb	8.3	580	0	0	1	0	0	aerenchymatous	1
15	FI-Hyy	Upland	Needleleaf forest	ENF	Dfc	3.1	671	1	1	0	1	1	tree	0
16	FI-Lom	Fen		WET	Dfc	−1.0	512	1	1	1	1	0	aerenchymatous	1
17	FI-Si2	Bog		WET	Dfc	3.2	664	0	1	1	1	1	moss_sphagnum	1
18	FI-Sii	Fen		WET	Dfc	3.2	666	0	1	1	0	0	moss_sphagnum	1
19	FR-LGt	Fen		WET	Cfb	11.0	707	0	1	1	1	0	aerenchymatous	0
20	HK-MPM	Mangrove		EBF	Cfa	22.7	1991	0	0	1	0	1	aerenchymatous	0
21	ID-Pag	Swamp		EBF	Af	27.4	2386	0	0	1	0	1	tree	0
22	IT-BCi	Upland	Crop − corn	CRO	Csa	16.3	1035	0	0	1	0	0	aerenchymatous	0
23	IT-Cas	Rice		CRO	Cfa	12.3	773	0	0	1	0	0	aerenchymatous	0
24	JP-BBY	Bog		WET	Dfb	6.7	1153	0	1	1	1	0	aerenchymatous	1
25	JP-Mse	Rice		CRO	Cfa	14.1	1305	0	0	1	0	0	aerenchymatous	0
26	JP-SwL	Lake		WAT	Dfb	10.2	1141	0	0	1	0	0	aerenchymatous	0
27	KR-CRK	Rice		CRO	Dwa	9.9	1234	0	0	1	0	0	aerenchymatous	0
28	MY-MLM	Swamp		EBF	Af	26.9	3401	0	0	0	0	1	tree	0
29	NL-Hor	Drained	Grassland	GRA	Cfb	9.7	827	0	0	1	0	0	aerenchymatous	0
30	NZ-Kop	Bog		EBF	Cfb	13.9	1343	0	1	1	0	0	aerenchymatous	1
31	PH-RiF	Rice		CRO	Am	26.9	2010	0	0	1	0	0	aerenchymatous	0
32	RU-Ch2	Wet tundra		WET	Dfc	−12.3	172	0	0	1	1	0	aerenchymatous	1
33	RU-Che	Drained		WET	Dfc	−12.3	172	0	0	1	1	0	aerenchymatous	0
34	RU-Cok	Wet tundra		OSH	Dfc	−14.1	210	0	1	1	1	0	moss_sphagnum	0
35	RU-Fy2	Upland	Needleleaf forest	ENF	Dfb	4.3	694	0	1	0	1	1	tree	0
36	SE-Deg	Fen		GRA	Dfc	1.7	620	0	1	1	1	0	moss_sphagnum	1
37	UK-LBT	Upland	Urban	URB	Cfb	11.0	646	0	0	0	0	0	no vegetation	0
38	US-A03	Wet tundra		BSV	ET	−11.9	144	0	1	1	0	0	moss_sphagnum	0
39	US-A10	Wet tundra		BSV	ET	−12.0	107	0	1	1	0	0	moss_sphagnum	0
40	US-Atq	Wet tundra		WET	ET	−10.3	133	1	0	1	1	0	aerenchymatous	1
41	US-Beo	Wet tundra		WET	ET	−11.9	109	1	1	1	0	0	aerenchymatous	1
42	US-Bes	Wet tundra		WET	ET	−12.0	109	0	1	1	0	0	aerenchymatous	1
43	US-Bi1	Drained	Crop − alfalfa	CRO	Csa	15.5	382	0	0	1	0	0	aerenchymatous	0
44	US-Bi2	Drained	Crop − corn	CRO	Csa	15.5	380	0	0	1	0	0	aerenchymatous	0
45	US-BZB	Bog		WET	Dfd	−2.4	292	0	1	1	1	0	eri_shrub	1
46	US-BZF	Fen		WET	Dfd	−2.5	294	1	1	1	0	0	aerenchymatous	1
47	US-BZS	Upland	Needleleaf forest	ENF	Dfd	−2.4	292	1	0	0	0	1	tree	0
48	US-CRT	Upland	Crop − soy	CRO	Dfa	9.7	855	0	0	1	0	0	aerenchymatous	0
49	US-DPW	Marsh		WET	Cwa	22.1	1223	0	0	1	0	0	aerenchymatous	1
50	US-EDN	Salt marsh		WET	Csa	14.9	403	0	0	1	0	0	aerenchymatous	0

Table B3. Continued.

	SITE _ID	SITE _CLASSIFICATION	UPLAND _CLASS	IGBP	KOP-PEN	MEAN_ANNUAL_TEMP _C_WORLDCLIM	MEAN_ANNUAL_PRECIP _MM_WORLDCLIM	MOSS _BROWN	MOSS _SPHAGNUM	AERENCHYMATOUS	ERI _SHRUB	TREE	DOM _VEG	IN_SEASONALITY _ANALYSIS
51	US-EML	Upland	Tundra	OSH	ET	−3.3	421	1	0	1	1	0	aerenchymatous	0
52	US-Ho1	Upland	Needleleaf forest	ENF	Dfb	5.7	1069	0	0	0	0	1	tree	0
53	US-HRA	Rice		CRO	Cfa	16.8	1290	0	0	1	0	0	aerenchymatous	0
54	US-HRC	Rice		CRO	Cfa	16.8	1290	0	0	1	0	0	aerenchymatous	0
55	US-ICs	Wet tundra		WET	ET	−8.9	242	0	0	1	1	0	aerenchymatous	1
56	US-Ivo	Wet tundra		WET	ET	−8.5	247	1	0	1	1	0	aerenchymatous	1
57	US-LA1	Salt marsh		WET	Cfa	20.4	1596	0	0	1	0	0	aerenchymatous	0
58	US-LA2	Marsh		WET	Cfa	20.0	1616	0	0	1	0	0	aerenchymatous	1
59	US-Los	Fen		WET	Dfb	4.1	833	0	0	1	1	1	eri_shrub	1
60	US-MAC	Drained	Grassland	WET	Cwa	22.7	1207	0	0	1	0	0	aerenchymatous	0
61	US-MRM	Salt marsh		WET	Cfa	12.0	1211	0	0	1	0	0	aerenchymatous	0
62	US-Myb	Marsh		WET	Csa	15.4	346	0	0	1	0	0	aerenchymatous	1
63	US-NC4	Swamp		WET	Cfa	16.5	1322	0	0	1	0	1	aerenchymatous	1
64	US-NGB	Wet tundra		SNO	ET	−11.9	109	0	1	1	0	0	moss_sphagnum	0
65	US-NGC	Wet tundra		GRA	ET	−3.1	413	0	1	1	1	0	eri_shrub	0
66	US-ORv	Marsh		WET	Cfa	11.0	954	0	0	1	0	0	aerenchymatous	1
67	US-OWC	Marsh		WET	Dfb	9.9	898	0	0	1	0	0	aerenchymatous	1
68	US-PFa	Upland	Mixed forest	MF	Dfb	4.3	826	0	0	0	0	1	tree	0
69	US-Snd	Drained	Grassland	GRA	Csa	15.5	340	0	0	1	0	0	aerenchymatous	0
70	US-Sne	Marsh		GRA	Csa	15.5	340	0	0	1	0	0	aerenchymatous	1
71	US-Srr	Salt marsh		WET	Csa	15.4	541	0	0	1	0	0	aerenchymatous	0
72	US-StJ	Salt marsh		WET	Cfa	13.0	1133	0	0	1	0	0	aerenchymatous	0
73	US-Tw1	Marsh		WET	Csa	15.4	371	0	0	1	0	0	aerenchymatous	1
74	US-Tw3	Drained	Crop − alfalfa	CRO	Csa	15.4	371	0	0	1	0	0	aerenchymatous	0
75	US-Tw4	Marsh		WET	Csa	15.4	370	0	0	1	0	0	aerenchymatous	1
76	US-Tw5	Marsh		WET	Csa	15.4	371	0	0	1	0	0	aerenchymatous	1
77	US-Twt	Rice		CRO	Csa	15.3	372	0	0	1	0	0	aerenchymatous	0
78	US-Uaf	Bog		ENF	Dwc	−2.8	298	1	1	1	1	1	moss_sphagnum	1
79	US-WPT	Marsh		WET	Dfa	9.9	881	0	0	1	0	0	aerenchymatous	1

https://doi.org/10.5194/essd-13-3607-2021

Table B3. Continued.

(c)	SITE_ID _ID	Mean_Air _Temp_C	Mean_Air _Temp_stdev_C	Ann_Flux_g _CH4−C_m−2	Ann_Flux_stdev _g_CH4−C_m−2	JFM_flux_g _CH4−C_m−2	JFM_flux_stdev _g_CH4−C_m−2	AMJ_flux_g _CH4−C_m−2	AMJ_flux_stdev _g_CH4−C_m−2	JAS_flux_g _CH4−C_m−2	JAS_flux_stdev _g_CH4−C_m−2	OND_flux_g _CH4−C_m−2	OND_flux_stdev _g_CH4−C_m−2
1	AT-Neu	6.60	0.51	0.32	0.09	0.03		0.05	0.04	0.16	0.07	0.09	0.01
2	BR-Npw	25.44	0.73	19.21	2.45	9.68	1.46	8.52	1.15	0.01	0.16	0.15	
3	BW-Gum	22.79		51.73				19.32					
4	BW-Nxr	23.06		47.32				8.88		16.90		18.09	
5	CA-SCB	−0.75	1.92	10.67	1.34			2.96	0.70	6.58	0.77	1.16	0.11
6	CA-SCC	−0.24	2.04	6.15	1.05			1.79	0.45	3.41	0.67		
7	CH−Cha	9.74	0.54	2.95	0.88	0.75	0.18	0.99	0.37	0.60	0.28	0.61	0.25
8	CH−Dav	4.37	0.09	1.21		0.28	0.05	0.37	0.21	0.13		0.24	
9	CH−Oe2	11.00		0.29						0.14		0.13	
10	CN-Hgu	3.77	1.31	0.82	0.01			0.23	0.04	0.28	0.15	0.15	
11	DE-Dgw	9.72	0.38	8.97	2.06	0.07	0.06	1.49	0.57	4.15	0.76	2.51	1.05
12	DE-Hte	10.04	0.54	48.11	7.41	2.98	0.72	17.18	3.66	24.28	4.07	6.17	1.46
13	DE-SfN	8.28	0.72	3.62		0.43	0.10	0.23		1.67	0.43	0.72	0.25
14	DE-Zrk	9.55	0.51	30.53	0.96	1.18	0.24	12.27	1.55	16.18	1.47	1.51	0.56
15	FI-Hyy	4.36								−0.02			
16	FI-Lom	−0.35	0.78	15.58	1.83	0.93	0.22	3.75	0.51	9.49	1.25	1.68	0.24
17	FI-Si2	5.14	0.84	9.74	0.67			2.71	0.59	5.83	1.15	1.19	0.08
18	FI-Sii	4.72	0.42	12.43	3.36	0.68	0.11	3.34	0.75	6.79	2.90	1.58	0.42
19	FR-LGt	11.07	0.37	2.45		0.02		1.09		0.85		0.29	
20	HK-MPM	23.75	0.10	11.09	0.51	0.97		2.33	0.52	5.56	0.34	2.95	0.26
21	ID-Pag	26.57	0.19	0.09	0.00	0.19		0.13		−0.24		0.05	
22	IT-BCi	16.69	0.39			−5.18						−2.69	
23	IT-Cas	12.58	0.58	21.62	5.40	0.60		5.59	3.71	15.31	2.24	0.42	0.12
24	JP-BBY	7.11	0.44	15.19	5.15	1.60	0.39	2.61	0.97	8.27	2.60	3.67	0.03
25	JP-Mse	13.75		9.50				1.59		7.42		0.45	
26	JP-SwL	11.67		66.68						39.86		18.53	
27	KR-CRK	10.96	0.46	27.92	1.81	0.92	0.15	8.81	0.92	16.69	1.77	1.25	0.11
28	MY-MLM	27.09	0.11	9.55		3.28		2.60	0.02	1.62		2.34	
29	NL-Hor	10.75	0.60										
30	NZ-Kop	13.68	0.28	17.34	4.46	3.99	0.84	3.03	1.63	3.63	0.52	5.87	0.30
31	PH-RiF	26.54	0.15	12.41		3.57	1.02	2.58	2.66	5.53	0.01	3.34	
32	RU-Ch2	−9.88	1.26	6.43	0.79	0.29		0.87	0.09	4.65	0.48	1.44	0.28
33	RU-Che	−9.77	1.25	4.09	0.22	0.37	0.00	0.47	0.08	2.18	0.12	1.19	0.04
34	RU-Cok	−12.38	0.92	4.45				0.74	0.09	3.42			
35	RU-Fy2	5.80	0.53	3.50	1.88	1.65	0.58	−0.27	0.04	−0.39	0.10	2.36	1.32
36	SE-Deg	2.57	0.77	10.74	0.88	0.59	0.55	3.30	0.29	5.70	0.78	1.44	0.09
37	UK-LBT	10.62	0.78	46.54	5.61	13.70	1.77	12.52		12.26	1.66	14.04	1.87
38	US-A03	−7.15	0.66	5.81	2.06			1.27	0.19	3.25	0.32		
39	US-A10									1.08			
40	US-Atq	−10.88	2.23	1.77	0.03	0.00		0.30	0.07	1.05	0.03	0.55	
41	US-Beo	−9.50	0.20	2.74		0.09		0.27		1.77		0.69	0.12
42	US-Bes	−10.46	0.21	3.19	0.18	0.09		0.58	0.26	2.20	0.18	0.71	
43	US-Bi1	13.87	1.20	0.69		0.45	0.43	−0.07	0.02	−0.13		0.17	0.05
44	US-Bi2	15.01	0.28	1.28	0.59	0.66		0.30	0.21	0.10	0.06	0.54	0.02
45	US-BZB	−0.62	0.55	9.05	2.23			2.41	0.39	6.06	1.43		
46	US-BZF	−0.31	0.55	8.72	2.98			3.21	2.77	6.35	2.24		
47	US-BZS	0.26	0.68	0.78	0.15			0.23	0.01	0.53	0.11		
48	US-CRT	11.32	0.91	2.21	0.00	0.58				0.26		0.59	
49	US-DPW	22.23	0.41	48.71	8.84	1.53	1.84	11.27	2.75	27.64	7.55	12.90	2.54
50	US-EDN	14.99		−0.04				−0.19		0.16			

Table B3. Continued.

	SITE_ID _ID	Mean_Air _Temp_C	Mean_Air _Temp_stdev_C	Ann_Flux_g _CH4−C_m−2	Ann_Flux_stdev _g_CH4−C_m−2	JFM_flux_g _CH4−C_m−2	JFM_flux_stdev _g_CH4−C_m−2	AMJ_flux_g _CH4−C_m−2	AMJ_flux_stdev _g_CH4−C_m−2	JAS_flux_g _CH4−C_m−2	JAS_flux_stdev _g_CH4−C_m−2	OND_flux_g _CH4−C_m−2	OND_flux_stdev _g_CH4−C_m−2
51	US-EML	−1.72	3.76	0.59	0.39	−0.03	0.27	0.06	0.17	0.35	0.12	0.27	
52	US-Ho1	6.48	1.32	−0.16	0.09	−0.04	0.01	−0.03	0.02	−0.02	0.05	−0.07	0.02
53	US-HRA	19.36		−0.24				1.28		6.08			
54	US-HRC	20.23		−0.24				3.07		8.38			
55	US-ICs	−6.02	0.48							1.23	0.30		
56	US-Ivo	−8.27	0.54	4.90	0.95	0.70	0.02	0.80	0.05	2.55	0.54	1.26	0.42
57	US-LA1	24.12	0.42	12.68		0.68		2.27		7.58		1.39	1.08
58	US-LA2	20.34	4.43	34.81	19.34	4.27		14.50	2.18	21.72	2.75	6.96	0.79
59	US-Los	5.01	1.23	6.51	1.28	0.36	0.07	1.71	0.46	3.57	0.96	0.81	0.25
60	US-MAC	23.15	0.96	15.82	10.34	1.32	0.02	3.71	2.07	14.70	5.53	2.81	0.25
61	US-MRM	13.14	0.88	0.34	0.05	0.09		0.07	0.01	0.11	0.01		
62	US-Myb	15.53	0.58	47.88	14.90	4.51	1.99	14.12	5.54	22.04	7.87	6.52	3.17
63	US-NC4	16.74	0.85	33.89	17.41	0.80	0.18	5.70	1.62	20.41	9.80	6.77	2.19
64	US-NGB	−9.45	0.92	2.41	0.15			0.26	0.15	2.00	0.26		
65	US-NGC	1.21	0.82	2.52	0.00					0.86	0.41		
66	US-ORv	12.20	0.92	7.20	2.51	0.88	0.10	2.55	0.93	3.14	1.16	0.99	0.17
67	US-OWC	13.02	1.72	113.99				31.03		66.03	10.07	9.81	
68	US-PFa	5.42	1.24	0.54	0.25	0.15	0.05	0.39	0.19	0.00	0.00		
69	US-Snd	14.76	1.16	4.71	1.71	2.00	1.79	1.11	0.74	1.35	0.61	1.74	1.14
70	US-Sne	15.04	0.45	42.80	4.48	2.44	0.71	14.95	5.12	12.61	10.68	4.71	3.54
71	US-Srr	15.93	0.45	0.83	0.08	0.09	0.06	0.31	0.04	0.42	0.09	0.08	0.07
72	US-StJ	13.96		9.55				1.40		5.24		2.92	
73	US-Tw1	15.16	0.74	39.51	11.03	4.92	1.91	10.13	3.74	18.02	4.08	7.11	2.49
74	US-Tw3	16.04	0.87									0.29	
75	US-Tw4	15.52	0.56	32.54	11.74	4.39	1.75	9.49	4.83	12.78	6.07	5.89	1.83
76	US-Tw5	15.03		59.72				21.49		29.78		8.45	
77	US-Twt	14.26	1.71	12.07	2.75	3.07	1.10	1.05	0.59	5.49	3.15	1.73	0.40
78	US-Uaf	−2.87	1.03	0.53	0.19			0.07		0.33	0.12		
79	US-WPT	11.40	0.99	49.59	7.48	1.66	0.22	16.31	3.99	28.75	3.05	3.26	0.12

https://doi.org/10.5194/essd-13-3607-2021

Table B3. Continued.

(d)	SITE_ID	SOIL_TEMP_PROBE_DEPTHS
1	AT-Neu	TS_1 = −0.05 cm; TS_2 = −0.1 cm; TS_3 = −0.2 cm
2	BR-Npw	
3	BW-Gum	
4	BW-Nxr	
5	CA-SCB	TS_1 = 0 cm; TS_2 = −0.02 cm; TS_3 = −0.04 cm; TS_4 = −0.08 cm; TS_5 = −0.16 cm; TS_6 = −0.32 cm; TS_7 = −0.64 cm ;TS_8 = −1.28 cm
6	CA-SCC	TS_1 = −0.1 cm; TS_2 = −0.15 cm; TS_3 = −0.2 cm; TS_4 = −0.25 cm; TS_5 = −0.3 cm; TS_6 = −0.5 cm; TS_7 = −0.6 cm; TS_8 = −0.7 cm
7	CH−Cha	TS_1 = −0.01 cm; TS_2 = −0.02 cm; TS_3 = −0.04 cm; TS_4 = −0.07 cm; TS_5 = −0.1 cm; TS_6 = −0.15 cm; TS_7 = −0.25 cm; TS_8 = −0.4 cm; TS_9 = −0.95 cm
8	CH−Dav	TS_1 = −0.05 cm; TS_2 = −0.15 cm; TS_3 = −0.5 cm
9	CH−Oe2	TS_1 = −0.05 cm; TS_2 = −0.1 cm; TS_3 = −0.15 cm; TS_5 = −0.3 cm; TS_6 = −0.5 cm
10	CN-Hgu	
11	DE-Dgw	
12	DE-Hte	TS_1 = 0 cm; TS_2 = −0.1 cm; TS_3 = −0.2 cm
13	DE-SfN	TS_1 = −0.02 cm; TS_3 = −0.1 cm; TS_4 = −0.2 cm; TS_5 = −0.5 cm
14	DE-Zrk	TS_1 = −0.05 cm; TS_2 = −0.1 cm; TS_3 = −0.2 cm; TS_4 = −0.3 cm; TS_5 = −0.5 cm
15	FI-Hyy	TS_1 = −0.02 cm; TS_2 = −0.04 cm; TS_3 = −0.12 cm; TS_4 = −0.25 cm; TS_5 = −0.5 cm
16	FI-Lom	TS_1 = −0.07 cm; TS_2 = −0.3 cm; TS_3 = −0.5 cm
17	FI-Si2	TS_1 = −0.05 cm; TS_2 = −0.2 cm; TS_3 = −0.35 cm; TS_4 = −0.5 cm; TS_1 = −0.05 cm; TS_2 = −0.2 cm; TS_3 = −0.35 cm; TS_4 = −0.5 cm
18	FI-Sii	before 2016(TS_1 = −0.05 cm; TS_2 = −0.2 cm; TS_3 = −0.35 cm; TS_4 = −0.5 cm; TS_2 = −0.2 cm; TS_3 = −0.35 cm; TS_4 = −0.5 cm) after 2017 (TS_1 = 0 cm; TS_2 = −0.5 cm; TS_3 = −0.1 cm; TS_4 = −0.15 cm; TS_5 = −0.25 cm; TS_6 = −0.45 cm; TS_7 = −0.95 cm)
19	FR-LGt	TS_1 = −0.02 cm; TS_2 = −0.05 cm; TS_3 = −0.1 cm; TS_4 = −0.2 cm; TS_5 = −0.4 cm
20	HK-MPM	
21	ID-Pag	TS_1 = −0.05 cm
22	IT-BCi	TS_1 = −0.05 cm; TS_2 = −0.1 cm; TS_3 = −0.3 cm; TS_4 = −0.5 cm; TS_5 = −1 cm
23	IT-Cas	TS_1 = −0.05 cm; TS_2 = −0.3 cm; TS_3 = −0.5 cm
24	JP-BBY	TS_1 = −0.183 cm; TS_2 = −0.233 cm; TS_3 = −0.283 cm; TS_ 4 = −0.383 cm; TS_5 = −0.483 cm
25	JP-Mse	TS_1 = −0.01 cm; TS_2 = −0.025 cm; TS_3 = −0.05 cm; TS_4 = −0.1 cm; TS_5 = −0.2 cm; TS_6 = −0.4 cm
26	JP-SwL	
27	KR-CRK	TS_1 = −0.05 cm; TS_2 = −0.15 cm
28	MY-MLM	TS_1 = −0.05 cm
29	NL-Hor	TS_1 = −0.01 cm; TS_2 = −0.02 cm; TS_3 = −0.04 cm; TS_4 = −0.05 cm; TS_5 = −0.1 cm; TS_6 = −0.15 cm; TS_7 = −0.25 cm; TS_8 = −0.4 cm; TS_9 = −0.6 cm
30	NZ-Kop	TS_1 = −0.5 cm; TS_2 = −0.1 cm; TS_3 = −0.2 cm
31	PH-RiF	
32	RU-Ch2	TS_1 = −0.04 cm; TS_2 = −0.08 cm; TS_3 = −0.16 cm
33	RU-Che	TS_1 = −0.04 cm; TS_2 = −0.08 cm; TS_3 = −0.16 cm
34	RU-Cok	
35	RU-Fy2	
36	SE-Deg	TS_1 = −0.02 cm; TS_2 = −0.05 cm; TS_3 = −0.1 cm; TS_4 = −0.15 cm; TS_5 = −0.3 cm; TS_6 = −0.5 cm
37	UK-LBT	
38	US-A03	TS_1 = −0.025 cm; TS_2 = −0.1 cm; TS_3 = −0.3 cm
39	US-A10	TS_1 = −0.025 cm; TS_2 = −0.1 cm; TS_3 = −0.3 cm
40	US-Atq	
41	US-Beo	
42	US-Bes	
43	US-Bi1	TS_1 = −0.02 cm; TS_2 = −0.04 cm; TS_3 = −0.08 cm; TS_4 = −0.16 cm; TS_5 = −0.32 cm
44	US-Bi2	TS_1 = −0.02 cm; TS_2 = −0.04 cm; TS_3 = −0.08 cm; TS_4 = −0.16 cm; TS_5 = −0.32 cm
45	US-BZB	TS_1 = −0.075 cm; TS_2 = −0.05 cm
46	US-BZF	TS_1 = −0.075 cm; TS_2 = −0.05 cm
47	US-BZS	
48	US-CRT	
49	US-DPW	
50	US-EDN	TS_1 = −0.25 cm; TS_2 = −0.15 cm; TS_3 = −0.05 cm; TS_4 = 0 cm; TS_5 = 0.05 cm; TS_6 = 0.1 cm; TS_7 = 0.2 cm; TS_8 = 0.3 cm
51	US-EML	TS_1 = −0.05 cm; TS_2 = −0.1 cm; TS_3 = −0.2 cm; TS_4 = −0.4 cm
52	US-Ho1	TS_1 = −0.05 cm; TS_2 = −0.1 cm
53	US-HRA	
54	US-HRC	

Table B3. Continued.

	SITE_ID	SOIL_TEMP_PROBE_DEPTHS
55	US-ICs	TS_1 = −0.075 cm; TS_2 = −0.05 cm
56	US-Ivo	TS_1 = −0.05 cm; TS_2 = −0.1 cm; TS_3 = −0.15 cm; TS_4 = −0.3 cm; TS_5 = −0.4 cm
57	US-LA1	TS = −0.1 cm
58	US-LA2	TS = −0.1 cm
59	US-Los	TS_1 = 0 cm; TS_2 = −0.05 cm; TS_3 = −0.1 cm; TS_4 = −0.2 cm; TS_5 = −0.5 cm
60	US-MAC	
61	US-MRM	
62	US-Myb	TS_1 = −0.02 cm; TS_2 = −0.04 cm; TS_3 = −0.08 cm; TS_4 = −0.16 cm; TS_5 = −0.32 cm
63	US-NC4	TS_1 = −0.05 cm; TS_2 = −0.2 cm
64	US-NGB	
65	US-NGC	
66	US-ORv	TS_1 = −0.08 cm
67	US-OWC	TS_1 = −0.05 cm; TS_2 = −0.3 cm
68	US-PFa	
69	US-Snd	TS_1 = −0.08 cm; TS_2 = −0.16 cm; TS_3 = nan cm; TS_4 = nan cm; TS_5 = nan cm; TS_6 = nan cm
70	US-Sne	TS_1 = −0.01 cm; TS_2 = −0.02 cm; TS_3 = −0.08 cm; TS_4 = −0.16 cm; TS_5 = −0.32 cm
71	US-Srr	
72	US-StJ	TS_2 = −0.05 cm; TS_3 = −0.1 cm
73	US-Tw1	TS_1 = −0.02 cm; TS_2 = −0.04 cm; TS_3 = −0.08 cm; TS_4 = −0.16 cm; TS_5 = −0.32 cm
74	US-Tw3	TS_1 = −0.02 cm; TS_2 = −0.04 cm; TS_3 = −0.08 cm; TS_4 = −0.16 cm; TS_5 = −0.32 cm
75	US-Tw4	TS_1 = −0.02 cm; TS_2 = −0.04 cm; TS_3 = −0.08 cm; TS_4 = −0.16 cm; TS_5 = −0.32 cm
76	US-Tw5	TS_1 = −0.02 cm; TS_2 = −0.1 cm; TS_3 = −0.02 cm; TS_4 = −0.08 cm; TS_5 = −0.16 cm
77	US-Twt	TS_1 = −0.02 cm; TS_2 = −0.04 cm; TS_3 = −0.08 cm; TS_4 = −0.16 cm; TS_5 = −0.32 cm
78	US-Uaf	TS_1 = −0.09 cm; TS_2 = −0.183 cm; TS_3 = −0.283 cm; TS_4 = −0.367 cm; TS_5 = −0.5 cm; TS_6 = −0.6 cm; TS_7 = −0.75 cm; TS_8 = −0.925 cm; TS_9 = −1 cm
79	US-WPT	TS_1 = −0.1 cm; TS_2 = −0.3 cm

Earth Syst. Sci. Data, 13, 3607–3689, 2021

https://doi.org/10.5194/essd-13-3607-2021

Column	Description
SITE_ID	Site identification code as assigned by regional flux data network
SITE_NAME	Site name determined by site personnel
SITE_PERSONNEL	People associated with site FLUXNET-CH_4 data
COUNTRY	Site country
LAT	Latitude
LON	Longitude
DATA_DOI	DOI link for site FLUXNET-CH_4 data
YEAR_START	Year data begin
YEAR_END	Year data end
UTC_OFFSET	Site data offset from coordinated universal time (in hours)
ORIGINAL_DATA_SOURCE	Regional network hosting the site's methane data that were incorporated into FLUXNET-CH_4
SITE_CLASSIFICATION	Site classification based on the literature description of sites
UPLAND_CLASS	For upland sites, category of upland type
IGBP	International Geosphere–Biosphere Programme (IGBP) ecosystem surface classification
KOPPEN	Koppen climate zone abbreviation
MEAN_ANNUAL_TEMP_C_WORLDCLIM	Mean annual temperature from WorldClim2 Global Climate Data
MEAN_ANNUAL_PRECIP_MM_WORLDCLIM	Mean annual precipitation from WorldClim2 Global Climate Data
MOSS_BROWN	Presence/absence (1/0) brown moss. Presence/absence designated by Avni Malhotra using site literature
MOSS_SPHAGNUM	Presence/absence (1/0) sphagnum moss. Presence/absence designated by Avni Malhotra using site literature
AERENCHYMATOUS	Presence/absence (1/0) aerenchymatous vegetation. Presence/absence designated by Avni Malhotra using site literature
ERI_SHRUB	Presence/absence (1/0) ericaceous shrubs. Presence/absence designated by Avni Malhotra using site literature
TREE	Presence/absence (1/0) trees. Presence/absence designated by Avni Malhotra using site literature
DOM_VEG	Dominant vegetation type in tower footprint. Dom_veg provided to Avni Malhotra by site personnel via survey, except 15 sites where principal investigators did not answer and Avni Malhotra estimated dominant vegetation type based on site literature
IN_SEASONALITY_ANALYSIS	Is site in freshwater wetland seasonality analysis? 1 = yes, 0 = no.
Mean_Air_Temp_C	Mean annual air temperature (C)
Mean_Air_Temp_stdev_C	Standard deviation of annual air temperature (C)
Ann_Flux_g_CH4-C_m−2	Mean annual methane flux ($g\,CH_4\text{-}C\,m^{-2}\,yr^1$)
Ann_Flux_stdev_g_CH4-C_m−2	Standard deviation of annual methane flux ($g\,CH_4\text{-}C\,m^{-2}\,yr^{-1}$)
JFM_flux_g_CH4-C_m−2	Mean methane flux in January, February, March ($g\,CH_4\text{-}C\,m^{-2}\,yr^{-1}$)
JFM_flux_stdev_g_CH4-C_m−2	Standard deviation of methane flux in January, February, March ($g\,CH_4\text{-}C\,m^{-2}\,yr^{-1}$)
AMJ_flux_g_CH4-C_m−2	Mean methane flux in April, May, June ($g\,CH_4\text{-}C\,m^{-2}\,yr^{-1}$)
AMJ_flux_stdev_g_CH4-C_m−2	Standard deviation of methane flux in April, May, June ($g\,CH_4\text{-}C\,m^{-2}\,yr^{-1}$)
JAS_flux_g_CH4-C_m−2	Mean methane flux in July, August, September ($g\,CH_4\text{-}C\,m^{-2}\,yr^{-1}$)
JAS_flux_stdev_g_CH4-C_m−2	Standard deviation of methane flux in July, August, September ($g\,CH_4\text{-}C\,m^{-2}\,yr^{-1}$)
OND_flux_g_CH4-C_m−2	Mean methane flux in October, November, December ($g\,CH_4\text{-}C\,m^{-2}\,yr^{-1}$)
OND_flux_stdev_g_CH4-C_m−2	Standard deviation of methane flux in October, November, December ($g\,CH_4\text{-}C\,m^{-2}\,yr^{-1}$)
SOIL_TEMP_PROBE_DEPTHS	Depth of soil temperature probe (m), with negative values being under the surface

Table B4. Table of bioclimatic predictor data used in the principal component analysis (PCA) of Fig. 6.

	SITE _ID	Enhanced_Vegetation _Index_(EVI)	Wong_Simple_Ratio _Water_Index_(SRWI)	Latent_Heat _(LE)	Mean_Annual _Temperature_(MAT)
1	BR-Npw	0.31	0.86	87.6	25.3
2	BW-Gum	0.28	0.87	60.9	23
3	BW-Nxr	0.22	0.82	52.6	23.5
4	CA-SCB	0.16	1.2	27.4	−2.7
5	DE-Hte	0.28	1.01	40.2	8.6
6	DE-SfN	0.41	1.03	48.5	8.2
7	DE-Zrk	0.33	1.05	42.5	8.2
8	FI-Lom	0.2	1.27	23.6	−1.5
9	FI-Si2	0.27	1.12	31.6	3.3
10	FI-Sii	0.27	1.12	31.6	3.3
11	FR-LGt	0.4	0.97	50	10.8
12	ID-Pag	0.5	1.1	119.7	27.2
13	JP-BBY	0.25	1.21	45.4	6.5
14	MY-MLM	0.42	1.17	116.6	26.9
15	NZ-Kop	0.53	1.06	71.2	13.9
16	RU-Ch2	−0.01	1.25	20	−12.1
17	RU-Cok	0.04	1.18	16.8	−14.2
18	SE-Deg	0.27	1.12	29	2
19	US-A03	−0.07	1.28	16.1	−11.4
20	US-Atq	−0.1	1.31	16.9	−10.2
21	US-BZB	0.17	1.09	26	−2.8
22	US-BZF	0.17	1.09	26	−2.8
23	US-DPW	0.32	0.88	71.8	22.2
24	US-ICs	−0.04	1.3	18.5	−8.8
25	US-Ivo	−0.08	1.34	18.4	−7.7
26	US-LA2	0.37	0.98	69.9	20
27	US-Los	0.29	1.1	46.6	4
28	US-Myb	0.23	0.86	51	15.5
29	US-NC4	0.34	0.96	68.4	16.5
30	US-NGC	0.1	1.24	22.3	−3.2
31	US-ORv	0.32	0.99	50.8	10.6
32	US-OWC	0.27	1.05	55.8	9.9
33	US-Sne	0.23	0.86	51	15.5
34	US-Tw1	0.26	0.91	51	15.5
35	US-Tw4	0.26	0.91	51	15.5
36	US-Tw5	0.26	0.91	51	15.5

Column	Description
SITE_ID	Site identification code as assigned by regional flux data network
Enhanced_Vegetation_Index_(EVI)	Enhanced vegetation index (unitless) from MOD13A3 (Didan, 2015), 2001–2018 monthly data
Wong_Simple_Ratio_Water_Index_(SRWI)	Simple ratio water index (unitless) from MOD09A1 (Vermote, 2015), ∼ 2001–2018 monthly data
Latent_Heat_(LE)	Latent heat (in $W\,m^{-2}$) from FLUXCOM (Jung et al., 2019), 2003–2013 monthly data
Mean_Annual_Temperature_(MAT)	Mean annual temperature (C) from BioClim (Fick and Hijman, 2017), 2001–2018 monthly data

Table B5. Seasonality parameters estimated using TIMESAT software for methane flux (FCH4), gross primary productivity (GPP), air temperature (TA), and soil temperature (TS, for shallowest probe at each site).

	SITE _ID	Year	Start_FCH4_(DOY)	End_FCH4_(DOY)	Base_value_FCH4 _FCH4_(nmol /m2/s)	Ampl_FCH4 _(nmolCH4/m2/s)	Peak_FCH4 _(DOY)	Peak_value _FCH4_(nmolCH4/m2/s)
1	AT-Neu	2010	NaN	NaN	NaN	NaN	NaN	NaN
2	AT-Neu	2011	NaN	NaN	NaN	NaN	NaN	NaN
3	AT-Neu	2012	NaN	NaN	NaN	NaN	NaN	NaN
4	BR-Npw	2014	NaN	NaN	NaN	NaN	NaN	NaN
5	BR-Npw	2015	NaN	NaN	NaN	NaN	NaN	NaN
6	BR-Npw	2016	192.7	345.8	−1.9	154.8	270	152.8
7	BW-Gum	2018	34.1	151.1	132.9	186.2	89.0	319.1
8	BW-Gum	2019	230.4	NaN	134.2	202.1	281.9	336.3
9	BW-Nxr	2018	65.1	NaN	29.2	208.7	287.5	237.9
10	CA-SCB	2014	138.8	299.1	17.5	72.3	222.4	89.9
11	CA-SCB	2015	NaN	NaN	NaN	NaN	NaN	NaN
12	CA-SCB	2016	109.2	290.4	11.8	82.0	207.9	93.8
13	CA-SCB	2017	118.0	300.4	14.0	58.9	221.5	72.9
14	CA-SCC	2013	NaN	NaN	NaN	NaN	203.4	44.8
15	CA-SCC	2014	128.4	313.1	3.1	40.1	215.0	43.3
16	CA-SCC	2015	98.0	303.9	1.7	54.6	210.9	56.3
17	CA-SCC	2016	102.7	NaN	1.7	NaN	208	59.6
18	DE-Dgw	2015	NaN	NaN	NaN	NaN	NaN	NaN
19	DE-Dgw	2016	NaN	NaN	NaN	NaN	NaN	NaN
20	DE-Dgw	2017	NaN	NaN	NaN	NaN	NaN	NaN
21	DE-Hte	2011	NaN	NaN	NaN	NaN	NaN	NaN
22	DE-Hte	2012	82.6	330.1	20.3	201.8	205.5	222.1
23	DE-Hte	2013	101.9	NaN	29.9	NaN	201.1	378.7
24	DE-Hte	2014	NaN	338.5	38.3	NaN	204.8	314.1
25	DE-Hte	2015	75.1	322.4	29.2	277.7	202	306.9
26	DE-Hte	2016	83.9	289.7	21.5	347.8	202	369.3
27	DE-Hte	2017	90.0	304.5	18.2	272.7	194	290.9
28	DE-Hte	2018	85.6	258.1	21.0	322.0	196.0	343.0
29	DE-SfN	2012	79.6	340.7	4.3	10.2	217.0	14.5
30	DE-SfN	2013	NaN	NaN	2.7	3.0	301.9	5.7
31	DE-SfN	2014	NaN	NaN	NaN	NaN	NaN	NaN
32	DE-Zrk	2013	NaN	NaN	NaN	NaN	NaN	NaN
33	DE-Zrk	2014	NaN	NaN	NaN	NaN	NaN	NaN
34	DE-Zrk	2015	87.0	273.0	9.3	242.5	208.7	251.9
35	DE-Zrk	2016	107.9	274.0	9.9	224.2	187.3	234.2
36	DE-Zrk	2017	110.0	270.1	11.2	203.6	190.0	214.8
37	DE-Zrk	2018	88.1	261.0	8.5	250.8	196.0	259.2
38	FI-Lom	2006	142.81	288.8	7.8	111.0	215.1	118.9
39	FI-Lom	2007	139.3	270.6	10.9	165.0	214.5	175.9
40	FI-Lom	2008	134.0	284.8	10.8	127.7	211.5	138.5
41	FI-Lom	2009	121.5	291.0	12.1	132.3	215.0	144.4
42	FI-Lom	2010	137.1	282.8	13.4	101.6	214.0	115.0
43	FI-Si2	2012	NaN	NaN	NaN	NaN	220.6	80.0
44	FI-Si2	2013	NaN	NaN	NaN	NaN	211.1	77.4
45	FI-Si2	2014	NaN	280.7	7.2	NaN	212.8	111.1
46	FI-Si2	2015	NaN	309.5	9.5	NaN	212.0	72.15
47	FI-Si2	2016	NaN	NaN	NaN	NaN	NaN	NaN
48	FI-Sii	2013	123.8	307.6	7.2	104.3	202.5	111.5
49	FI-Sii	2014	118.8	NaN	2.3	NaN	215.1	112.7
50	FI-Sii	2015	NaN	NaN	NaN	NaN	236.0	112.7

https://doi.org/10.5194/essd-13-3607-2021

Table B5. Continued.

	SITE_ID	Year	Start_FCH4_(DOY)	End_FCH4_(DOY)	Base_value_FCH4 _FCH4_(nmolCH4/m2/s)	Ampl_FCH4 _(nmolCH4/m2/s)	Peak_FCH4 _(DOY)	Peak_value _FCH4_(nmolCH4/m2/s)
51	FI-Sii	2016	114.5	311.3	8.9	121.1	214.0	130.0
52	FI-Sii	2017	118.9	300.4	6.5	57.1	203.0	63.6
53	FI-Sii	2018	116.3	295.1	7.5	53.8	187.0	61.3
54	HK-MPM	2016	NaN	NaN	NaN	NaN	NaN	NaN
55	HK-MPM	2017	NaN	NaN	NaN	NaN	NaN	NaN
56	HK-MPM	2018	NaN	NaN	NaN	NaN	NaN	NaN
57	ID-Pag	2016	274.1	NaN	−2.8	5.1	NaN	2.3
58	JP-BBY	2015	166.7	NaN	18.2	NaN	237.7	71.4
59	JP-BBY	2016	NaN	325.0	18.3	105.7	244.3	124.0
60	JP-BBY	2017	138.5	323.1	15.2	130.1	236.0	145.3
61	JP-BBY	2018	NaN	332.1	17.8	74.7	221.0	92.6
62	JP-Mse	2012	NaN	NaN	NaN	NaN	NaN	NaN
63	KR-CRK	2015	NaN	NaN	NaN	NaN	NaN	NaN
64	KR-CRK	2016	NaN	NaN	NaN	NaN	NaN	NaN
65	KR-CRK	2017	NaN	NaN	NaN	NaN	NaN	NaN
66	KR-CRK	2018	NaN	NaN	NaN	NaN	NaN	NaN
67	MY-MLM	2014	229.6	562.4	15.5	19.8	64.2	35.3
68	MY-MLM	2015	NaN	NaN	NaN	NaN	NaN	NaN
69	NZ-Kop	2012	−94.5	227.6	36.9	28.3	176.2	65.2
70	NZ-Kop	2013	7.2	251.5	21.1	61.7	182.0	82.8
71	NZ-Kop	2014	10.0	228.4	22.6	42.7	161	65.2
72	NZ-Kop	2015	−8.5	NaN	23.0	34.7	150.0	57.8
73	PH-RiF	2012	154.2	303.9	4.0	62.9	239.1	66.9
74	PH-RiF	2013	304.1	455.0	5.3	54.0	380.3	59.3
75	PH-RiF	2014	133.9	265.7	6.1	121.8	178.3	127.9
76	PH-RiF	2015	NaN	NaN	3.8	56.2	NaN	60.1
77	RU-Ch2	2014	150.8	312.2	0.7	70.2	216.5	70.9
78	RU-Ch2	2015	153.3	NaN	8.0	NaN	209.0	56.1
79	RU-Ch2	2016	NaN	NaN	NaN	NaN	218.8	68.3
80	RU-Che	2014	NaN	NaN	NaN	NaN	NaN	NaN
81	RU-Che	2015	NaN	NaN	NaN	NaN	NaN	NaN
82	RU-Che	2016	NaN	NaN	NaN	NaN	NaN	NaN
83	SE-Deg	2014	NaN	NaN	NaN	80.8	204.2	91.7
84	SE-Deg	2015	103.3	318.7	5.1	73.7	211.3	78.8
85	SE-Deg	2016	102.5	324.1	4.3	74.3	205.3	78.7
86	SE-Deg	2017	NaN	NaN	NaN	NaN	NaN	NaN
87	SE-Deg	2018	117.2	327.6	6.9	50.9	192.0	57.8
88	US-Atq	2013	NaN	NaN	NaN	NaN	NaN	NaN
89	US-Atq	2014	145.7	328.7	0.9	13.2	215.0	14.1
90	US-Atq	2015	153.3	264.0	1.0	18.6	193.2	19.6
91	US-Beo	2013	NaN	NaN	NaN	NaN	NaN	NaN
92	US-Beo	2014	157.0	356.3	0.4	23.0	211.4	23.4
93	US-Bes	2013	NaN	NaN	NaN	NaN	NaN	NaN
94	US-Bes	2014	157.3	312.6	0.6	34.3	206.5	35.0
95	US-Bes	2015	146.8	283.8	0.6	35.0	193.1	35.7
96	US-BZB	2014	NaN	NaN	NaN	NaN	226.9	67.5
97	US-BZB	2015	NaN	NaN	NaN	NaN	219.4	68.4
98	US-BZB	2016	NaN	NaN	NaN	NaN	226.1	98.4
99	US-BZF	2014	NaN	NaN	NaN	NaN	231.6	57.7
100	US-BZF	2015	NaN	NaN	NaN	NaN	179	87.0

Table B5. Continued.

	SITE _ID	Year	Start_FCH4_(DOY)	End_FCH4_(DOY)	Base_value_FCH4 _FCH4_(nmolCH4/m2/s)	Ampl_FCH4 _(nmolCH4/m2/s)	Peak_FCH4 _(DOY)	Peak_value _FCH4_(nmolCH4/m2/s)
101	US-BZF	2016	NaN	NaN	NaN	NaN	220.1	119.1
102	US-BZS	2015	NaN	NaN	NaN	NaN	NaN	NaN
103	US-BZS	2016	NaN	NaN	NaN	NaN	NaN	NaN
104	US-DPW	2013	151.7	364.0	16.4	395.0	240.7	411.4
105	US-DPW	2014	98.9	332.5	34.5	338.0	228.9	372.4
106	US-DPW	2015	NaN	376.3	25.0	NaN	248.6	247.3
107	US-DPW	2016	84.2	389.2	23.5	184.3	237.0	207.8
108	US-HRA	2017	NaN	NaN	NaN	NaN	NaN	NaN
109	US-HRC	2018	NaN	NaN	NaN	NaN	NaN	NaN
110	US-ICs	2014	NaN	NaN	NaN	NaN	NaN	NaN
111	US-ICs	2015	NaN	NaN	NaN	NaN	NaN	NaN
112	US-ICs	2016	138.2	302.1	0.2	18.0	200.5	18.2
113	US-Ivo	2013	NaN	400.0	1.9	29.9	238.9	31.9
114	US-Ivo	2014	158.5	301.8	6.7	30.0	226.8	36.7
115	US-Ivo	2015	156.8	278.0	6.9	19.4	231.1	26.3
116	US-Ivo	2016	164.7	352.4	6.1	32.5	232.0	38.7
117	US-LA1	2012	NaN	NaN	NaN	NaN	NaN	NaN
118	US-LA2	2012	62.8	NaN	38.8	225.7	229.2	264.5
119	US-LA2	2013	NaN	NaN	25.1	193.2	216.2	218.3
120	US-Los	2014	127.1	309.8	4.0	35.1	219.3	39.1
121	US-Los	2015	143.4	324.4	3.2	34.6	220.7	37.8
122	US-Los	2016	143.8	310.1	3.3	75.8	193.6	79.1
123	US-Los	2017	134.1	255.2	3.6	58.3	185.0	61.9
124	US-Los	2018	143.0	288.8	3.0	52.4	191.0	55.4
125	US-MAC	2013	NaN	NaN	NaN	NaN	NaN	NaN
126	US-MAC	2014	NaN	NaN	NaN	NaN	NaN	NaN
127	US-MAC	2015	NaN	NaN	NaN	NaN	NaN	NaN
128	US-Myb	2010	NaN	NaN	NaN	NaN	NaN	NaN
129	US-Myb	2011	72.4	369.3	18.3	174.2	253.5	192.5
130	US-Myb	2012	97.2	345.3	18.9	366.6	214.7	385.5
131	US-Myb	2013	46.8	336.3	39.0	265.4	220.2	304.3
132	US-Myb	2014	57.4	334.7	37.1	276.9	206.0	314.0
133	US-Myb	2015	23.7	330.0	21.6	285.7	201.0	307.3
134	US-Myb	2016	37.0	306.0	21.9	216.0	191.0	237.9
135	US-Myb	2017	175.8	332.2	30.5	191.7	235.0	222.2
136	US-Myb	2018	33.1	322.6	28.8	99.3	169.0	128.1
137	US-NC4	2012	132.9	307.9	9.5	323.8	232.2	333.3
138	US-NC4	2013	97.2	365.1	4.3	113.3	240.7	117.5
139	US-NC4	2014	110.6	332.3	−0.1	181.8	253.9	181.6
140	US-NC4	2015	68.4	414.1	−0.8	122.5	245.0	121.7
141	US-NC4	2016	128.4	350.6	2.7	373.6	259.0	376.2
142	US-ORv	2011	NaN	297.3	7.3	15.2	178.5	22.4
143	US-ORv	2012	120.1	269.1	8.3	65.2	189.7	73.4
144	US-ORv	2013	72.4	308.4	9.0	27.4	189.4	36.4
145	US-ORv	2014	87.6	292.2	9.1	32.4	201.0	41.5
146	US-ORv	2015	86.0	NaN	9.0	38.5	170.0	47.41
147	US-OWC	2015	NaN	NaN	NaN	NaN	NaN	NaN
148	US-OWC	2016	NaN	NaN	NaN	NaN	219.2	883.0
149	US-Sne	2016	NaN	NaN	NaN	NaN	NaN	NaN

https://doi.org/10.5194/essd-13-3607-2021

Table B5. Continued.

	SITE _ID	Year	Start_FCH4_(DOY)	End_FCH4_(DOY)	Base_value_FCH4 _FCH4_(nmolCH4/m2/s)	Ampl_FCH4 _(nmolCH4/m2/s)	Peak_FCH4 _(DOY)	Peak_value _FCH4_(nmolCH4/m2/s)
150	US-Sne	2017	76.2	337.1	14.9	244.2	187.8	259.0
151	US-Sne	2018	60.6	341.6	21.4	168.3	222.6	189.8
152	US-Srr	2014	NaN	NaN	NaN	NaN	NaN	NaN
153	US-Srr	2015	NaN	NaN	NaN	NaN	NaN	NaN
154	US-Srr	2016	NaN	NaN	NaN	NaN	NaN	NaN
155	US-Srr	2017	NaN	NaN	NaN	NaN	NaN	NaN
156	US-StJ	2016	NaN	NaN	NaN	NaN	NaN	NaN
157	US-Tw1	2011	140.5	352.4	36.3	104.5	233.8	140.8
158	US-Tw1	2012	NaN	309.6	28.1	243.5	242.9	271.6
159	US-Tw1	2013	33.4	307.1	42.2	114.3	218.0	156.5
160	US-Tw1	2014	174.6	331.5	65.3	253.2	240.0	318.5
161	US-Tw1	2015	62.3	330.3	63.8	204.1	207.0	267.9
162	US-Tw1	2016	32.3	323.8	48.5	160.0	221.0	208.5
163	US-Tw1	2017	27.8	305.0	43.0	138.1	226.0	181.1
164	US-Tw1	2018	155.0	314.9	38.7	127.5	228.0	166.3
165	US-Tw4	2014	93.8	461.3	27.4	36.5	226.8	63.8
166	US-Tw4	2015	114.5	334.1	39.8	86.5	228.2	126.3
167	US-Tw4	2016	42.8	357.1	43.2	101.8	215.6	144.9
168	US-Tw4	2017	110.7	318.8	55.1	201.2	222.0	256.3
169	US-Tw4	2018	63.0	237.3	53.0	165.1	173.0	218.1
170	US-Tw5	2018	NaN	331.9	26.5	339.3	196.9	365.8
171	US-Twt	2009	NaN	NaN	NaN	NaN	NaN	NaN
172	US-Twt	2010	NaN	NaN	NaN	NaN	NaN	NaN
173	US-Twt	2011	NaN	NaN	NaN	NaN	NaN	NaN
174	US-Twt	2012	NaN	NaN	NaN	NaN	NaN	NaN
175	US-Twt	2013	NaN	NaN	NaN	NaN	NaN	NaN
176	US-Twt	2014	NaN	NaN	NaN	NaN	NaN	NaN
177	US-Twt	2015	NaN	NaN	NaN	NaN	NaN	NaN
178	US-Twt	2016	NaN	NaN	NaN	NaN	NaN	NaN
179	US-Uaf	2011	157.6	NaN	0.8	2.1	242.0	2.8
180	US-Uaf	2012	151.8	NaN	0.7	1.6	265.9	2.3
181	US-Uaf	2013	167.0	NaN	0.8	1.4	267.0	2.2
182	US-Uaf	2014	182.2	NaN	0.9	3.2	247.0	4.1
183	US-Uaf	2015	176.0	NaN	0.8	3.5	245.0	4.3
184	US-Uaf	2016	184.7	NaN	0.9	7.3	248.0	8.2
185	US-Uaf	2017	182.0	NaN	0.9	6.0	248.0	6.8
186	US-Uaf	2018	158.5	NaN	0.9	4.9	250.0	5.8
187	US-WPT	2011	103.5	294.1	5.6	355.3	207.1	360.9
188	US-WPT	2012	90.0	296.5	9.0	380.5	195.6	389.5
189	US-WPT	2013	72.5	296.9	7.5	343.3	220.0	350.8

Table B5. Continued.

	SITE _ID	Year	Start_GPP _DT_(DOY)	End_GPP _DT_(DOY)	Base_value_GPP _DT_(µmolCO2/m2/s)	Ampl_GPP_DT _(µmolCO2/m2/s)	Peak_GPP_DT _(DOY)	Peak_value_GPP _DT_(µmolCO2/m2/s)
1	AT-Neu	2010	61.4	332.2	−0.2	9.7	175.9	9.5
2	AT-Neu	2011	76.7	303.7	0.2	11.4	167.9	11.5
3	AT-Neu	2012	84.7	305.5	0.3	9.8	179.0	10.0
4	BR-Npw	2014	59.5	367.8	2.0	5.1	242.9	7.1
5	BR-Npw	2015	61.5	385.1	2.0	5.2	228.0	7.2
6	BR-Npw	2016	83.8	375.6	2.4	4.7	203.0	7.2
7	BW-Gum	2018	NaN	NaN	NaN	NaN	NaN	NaN
8	BW-Gum	2019	NaN	NaN	NaN	NaN	NaN	NaN
9	BW-Nxr	2018	NaN	NaN	NaN	NaN	NaN	NaN
10	CA-SCB	2014	127.5	266.1	0.1	2.7	210.0	2.8
11	CA-SCB	2015	60.2	275.2	0.1	3.4	199.4	3.5
12	CA-SCB	2016	123.0	277.1	0.0	3.7	191.9	3.7
13	CA-SCB	2017	113.8	274.6	0.0	3.0	202.0	3.0
14	CA-SCC	2013	126.4	273.7	0.2	3.2	198.8	3.4
15	CA-SCC	2014	130.1	269.3	0.3	3.2	194.3	3.5
16	CA-SCC	2015	104.4	270.0	0.3	4.5	196.9	4.8
17	CA-SCC	2016	106.9	284.8	0.1	3.7	191.0	3.8
18	DE-Dgw	2015	13.4	348.6	0.0	0.4	227.3	0.4
19	DE-Dgw	2016	31.3	294.3	0.0	0.5	167.6	0.5
20	DE-Dgw	2017	80.6	293.5	0.0	0.5	191.0	0.5
21	DE-Hte	2011	111.7	280.5	0.1	6.9	170.1	6.9
22	DE-Hte	2012	122.6	296.5	0.3	7.1	200.1	7.4
23	DE-Hte	2013	133.5	294.0	0.3	6.1	206.4	6.4
24	DE-Hte	2014	37.5	277.7	0.3	5.5	160.0	5.8
25	DE-Hte	2015	127.8	303.3	0.3	5.3	191.0	5.6
26	DE-Hte	2016	118.0	328.5	0.2	5.4	184.0	5.6
27	DE-Hte	2017	123.8	301.6	0.1	5.7	177.0	5.8
28	DE-Hte	2018	121.0	334.1	0.1	7.0	190.0	7.0
29	DE-SfN	2012	−13.8	320.9	0.4	4.3	168.1	4.7
30	DE-SfN	2013	64.4	316.6	0.3	4.0	198.0	4.3
31	DE-SfN	2014	44.0	335.8	0.4	4.1	193.0	4.5
32	DE-Zrk	2013	110.2	283.5	0.1	4.3	186.3	4.4
33	DE-Zrk	2014	86.6	309.8	0.1	3.6	180.4	3.6
34	DE-Zrk	2015	99.4	264.2	0.1	3.5	186.6	3.6
35	DE-Zrk	2016	90.3	301.9	0.1	4.4	218.0	4.5
36	DE-Zrk	2017	92.9	303.9	0.1	4.1	180.0	4.2
37	DE-Zrk	2018	105.2	314.6	0.1	6.9	212.0	7.0
38	FI-Lom	2006	147.8	261.4	0.1	5.9	197.4	6.0
39	FI-Lom	2007	145.8	257.6	0.1	6.4	197.9	6.4
40	FI-Lom	2008	151.6	258.9	0.1	7.2	200.0	7.3
41	FI-Lom	2009	147.6	262.6	0.0	6.5	197.0	6.6
42	FI-Lom	2010	153.9	262.6	0.0	6.4	199.0	6.4
43	FI-Si2	2012	33.7	276.8	0.1	1.5	209.0	1.6
44	FI-Si2	2013	106.8	338.1	0.1	1.6	182.9	1.8

https://doi.org/10.5194/essd-13-3607-2021

Table B5. Continued.

	SITE _ID	Year	Start_GPP _DT_(DOY)	End_GPP _DT_(DOY)	Base_value_GPP _DT_(µmolCO2/m2/s)	Ampl_GPP_DT _(µmolCO2/m2/s)	Peak_GPP_DT _(DOY)	Peak_value_GPP _DT_(µmolCO2/m2/s)
45	FI-Si2	2014	40.9	290.0	0.1	2.2	146.0	2.3
46	FI-Si2	2015	113.2	267.8	0.1	1.9	197.0	2.1
47	FI-Si2	2016	43.9	284.9	0.1	1.8	166.0	2.0
48	FI-Sii	2013	119.0	282.5	0.0	3.7	185.7	3.7
49	FI-Sii	2014	100.3	294.4	0.0	2.4	199.7	2.4
50	FI-Sii	2015	84.6	321.9	0.1	2.6	204.3	2.7
51	FI-Sii	2016	118.7	284.1	0.1	3.4	200.0	3.5
52	FI-Sii	2017	117.5	290.5	0.1	3.0	206.0	3.1
53	FI-Sii	2018	113.6	295.6	0.0	2.3	185.0	2.4
54	HK-MPM	2016	NaN	NaN	NaN	NaN	NaN	NaN
55	HK-MPM	2017	NaN	NaN	NaN	NaN	NaN	NaN
56	HK-MPM	2018	NaN	NaN	NaN	NaN	NaN	NaN
57	ID-Pag	2016	NaN	NaN	NaN	NaN	NaN	NaN
58	JP-BBY	2015	123.6	304.3	0.2	5.3	203.4	5.6
59	JP-BBY	2016	114.1	302.4	0.0	7.9	203.2	8.0
60	JP-BBY	2017	119.9	300.4	0.0	7.6	199.8	7.6
61	JP-BBY	2018	96.3	311.6	0.0	5.4	217.0	5.5
62	JP-Mse	2012	144.6	266.9	0.6	9.8	209.7	10.4
63	KR-CRK	2015	135.0	267.8	0.1	10.7	202.1	10.8
64	KR-CRK	2016	137.2	262.4	0.1	12.4	198.8	12.5
65	KR-CRK	2017	143.3	266.2	0.1	12.2	193.5	12.3
66	KR-CRK	2018	139.0	263.8	0.2	11.0	198.0	11.1
67	MY-MLM	2014	180.0	437.9	8.5	2.7	272.6	11.2
68	MY-MLM	2015	194.2	NaN	8.8	8.3	271.1	17.1
69	NZ-Kop	2012	38.7	334.9	1.3	2.5	194.8	3.8
70	NZ-Kop	2013	58.1	351.6	1.5	2.6	190.0	4.1
71	NZ-Kop	2014	42.2	355.0	1.4	2.8	209.0	4.2
72	NZ-Kop	2015	44.3	366.2	1.2	3.3	193.0	4.5
73	PH-RiF	2012	NaN	NaN	NaN	NaN	NaN	NaN
74	PH-RiF	2013	NaN	NaN	NaN	NaN	NaN	NaN
75	PH-RiF	2014	NaN	NaN	NaN	NaN	NaN	NaN
76	PH-RiF	2015	NaN	NaN	NaN	NaN	NaN	NaN
77	RU-Ch2	2014	142.9	252.8	0.0	5.1	210.3	5.1
78	RU-Ch2	2015	157.5	247.9	0.0	5.0	202.6	5.0
79	RU-Ch2	2016	145.3	257.9	0.0	4.1	201.5	4.1
80	RU-Che	2014	161.7	258.8	0.1	5.5	206.9	5.6
81	RU-Che	2015	157.0	250.3	0.0	5.4	203.3	5.4
82	RU-Che	2016	140.6	258.3	−0.1	6.9	188.6	6.8
83	SE-Deg	2014	115.4	285.9	0.0	2.8	196.3	2.8
84	SE-Deg	2015	113.5	278.7	0.0	2.7	203.4	2.7
85	SE-Deg	2016	118.8	290.3	0.0	2.3	195.5	2.3
86	SE-Deg	2017	121.9	276.1	0.0	2.4	199.0	2.5

Table B5. Continued.

	SITE _ID	Year	Start_GPP _DT_(DOY)	End_GPP _DT_(DOY)	Base_value_GPP _DT_(µmolCO2/m2/s)	Ampl_GPP_DT _(µmolCO2/m2/s)	Peak_GPP_DT _(DOY)	Peak_value_GPP _DT_(µmolCO2/m2/s)
87	SE-Deg	2018	118.5	276.6	0.0	1.7	188.0	1.7
88	US-Atq	2013	33.2	256.5	0.0	3.1	161.7	3.1
89	US-Atq	2014	139.1	244.9	0.1	1.8	194.3	1.9
90	US-Atq	2015	132.8	244.0	0.1	3.4	191.0	3.5
91	US-Beo	2013	39.3	285.3	0.0	0.9	159.8	0.9
92	US-Beo	2014	88.2	261.5	0.0	2.0	200.0	2.0
93	US-Bes	2013	49.4	269.4	0.0	0.8	187.9	0.9
94	US-Bes	2014	174.6	262.2	0.0	1.6	220.7	1.6
95	US-Bes	2015	160.5	248.8	0.0	2.5	198.4	2.6
96	US-BZB	2014	NaN	NaN	NaN	NaN	NaN	NaN
97	US-BZB	2015	NaN	NaN	NaN	NaN	NaN	NaN
98	US-BZB	2016	NaN	NaN	NaN	NaN	NaN	NaN
99	US-BZF	2014	132.7	201.3	0.2	5.8	167.5	6.0
100	US-BZF	2015	129.1	258.7	0.2	6.9	187.5	7.1
101	US-BZF	2016	128.6	228.0	0.2	9.1	175.0	9.3
102	US-BZS	2015	NaN	NaN	NaN	NaN	NaN	NaN
103	US-BZS	2016	NaN	NaN	NaN	NaN	NaN	NaN
104	US-DPW	2013	NaN	NaN	NaN	NaN	NaN	NaN
105	US-DPW	2014	55.7	332.1	0.6	4.6	183.5	5.2
106	US-DPW	2015	53.7	372.9	0.7	4.8	174.8	5.5
107	US-DPW	2016	71.2	343.9	0.8	4.8	197.0	5.7
108	US-HRA	2017	131.3	244.8	0.4	20.1	183.1	20.5
109	US-HRC	2018	135.7	237.6	1.3	18.8	182.2	20.1
110	US-ICs	2014	150.4	253.4	0.2	3.5	201.6	3.7
111	US-ICs	2015	142.8	263.2	0.2	4.4	189.9	4.6
112	US-ICs	2016	154.4	245.7	0.1	3.2	192.8	3.3
113	US-Ivo	2013	149.1	258.0	0.1	3.9	201.9	3.9
114	US-Ivo	2014	151.6	257.8	0.1	3.6	199.1	3.7
115	US-Ivo	2015	121.7	248.3	0.1	4.0	187.1	4.0
116	US-Ivo	2016	154.7	254.5	0.1	5.3	194.0	5.4
117	US-LA1	2012	−8.0	216.9	0.5	2.3	142.8	2.8
118	US-LA2	2012	47.0	334.0	0.3	5.6	146.8	6.0
119	US-LA2	2013	93.7	335.8	0.3	6.9	166.3	7.3
120	US-Los	2014	131.4	288.1	0.0	6.7	198.2	6.6
121	US-Los	2015	130.4	288.1	0.1	6.3	201.5	6.4
122	US-Los	2016	130.9	291.5	0.2	7.2	198.2	7.3
123	US-Los	2017	136.0	292.4	0.1	7.4	199.0	7.5
124	US-Los	2018	135.0	285.6	0.1	7.2	199.0	7.3
125	US-MAC	2013	NaN	378.1	2.5	5.4	222.7	9.5

Earth Syst. Sci. Data, 13, 3607–3689, 2021 https://doi.org/10.5194/essd-13-3607-2021

Table B5. Continued.

	SITE _ID	Year	Start_GPP _DT_(DOY)	End_GPP _DT_(DOY)	Base_value_GPP _DT_(µmolCO2/m2/s)	Ampl_GPP_DT _(µmolCO2/m2/s)	Peak_GPP_DT _(DOY)	Peak_value_GPP _DT_(µmolCO2/m2/s)
126	US-MAC	2014	47.0	334.2	2.5	9.2	180.7	11.7
127	US-MAC	2015	46.5	356.6	2.9	5.9	154.1	8.8
128	US-Myb	2010	28.6	305.2	0.6	1.4	183.4	2.0
129	US-Myb	2011	200.4	367.3	0.3	3.6	265.5	3.9
130	US-Myb	2012	88.4	331.9	−0.1	13.7	204.5	13.6
131	US-Myb	2013	47.4	341.9	−0.1	8.0	200.0	7.8
132	US-Myb	2014	86.8	310.7	0.2	8.2	168.0	8.4
133	US-Myb	2015	76.1	323.2	0.2	7.3	202.0	7.5
134	US-Myb	2016	24.1	328.4	0.0	4.0	176.0	4.0
135	US-Myb	2017	67.5	395.2	−0.2	5.8	202.0	5.5
136	US-Myb	2018	83.7	331.3	−0.3	10.5	201.0	10.3
137	US-NC4	2012	NaN	NaN	NaN	NaN	NaN	NaN
138	US-NC4	2013	94.4	304.8	0.8	7.0	181.0	7.7
139	US-NC4	2014	97.5	354.5	0.6	6.1	173.7	6.7
140	US-NC4	2015	92.0	315.1	0.7	9.7	185.0	10.5
141	US-NC4	2016	99.6	327.0	0.9	8.2	183.0	9.1
142	US-ORv	2011	88.8	316.4	−0.1	7.4	180.4	7.3
143	US-ORv	2012	93.5	303.4	0.3	9.3	181.0	9.6
144	US-ORv	2013	107.6	305.2	0.4	10.1	192.4	10.5
145	US-ORv	2014	109.3	299.2	0.2	10.1	190.0	10.4
146	US-ORv	2015	105.0	301.6	0.3	9.6	194.0	9.9
147	US-OWC	2015	NaN	301.4	0.3	6.7	151.3	7.0
148	US-OWC	2016	116.0	309.2	0.3	6.4	204.0	6.7
149	US-Sne	2016	−21.8	306.2	0.3	8.0	190.3	8.3
150	US-Sne	2017	NaN	NaN	NaN	NaN	NaN	NaN
151	US-Sne	2018	84.6	370.3	0.3	2.4	202.0	2.8
152	US-Srr	2014	47.0	307.5	0.8	6.0	175.6	6.8
153	US-Srr	2015	35.5	320.9	0.3	8.0	158.6	8.3
154	US-Srr	2016	44.8	318.9	0.4	8.9	170.8	9.2
155	US-Srr	2017	56.8	309.8	0.3	10.5	185.0	10.8
156	US-StJ	2016	120.7	280.7	1.3	12.0	193.8	13.3
157	US-Tw1	2011	NaN	NaN	NaN	NaN	NaN	NaN
158	US-Tw1	2012	102.1	325.5	0.0	12.8	216.1	12.8
159	US-Tw1	2013	98.3	338.0	−0.2	13.1	208.4	12.9
160	US-Tw1	2014	95.7	326.3	0.1	10.5	208.0	10.6
161	US-Tw1	2015	105.5	344.1	0.3	9.9	215.0	10.1
162	US-Tw1	2016	91.8	313.1	0.0	10.1	209.0	10.1
163	US-Tw1	2017	93.4	329.8	0.0	11.3	214.0	11.2
164	US-Tw1	2018	119.0	363.8	0.0	12.7	217.0	12.7

Table B5. Continued.

	SITE _ID	Year	Start_GPP _DT_(DOY)	End_GPP _DT_(DOY)	Base_value_GPP _DT_(µmolCO2/m2/s)	Ampl_GPP_DT _(µmolCO2/m2/s)	Peak_GPP_DT _(DOY)	Peak_value_GPP _DT_(µmolCO2/m2/s)
165	US-Tw4	2014	160.0	363.2	0.0	4.7	236.6	4.7
166	US-Tw4	2015	57.2	335.9	0.0	8.1	213.0	8.1
167	US-Tw4	2016	76.1	311.3	0.2	8.2	185.0	8.4
168	US-Tw4	2017	100.2	332.9	0.1	8.8	214.0	8.9
169	US-Tw4	2018	98.4	337.8	0.0	11.8	206.0	11.9
170	US-Tw5	2018	115.9	321.3	1.8	6.7	231.1	8.5
171	US-Twt	2009	150.0	293.0	0.2	12.5	212.0	12.7
172	US-Twt	2010	141.1	311.9	0.1	13.7	224.4	13.8
173	US-Twt	2011	158.5	288.7	0.1	14.2	215.9	14.3
174	US-Twt	2012	166.8	308.8	0.2	12.3	233.0	12.5
175	US-Twt	2013	138.2	272.4	0.3	16.7	202.0	17.0
176	US-Twt	2014	148.1	281.4	0.2	15.0	205.0	15.2
177	US-Twt	2015	137.1	277.2	0.2	11.5	218.0	11.7
178	US-Twt	2016	169.1	289.9	0.3	13.8	224.0	14.1
179	US-Uaf	2011	114.6	283.5	0.1	6.0	196.9	6.2
180	US-Uaf	2012	88.0	271.2	0.2	6.6	187.3	6.8
181	US-Uaf	2013	124.1	271.6	0.2	5.8	192.1	6.0
182	US-Uaf	2014	84.6	269.3	0.1	5.3	188.0	5.5
183	US-Uaf	2015	90.5	264.3	0.1	5.2	196.0	5.3
184	US-Uaf	2016	103.1	270.8	0.1	4.7	192.0	4.8
185	US-Uaf	2017	102.3	275.6	0.1	6.1	198.0	6.2
186	US-Uaf	2018	111.6	291.5	0.0	5.6	190.0	5.6
187	US-WPT	2011	135.0	285.6	0.2	7.4	206.1	7.7
188	US-WPT	2012	129.0	293.7	0.1	7.0	205.9	7.0
189	US-WPT	2013	134.9	278.1	0.0	6.2	200.9	6.2

Earth Syst. Sci. Data, 13, 3607–3689, 2021

https://doi.org/10.5194/essd-13-3607-2021

Table B5. Continued.

	SITE_ID	Year	Probe_name	Soil_temp_depth_m	Start_TS_(DOY)	End_TS_(DOY)	Base_value_TS_(C)	Ampl_TS_(C)	Peak_TS_(DOY)	Peak_value_TS_(C)
1	AT-Neu	2010	TS_1	−0.1	61.3	339.4	0.2	17.5	200.9	17.7
2	AT-Neu	2011	TS_1	−0.1	51.0	328.8	0.4	16.4	201.0	16.8
3	AT-Neu	2012	TS_1	−0.1	61.1	341.9	0.7	17.6	202.9	18.3
4	BR-Npw	2014	NaN	NaN	NaN	NaN	NaN	NaN	NaN	NaN
5	BR-Npw	2015	NaN	NaN	NaN	NaN	NaN	NaN	NaN	NaN
6	BR-Npw	2016	TS_1	NaN	18.4	343.2	22.4	6.0	188.0	28.4
7	BW-Gum	2018	NaN	NaN	NaN	NaN	NaN	NaN	NaN	NaN
8	BW-Gum	2019	NaN	NaN	NaN	NaN	NaN	NaN	NaN	NaN
9	BW-Nxr	2018	NaN	NaN	NaN	NaN	NaN	NaN	NaN	NaN
10	CA-SCB	2014	TS_1	0.0	105.9	292.2	−0.6	20.6	196.6	20.0
11	CA-SCB	2015	TS_1	0.0	106.9	287.1	−0.4	17.2	186.8	16.8
12	CA-SCB	2016	TS_1	0.0	101.6	284.1	−0.3	19.1	193.2	18.8
13	CA-SCB	2017	TS_1	0.0	107.4	289.7	−0.3	17.7	198.0	17.4
14	CA-SCC	2013	NaN	NaN	NaN	NaN	NaN	NaN	NaN	NaN
15	CA-SCC	2014	TS_1	−0.1	123.4	287.1	−0.5	15.6	203.0	15.1
16	CA-SCC	2015	TS_1	−0.1	113.9	285.2	−0.3	16.3	189.2	16.0
17	CA-SCC	2016	TS_1	−0.1	108.1	260.1	−0.3	18.4	190.9	18.0
18	DE-Dgw	2015	NaN	NaN	NaN	NaN	NaN	NaN	NaN	NaN
19	DE-Dgw	2016	NaN	NaN	NaN	NaN	NaN	NaN	NaN	NaN
20	DE-Dgw	2017	NaN	NaN	NaN	NaN	NaN	NaN	NaN	NaN
21	DE-Hte	2011	NaN	NaN	NaN	NaN	NaN	NaN	NaN	NaN
22	DE-Hte	2012	TS_3	−0.2	77.0	344.0	5.0	12.3	215.5	17.2
23	DE-Hte	2013	TS_3	−0.2	60.9	378.0	4.0	12.0	207.9	16.0
24	DE-Hte	2014	TS_1	0.0	NaN	327.8	8.5	8.3	205.6	16.9
25	DE-Hte	2015	TS_1	0.0	62.9	360.6	5.2	11.7	187.4	16.8
26	DE-Hte	2016	TS_1	0.0	71.9	NaN	4.9	12.4	175.6	17.3
27	DE-Hte	2017	TS_1	0.0	61.6	343.3	4.5	11.8	186.0	16.3
28	DE-Hte	2018	NaN	NaN	NaN	NaN	NaN	NaN	NaN	NaN
29	DE-SfN	2012	TS_1	0.0	NaN	372.6	0.0	23.6	206.5	15.3
30	DE-SfN	2013	TS_1	0.0	55.8	381.5	0.9	13.6	216.4	14.5
31	DE-SfN	2014	NaN	NaN	NaN	NaN	NaN	NaN	NaN	NaN
32	DE-Zrk	2013	NaN	NaN	NaN	NaN	NaN	NaN	NaN	NaN
33	DE-Zrk	2014	TS_1	−0.1	54.8	361.6	4.4	13.9	202.3	18.3
34	DE-Zrk	2015	TS_1	−0.1	58.3	359.3	4.3	13.2	215.5	17.5
35	DE-Zrk	2016	TS_1	−0.1	72.8	332.0	4.3	14.9	200.4	19.2
36	DE-Zrk	2017	TS_1	−0.1	69.1	351.4	4.4	14.7	199.0	19.1
37	DE-Zrk	2018	TS_1	−0.1	84.5	336.1	4.8	12.3	203.0	17.1
38	FI-Lom	2006	TS_1	−0.1	114.1	290.8	−0.1	13.4	204.8	13.3
39	FI-Lom	2007	TS_1	−0.1	126.8	302.0	0.1	13.1	200.0	13.2
40	FI-Lom	2008	TS_1	−0.1	135.6	296.7	0.2	12.7	202.9	12.9
41	FI-Lom	2009	TS_1	−0.1	117.2	291.9	0.1	11.7	214.0	11.9
42	FI-Lom	2010	TS_1	−0.1	129.9	318.5	0.0	12.1	208.0	12.2
43	FI-Si2	2012	TS_1	−0.1	NaN	323.5	0.0	19.9	204.6	16.0
44	FI-Si2	2013	TS_1	−0.1	106.9	341.0	−0.1	16.0	199.4	16.0
45	FI-Si2	2014	TS_1	−0.1	104.6	331.1	0.0	17.1	208.5	17.0
46	FI-Si2	2015	TS_1	−0.1	76.5	352.3	−0.9	16.3	211.0	15.4

Table B5. Continued.

	SITE_ID	Year	Probe_name	Soil_temp_depth_m	Start_TS_(DOY)	End_TS_(DOY)	Base_value_TS_(C)	Ampl_TS_(C)	Peak_TS_(DOY)	Peak_value_TS_(C)
47	FI-Si2	2016	TS_1	−0.1	102.6	329.4	−0.9	16.5	206.0	15.6
48	FI-Sii	2013	NaN	NaN	NaN	NaN	NaN	NaN	NaN	NaN
49	FI-Sii	2014	NaN	NaN	NaN	NaN	NaN	NaN	NaN	NaN
50	FI-Sii	2015	NaN	NaN	NaN	NaN	NaN	NaN	NaN	NaN
51	FI-Sii	2016	NaN	NaN	NaN	NaN	NaN	NaN	NaN	NaN
52	FI-Sii	2017	NaN	NaN	NaN	NaN	NaN	NaN	NaN	NaN
53	FI-Sii	2018	NaN	NaN	NaN	NaN	NaN	NaN	NaN	NaN
54	HK-MPM	2016	TS_2	NaN	NaN	566.9	0.0	7.8	219.8	28.9
55	HK-MPM	2017	TS_2	NaN	NaN	NaN	0.0	8.7	218.5	29.1
56	HK-MPM	2018	TS_2	NaN	NaN	NaN	0.0	7.2	204.9	28.7
57	ID-Pag	2016	NaN	NaN	NaN	NaN	NaN	NaN	NaN	NaN
58	JP-BBY	2015	TS_1	−0.2	87.8	340.8	0.9	21.6	218.1	22.5
59	JP-BBY	2016	TS_1	−0.2	80.8	330.6	0.4	22.2	217.8	22.6
60	JP-BBY	2017	TS_1	−0.2	80.4	347.8	0.2	21.8	213.8	22.0
61	JP-BBY	2018	TS_1	−0.2	78.3	355.4	0.5	20.4	222.0	20.9
62	JP-Mse	2012	TS_1	0.0	60.4	348.9	2.1	23.8	211.8	25.9
63	KR-CRK	2015	NaN	NaN	NaN	NaN	NaN	NaN	NaN	NaN
64	KR-CRK	2016	NaN	NaN	NaN	NaN	NaN	NaN	NaN	NaN
65	KR-CRK	2017	NaN	NaN	NaN	NaN	NaN	NaN	NaN	NaN
66	KR-CRK	2018	NaN	NaN	NaN	NaN	NaN	NaN	NaN	NaN
67	MY-MLM	2014	TS	NaN	NaN	358.4	25.1	4.0	194.5	29.0
68	MY-MLM	2015	TS	NaN	27.3	NaN	25.6	2.0	172.7	27.6
69	NZ-Kop	2012	TS_1	−0.5	62.5	360.3	8.3	8.4	219.8	16.7
70	NZ-Kop	2013	TS_1	−0.5	45.6	367.0	8.4	7.6	210.5	16.0
71	NZ-Kop	2014	TS_1	−0.5	56.9	365.7	8.2	8.8	219.0	17.0
72	NZ-Kop	2015	TS_1	−0.5	56.5	371.8	7.7	9.4	214.0	17.1
73	PH-RiF	2012	NaN	NaN	NaN	NaN	NaN	NaN	NaN	NaN
74	PH-RiF	2013	NaN	NaN	NaN	NaN	NaN	NaN	NaN	NaN
75	PH-RiF	2014	NaN	NaN	NaN	NaN	NaN	NaN	NaN	NaN
76	PH-RiF	2015	NaN	NaN	NaN	NaN	NaN	NaN	NaN	NaN
77	RU-Ch2	2014	TS_1	0.0	138.8	263.8	−0.1	14.4	206.6	14.3
78	RU-Ch2	2015	TS_1	0.0	143.9	269.6	−0.1	14.0	193.3	13.8
79	RU-Ch2	2016	TS_1	0.0	127.0	273.5	−0.2	11.6	200.2	11.5
80	RU-Che	2014	TS_1	0.0	138.0	267.6	−0.1	15.0	208.0	14.9
81	RU-Che	2015	TS_1	0.0	143.8	274.7	−0.2	14.8	193.7	14.6
82	RU-Che	2016	TS_1	0.0	126.7	274.0	−0.2	13.0	200.4	12.8
83	SE-Deg	2014	TS_1	0.0	111.8	303.6	−0.5	17.2	201.6	16.7
84	SE-Deg	2015	TS_1	0.0	104.2	310.6	−0.3	15.2	207.2	14.9
85	SE-Deg	2016	TS_1	0.0	108.1	306.4	−0.2	14.9	200.3	14.7
86	SE-Deg	2017	TS_1	0.0	133.4	326.9	−0.2	12.4	215.0	12.2
87	SE-Deg	2018	TS_1	0.0	111.7	310.2	−0.2	14.7	198.0	14.5
88	US-Atq	2013	NaN	NaN	NaN	NaN	NaN	NaN	NaN	NaN
89	US-Atq	2014	TS_1	NaN	10.7	139.5	−0.2	8.1	61.0	7.9
90	US-Atq	2015	NaN	NaN	NaN	NaN	NaN	NaN	NaN	NaN
91	US-Beo	2013	NaN	NaN	NaN	NaN	NaN	NaN	NaN	NaN
92	US-Beo	2014	TS_1	NaN	155.1	270.1	0.0	4.9	211.1	4.8
93	US-Bes	2013	TS_1	NaN	143.2	262.0	0.0	5.6	201.3	5.6

Earth Syst. Sci. Data, 13, 3607–3689, 2021 https://doi.org/10.5194/essd-13-3607-2021

Table B5. Continued.

	SITE_ID	Year	Probe_name	Soil_temp_depth_m	Start_TS_(DOY)	End_TS_(DOY)	Base_value_TS_(C)	Ampl_TS_(C)	Peak_TS_(DOY)	Peak_value_TS_(C)
94	US-Bes	2014	TS_1	NaN	151.8	282.3	−0.1	3.9	198.5	3.8
95	US-Bes	2015	TS_1	NaN	140.4	271.0	−0.1	4.8	195.3	4.7
96	US-BZB	2014	TS_1	−0.1	123.1	298.4	−0.4	15.4	215.8	14.9
97	US-BZB	2015	TS_1	−0.1	107.8	295.6	−0.4	14.0	210.2	13.7
98	US-BZB	2016	TS_1	−0.1	125.1	292.4	−0.3	16.4	214.3	16.1
99	US-BZF	2014	TS_1	−0.1	96.1	322.8	−1.6	16.1	205.4	14.6
100	US-BZF	2015	TS_1	−0.1	108.4	331.1	−1.2	14.9	197.5	13.7
101	US-BZF	2016	TS_1	−0.1	95.5	315.9	−1.0	17.2	205.1	16.2
102	US-BZS	2015	TS_1	NaN	116.5	275.2	−0.1	4.9	202.9	4.8
103	US-BZS	2016	TS_1	NaN	119.1	278.9	0.0	5.6	208.4	5.5
104	US-DPW	2013	NaN	NaN	NaN	NaN	NaN	NaN	NaN	NaN
105	US-DPW	2014	NaN	NaN	NaN	NaN	NaN	NaN	NaN	NaN
106	US-DPW	2015	NaN	NaN	NaN	NaN	NaN	NaN	NaN	NaN
107	US-DPW	2016	NaN	NaN	NaN	NaN	NaN	NaN	NaN	NaN
108	US-HRA	2017	NaN	NaN	NaN	NaN	NaN	NaN	NaN	NaN
109	US-HRC	2018	NaN	NaN	NaN	NaN	NaN	NaN	NaN	NaN
110	US-ICs	2014	TS_1	−0.1	147.3	263.1	−0.1	5.5	205.6	5.4
111	US-ICs	2015	TS_1	−0.1	141.6	255.7	0.0	6.1	195.2	6.1
112	US-ICs	2016	TS_1	−0.1	146.7	265.9	0.0	5.7	206.2	5.6
113	US-Ivo	2013	NaN	NaN	NaN	NaN	NaN	NaN	NaN	NaN
114	US-Ivo	2014	TS_1	−0.1	136.9	264.3	−0.2	10.8	195.7	10.6
115	US-Ivo	2015	TS_1	−0.1	139.4	257.1	−0.1	14.9	185.6	14.7
116	US-Ivo	2016	TS_1	−0.1	133.6	262.4	−0.1	8.9	197.3	8.8
117	US-LA1	2012	TS_1	−0.1	29.1	331.4	15.6	13.5	197.2	29.1
118	US-LA2	2012	TS_1	−0.1	36.6	336.1	15.0	14.4	193.2	29.4
119	US-LA2	2013	TS_1	−0.1	65.8	377.9	14.7	16.1	201.5	30.8
120	US-Los	2014	TS_1	0.0	136.2	417.4	2.0	8.3	244.3	10.2
121	US-Los	2015	TS_1	0.0	148.2	422.3	2.4	7.8	258.7	10.2
122	US-Los	2016	TS_1	0.0	135.2	415.7	2.5	8.1	255.1	10.6
123	US-Los	2017	TS_1	0.0	141.1	414.6	1.9	7.5	256.0	9.3
124	US-Los	2018	TS_1	0.0	169.8	421.8	1.5	7.4	260.0	8.9
125	US-MAC	2013	NaN	NaN	NaN	NaN	NaN	NaN	NaN	NaN
126	US-MAC	2014	NaN	NaN	NaN	NaN	NaN	NaN	NaN	NaN
127	US-MAC	2015	NaN	NaN	NaN	NaN	NaN	NaN	NaN	NaN
128	US-Myb	2010	NaN	NaN	NaN	NaN	NaN	NaN	NaN	NaN
129	US-Myb	2011	TS_3	−0.1	NaN	329.5	12.1	8.9	231.7	21.0
130	US-Myb	2012	TS_3	−0.1	35.6	372.2	9.4	11.0	216.1	20.4
131	US-Myb	2013	TS_3	−0.1	34.4	354.7	9.2	11.3	210.9	20.5
132	US-Myb	2014	TS_3	−0.1	26.0	365.9	9.6	12.3	210.0	21.9
133	US-Myb	2015	TS_3	−0.1	17.3	340.7	9.8	11.9	212.0	21.6
134	US-Myb	2016	TS_3	−0.1	5.1	357.8	9.6	11.2	201.0	20.8
135	US-Myb	2017	TS_3	−0.1	27.3	352.9	9.9	13.1	214.0	23.0
136	US-Myb	2018	TS_3	−0.1	36.3	326.1	10.2	10.7	207.0	20.9
137	US-NC4	2012	TS_1	−0.1	42.4	336.0	7.9	15.8	215.4	23.6
138	US-NC4	2013	TS_1	−0.1	60.0	368.8	6.9	16.8	210.5	23.7
139	US-NC4	2014	TS_1	−0.1	54.4	362.3	6.7	16.8	208.5	23.5

Table B5. Continued.

	SITE_ID	Year	Probe_name	Soil_temp_depth_m	Start_TS_(DOY)	End_TS_(DOY)	Base_value_TS_(C)	Ampl_TS_(C)	Peak_TS_(DOY)	Peak_value_TS_(C)
140	US-NC4	2015	TS_1	−0.1	68.1	387.3	8.3	16.1	205.0	24.3
141	US-NC4	2016	TS_1	−0.1	53.0	351.4	9.4	15.0	220.0	24.5
142	US-ORv	2011	NaN	NaN	NaN	NaN	NaN	NaN	NaN	NaN
143	US-ORv	2012	TS	NaN	57.4	352.6	4.4	20.6	203.9	25.0
144	US-ORv	2013	TS	NaN	63.7	356.7	2.9	20.0	210.8	22.9
145	US-ORv	2014	TS	NaN	68.1	365.0	2.1	20.2	205.3	22.3
146	US-ORv	2015	TS	NaN	68.8	387.8	1.8	21.3	206.0	23.0
147	US-OWC	2015	NaN	NaN	NaN	NaN	NaN	NaN	NaN	NaN
148	US-OWC	2016	TS_1	−0.1	0.0	0.0	0.0	0.0	211.2	23.9
149	US-Sne	2016	NaN	NaN	NaN	NaN	NaN	NaN	NaN	NaN
150	US-Sne	2017	TS_1	0.0	46.1	337.9	10.3	13.1	212.7	23.5
151	US-Sne	2018	TS_1	0.0	48.4	325.1	10.3	12.2	217.3	22.4
152	US-Srr	2014	NaN	NaN	NaN	NaN	NaN	NaN	NaN	NaN
153	US-Srr	2015	NaN	NaN	NaN	NaN	NaN	NaN	NaN	NaN
154	US-Srr	2016	TS_1	NaN	NaN	326.3	10.0	10.7	200.5	20.7
155	US-Srr	2017	TS_1	NaN	11.3	346.8	7.2	13.7	199.5	20.9
156	US-StJ	2016	TS_2	−0.1	68.4	347.4	4.1	16.2	213.7	20.3
157	US-Tw1	2011	NaN	NaN	NaN	NaN	NaN	NaN	NaN	NaN
158	US-Tw1	2012	TS_1	0.0	50.5	360.0	6.0	11.5	225.2	17.5
159	US-Tw1	2013	TS_1	0.0	35.8	337.6	4.4	14.6	206.6	19.0
160	US-Tw1	2014	TS_1	0.0	41.2	395.4	6.7	10.9	208.3	17.6
161	US-Tw1	2015	TS_1	0.0	50.7	342.5	9.0	7.8	235.0	16.9
162	US-Tw1	2016	TS_1	0.0	34.6	361.1	8.8	7.9	218.0	16.7
163	US-Tw1	2017	TS_1	0.0	41.2	343.7	7.5	10.2	228.0	17.8
164	US-Tw1	2018	TS_1	0.0	60.5	327.4	6.7	10.4	222.0	17.1
165	US-Tw4	2014	NaN	NaN	NaN	NaN	NaN	NaN	NaN	NaN
166	US-Tw4	2015	TS_1	0.0	15.9	327.2	10.0	11.6	199.4	21.6
167	US-Tw4	2016	TS_1	0.0	9.6	358.7	8.2	11.3	201.7	19.5
168	US-Tw4	2017	TS_1	0.0	38.3	347.3	8.1	11.5	211.9	19.6
169	US-Tw4	2018	TS_1	0.0	58.1	344.9	8.0	10.9	218.0	18.9
170	US-Tw5	2018	TS_1	0.0	NaN	414.8	0.0	8.9	222.2	18.4
171	US-Twt	2009	NaN	NaN	NaN	NaN	NaN	NaN	NaN	NaN
172	US-Twt	2010	NaN	NaN	NaN	NaN	NaN	NaN	NaN	NaN
173	US-Twt	2011	NaN	NaN	NaN	NaN	NaN	NaN	NaN	NaN
174	US-Twt	2012	NaN	NaN	NaN	NaN	NaN	NaN	NaN	NaN
175	US-Twt	2013	NaN	NaN	NaN	NaN	NaN	NaN	NaN	NaN
176	US-Twt	2014	NaN	NaN	NaN	NaN	NaN	NaN	NaN	NaN
177	US-Twt	2015	NaN	NaN	NaN	NaN	NaN	NaN	NaN	NaN
178	US-Twt	2016	NaN	NaN	NaN	NaN	NaN	NaN	NaN	NaN
179	US-Uaf	2011	TS_1	−0.1	86.2	372.5	−12.3	22.0	199.6	9.7

Earth Syst. Sci. Data, 13, 3607–3689, 2021 https://doi.org/10.5194/essd-13-3607-2021

Table B5. Continued.

	SITE_ID	Year	Probe_name	Soil_temp_depth_m	Start_TS_(DOY)	End_TS_(DOY)	Base_value_TS_(C)	Ampl_TS_(C)	Peak_TS_(DOY)	Peak_value_TS_(C)
180	US-Uaf	2012	TS_1	−0.1	73.8	338.5	−11.8	20.9	202.4	9.0
181	US-Uaf	2013	TS_1	−0.1	109.6	395.5	−10.1	20.5	200.4	10.4
182	US-Uaf	2014	TS_1	−0.1	76.1	365.4	−10.9	19.9	206.0	9.0
183	US-Uaf	2015	TS_1	−0.1	81.0	423.2	-9.8	19.8	190.0	10.0
184	US-Uaf	2016	TS_1	−0.1	77.4	315.8	−7.7	19.1	198.0	11.4
185	US-Uaf	2017	TS_1	−0.1	84.9	380.2	−7.4	19.1	196.0	11.7
186	US-Uaf	2018	TS_1	−0.1	96.0	333.3	−5.6	17.7	199.0	12.1
187	US-WPT	2011	TS_1	−0.1	81.0	342.2	5.3	19.3	202.6	24.5
188	US-WPT	2012	TS_1	−0.1	40.3	345.6	3.7	21.6	197.4	25.3
189	US-WPT	2013	TS_1	−0.1	74.6	340.5	3.7	18.2	207.2	22.0

Table B5. Continued.

	SITE_ID	Year	Start_TA_(DOY)	End_TA_(DOY)	Base_value_TA_(C)	Ampl_TA_(C)	Peak_TA_(DOY)	Peak_value_TA_(C)
1	AT-Neu	2010	43.2	351.7	−4.8	20.9	195.9	16.1
2	AT-Neu	2011	18.5	359.9	−5.1	20.6	198.5	15.5
3	AT-Neu	2012	38.0	366.6	−5.6	22.4	197.2	16.8
4	BR-Npw	2014	NaN	NaN	NaN	NaN	NaN	NaN
5	BR-Npw	2015	NaN	NaN	NaN	NaN	NaN	NaN
6	BR-Npw	2016	7.5	348.7	19.6	7.5	211.0	27.1
7	BW-Gum	2018	NaN	NaN	NaN	NaN	NaN	NaN
8	BW-Gum	2019	NaN	NaN	NaN	NaN	NaN	NaN
9	BW-Nxr	2018	NaN	NaN	NaN	NaN	NaN	NaN
10	CA-SCB	2014	60.2	335.3	−23.3	41.3	197.4	18.0
11	CA-SCB	2015	45.1	360.8	−21.8	39.1	186.4	17.4
12	CA-SCB	2016	49.8	335.8	−18.9	37.3	193.9	18.4
13	CA-SCB	2017	64.7	327.3	−18.5	36.0	201.0	17.5
14	CA-SCC	2013	67.6	338.2	−21.1	39.1	203.8	18.1
15	CA-SCC	2014	54.1	337.8	−22.3	41.0	196.7	18.7
16	CA-SCC	2015	46.4	359.4	−20.1	37.9	187.1	17.8
17	CA-SCC	2016	47.3	350.2	−18.8	37.7	194.0	18.9
18	DE-Dgw	2015	72.5	347.6	2.2	16.3	203.8	18.4
19	DE-Dgw	2016	64.5	324.7	1.3	17.4	205.4	18.7
20	DE-Dgw	2017	43.8	375.3	−0.2	18.5	202.2	18.3
21	DE-Hte	2011	NaN	NaN	NaN	NaN	NaN	NaN
22	DE-Hte	2012	50.3	352.5	0.8	17.0	207.6	17.8
23	DE-Hte	2013	83.5	365.3	1.6	17.1	202.5	18.7
24	DE-Hte	2014	48.7	352.5	2.9	15.8	213.0	18.7
25	DE-Hte	2015	57.6	366.3	2.6	15.3	211.0	17.9
26	DE-Hte	2016	67.5	323.1	2.7	16.0	211.0	18.8
27	DE-Hte	2017	58.9	370.1	1.8	16.2	212.0	18.0
28	DE-Hte	2018	74.5	368.0	0.9	19.1	203.0	20.1
29	DE-SfN	2012	54.9	355.2	−2.1	20.3	196.3	18.2
30	DE-SfN	2013	64.6	344.0	−0.3	18.6	202.8	18.2
31	DE-SfN	2014	NaN	NaN	NaN	NaN	NaN	NaN
32	DE-Zrk	2013	NaN	NaN	NaN	NaN	NaN	NaN
33	DE-Zrk	2014	NaN	NaN	NaN	NaN	NaN	NaN
34	DE-Zrk	2015	49.7	355.4	2.1	15.3	203.4	17.5
35	DE-Zrk	2016	63.3	323.8	1.9	16.5	204.0	18.3
36	DE-Zrk	2017	45.2	372.5	0.5	17.4	205.0	17.9
37	DE-Zrk	2018	75.8	358.9	−0.1	18.8	190.0	18.7
38	FI-Lom	2006	72.5	355.6	−12.2	26.7	195.0	14.5
39	FI-Lom	2007	56.2	372.5	−11.0	22.6	193.4	11.6
40	FI-Lom	2008	73.5	348.1	−10.4	22.3	200.4	12.0
41	FI-Lom	2009	56.7	356.3	−13.6	27.1	205.0	13.5
42	FI-Lom	2010	54.8	346.0	−16.1	27.8	200.0	11.7
43	FI-Si2	2012	70.4	349.7	−6.9	22.7	199.1	15.8
44	FI-Si2	2013	88.2	369.5	−6.0	23.7	188.6	17.8

Earth Syst. Sci. Data, 13, 3607–3689, 2021 https://doi.org/10.5194/essd-13-3607-2021

Table B5. Continued.

	SITE_ID	Year	Start_TA_(DOY)	End_TA_(DOY)	Base_value_TA_(C)	Ampl_TA_(C)	Peak_TA_(DOY)	Peak_value_TA_(C)
45	FI-Si2	2014	53.3	350.4	−4.4	21.5	200.3	17.1
46	FI-Si2	2015	39.6	359.2	−5.0	19.4	212.0	14.4
47	FI-Si2	2016	42.6	345.0	−6.7	23.2	199.0	16.5
48	FI-Sii	2013	89.3	363.9	−5.7	22.2	189.1	16.5
49	FI-Sii	2014	52.0	339.8	−4.4	21.5	200.9	17.2
50	FI-Sii	2015	34.4	357.7	−5.4	19.7	209.5	14.3
51	FI-Sii	2016	55.0	320.6	−5.2	20.9	195.0	15.7
52	FI-Sii	2017	61.6	377.3	−6.3	20.9	208.0	14.6
53	FI-Sii	2018	74.2	378.7	-9.0	27.4	195.0	18.4
54	HK-MPM	2016	53.6	378.9	16.0	13.3	198.1	29.2
55	HK-MPM	2017	49.1	357.3	16.3	13.1	215.6	29.3
56	HK-MPM	2018	42.1	383.0	15.3	14.1	199.0	29.3
57	ID-Pag	2016	NaN	NaN	NaN	NaN	NaN	NaN
58	JP-BBY	2015	56.2	355.7	−5.3	25.9	209.5	20.6
59	JP-BBY	2016	46.1	348.0	−7.1	28.0	212.0	20.9
60	JP-BBY	2017	44.7	361.6	−7.5	28.2	208.7	20.7
61	JP-BBY	2018	45.6	367.9	−7.6	27.1	210.0	19.6
62	JP-Mse	2012	54.5	351.8	1.5	24.6	219.9	26.1
63	KR-CRK	2015	NaN	NaN	NaN	NaN	NaN	NaN
64	KR-CRK	2016	NaN	NaN	NaN	NaN	NaN	NaN
65	KR-CRK	2017	NaN	NaN	NaN	NaN	NaN	NaN
66	KR-CRK	2018	NaN	NaN	NaN	NaN	NaN	NaN
67	MY-MLM	2014	17.5	365.8	26.0	1.9	179.4	27.9
68	MY-MLM	2015	NaN	NaN	NaN	NaN	NaN	NaN
69	NZ-Kop	2012	50.8	347.1	9.1	9.7	219.9	18.8
70	NZ-Kop	2013	39.3	352.9	9.3	8.3	209.6	17.6
71	NZ-Kop	2014	53.5	352.7	9.1	9.7	215.0	18.8
72	NZ-Kop	2015	51.0	357.8	8.5	10.4	212.0	19.0
73	PH-RiF	2012	NaN	NaN	NaN	NaN	NaN	NaN
74	PH-RiF	2013	NaN	NaN	NaN	NaN	NaN	NaN
75	PH-RiF	2014	NaN	NaN	NaN	NaN	NaN	NaN
76	PH-RiF	2015	NaN	NaN	NaN	NaN	NaN	NaN
77	RU-Ch2	2014	62.1	339.9	−31.6	46.0	208.4	14.4
78	RU-Ch2	2015	54.1	340.0	−34.4	47.6	204.4	13.2
79	RU-Ch2	2016	56.4	373.2	−34.4	48.4	201.9	14.0
80	RU-Che	2014	61.3	340.0	−31.5	45.9	208.0	14.4
81	RU-Che	2015	53.2	340.1	−34.3	47.6	204.3	13.3
82	RU-Che	2016	55.9	372.3	−34.3	48.4	201.7	14.1
83	SE-Deg	2014	69.6	327.7	−5.2	21.4	201.0	16.2
84	SE-Deg	2015	29.7	352.2	−7.4	19.3	213.9	11.9
85	SE-Deg	2016	54.7	331.3	−7.3	21.0	197.1	13.7
86	SE-Deg	2017	61.9	353.2	−8.3	21.3	210.0	13.0
87	SE-Deg	2018	74.4	373.7	−11.3	26.5	193.0	15.2
88	US-Atq	2013	NaN	NaN	NaN	NaN	NaN	NaN
89	US-Atq	2014	70.0	360.8	−25.8	32.2	203.4	6.4
90	US-Atq	2015	84.1	347.2	−26.1	34.7	196.7	8.6
91	US-Beo	2013	NaN	NaN	NaN	NaN	NaN	NaN

Table B5. Continued.

	SITE_ID	Year	Start_TA_(DOY)	End_TA_(DOY)	Base_value_TA_(C)	Ampl_TA_(C)	Peak_TA_(DOY)	Peak_value_TA_(C)
92	US-Beo	2014	63.3	351.3	−22.7	25.6	203.2	2.9
93	US-Bes	2013	NaN	NaN	NaN	NaN	NaN	NaN
94	US-Bes	2014	76.6	357.3	−24.7	26.6	208.3	1.8
95	US-Bes	2015	82.7	344.0	−25.2	29.5	203.3	4.3
96	US-BZB	2014	65.0	339.3	−17.1	32.1	189.6	15.0
97	US-BZB	2015	52.2	340.0	−17.3	33.9	181.6	16.6
98	US-BZB	2016	35.7	321.0	−16.9	33.5	192.5	16.6
99	US-BZF	2014	64.6	341.5	−16.8	32.0	190.5	15.2
100	US-BZF	2015	52.2	341.0	−16.9	33.4	181.5	16.5
101	US-BZF	2016	34.6	321.3	−16.6	33.2	194.0	16.6
102	US-BZS	2015	46.2	343.6	−17.4	34.6	180.2	17.2
103	US-BZS	2016	32.5	320.3	−15.9	33.0	193.8	17.1
104	US-DPW	2013	59.4	361.7	16.3	10.9	220.8	27.2
105	US-DPW	2014	38.7	326.8	16.0	11.8	210.3	27.8
106	US-DPW	2015	33.6	381.2	15.9	10.0	211.8	25.9
107	US-DPW	2016	45.5	367.1	15.7	12.8	203.0	28.5
108	US-HRA	2017	NaN	NaN	NaN	NaN	NaN	NaN
109	US-HRC	2018	NaN	NaN	NaN	NaN	NaN	NaN
110	US-ICs	2014	NaN	NaN	NaN	NaN	NaN	NaN
111	US-ICs	2015	NaN	NaN	NaN	NaN	NaN	NaN
112	US-ICs	2016	68.1	328.8	−16.9	26.3	196.8	9.4
113	US-Ivo	2013	93.1	360.4	−23.4	36.2	193.6	12.8
114	US-Ivo	2014	69.0	341.9	−21.4	30.7	193.5	9.3
115	US-Ivo	2015	90.8	326.8	−21.5	31.9	188.6	10.4
116	US-Ivo	2016	90.0	340.0	−21.6	31.3	197.0	9.7
117	US-LA1	2012	31.0	302.5	19.1	8.8	177.6	27.9
118	US-LA2	2012	35.2	316.9	16.7	11.6	197.4	28.3
119	US-LA2	2013	71.4	321.2	15.9	13.3	210.6	29.2
120	US-Los	2014	58.0	365.5	−14.2	33.1	195.4	18.9
121	US-Los	2015	50.4	367.6	−10.8	29.4	203.5	18.6
122	US-Los	2016	39.2	356.4	−9.1	29.1	209.4	20.0
123	US-Los	2017	30.7	345.4	−9.8	28.1	212.0	18.3
124	US-Los	2018	69.6	336.0	−9.7	29.8	197.0	20.0
125	US-MAC	2013	NaN	NaN	NaN	NaN	NaN	NaN
126	US-MAC	2014	42.4	324.0	17.1	9.8	211.2	26.9
127	US-MAC	2015	39.5	328.0	16.9	9.6	200.6	26.6
128	US-Myb	2010	NaN	NaN	NaN	NaN	NaN	NaN
129	US-Myb	2011	31.1	331.8	8.2	12.6	223.6	20.8
130	US-Myb	2012	16.5	358.5	7.2	13.5	214.9	20.7
131	US-Myb	2013	24.4	342.3	7.3	13.4	197.0	20.7
132	US-Myb	2014	11.5	353.5	8.8	12.8	211.0	21.5
133	US-Myb	2015	−1.0	325.6	8.9	13.1	228.0	22.0
134	US-Myb	2016	−3.3	351.7	8.0	13.0	208.0	20.9
135	US-Myb	2017	27.3	345.8	8.3	13.9	214.0	22.2

https://doi.org/10.5194/essd-13-3607-2021

Table B5. Continued.

	SITE_ID	Year	Start_TA_(DOY)	End_TA_(DOY)	Base_value_TA_(C)	Ampl_TA_(C)	Peak_TA_(DOY)	Peak_value_TA_(C)
136	US-Myb	2018	44.4	332.6	9.0	11.5	218.0	20.5
137	US-NC4	2012	57.3	339.3	9.0	17.5	208.7	26.5
138	US-NC4	2013	69.3	352.4	6.8	19.0	204.6	25.8
139	US-NC4	2014	49.2	367.7	5.4	18.3	206.3	23.7
140	US-NC4	2015	64.4	392.2	6.9	19.4	202.0	26.3
141	US-NC4	2016	54.0	350.6	8.1	19.1	215.0	27.2
142	US-ORv	2011	64.0	358.3	0.5	25.1	195.2	25.6
143	US-ORv	2012	32.9	351.3	0.8	24.9	195.9	25.8
144	US-ORv	2013	51.2	355.8	−2.4	25.9	203.6	23.5
145	US-ORv	2014	51.3	370.0	−4.3	28.0	196.0	23.6
146	US-ORv	2015	62.5	393.6	−4.6	27.9	199.0	23.3
147	US-OWC	2015	NaN	NaN	NaN	NaN	NaN	NaN
148	US-OWC	2016	56.2	365.0	2.2	22.7	211.8	24.9
149	US-Sne	2016	NaN	NaN	NaN	NaN	NaN	NaN
150	US-Sne	2017	9.2	344.4	7.3	14.5	217.9	21.8
151	US-Sne	2018	49.6	357.4	7.1	14.0	220.9	21.1
152	US-Srr	2014	50.6	337.4	10.7	10.1	217.3	20.8
153	US-Srr	2015	5.0	323.3	9.5	12.2	235.3	21.7
154	US-Srr	2016	−6.2	346.2	8.3	11.7	211.9	20.0
155	US-Srr	2017	17.2	346.4	7.9	13.4	216.0	21.4
156	US-StJ	2016	67.3	347.1	3.0	23.4	214.0	26.4
157	US-Tw1	2011	59.5	328.0	7.8	13.5	222.1	21.3
158	US-Tw1	2012	18.5	356.8	6.7	14.9	216.3	21.6
159	US-Tw1	2013	29.3	344.8	7.1	14.3	196.8	21.4
160	US-Tw1	2014	14.7	349.8	8.5	13.6	204.0	22.1
161	US-Tw1	2015	7.0	324.1	8.2	13.5	222.0	21.6
162	US-Tw1	2016	4.4	350.6	7.2	13.9	203.0	21.1
163	US-Tw1	2017	25.1	343.3	7.2	15.1	206.0	22.4
164	US-Tw1	2018	50.8	337.8	7.4	13.4	211.0	20.8
165	US-Tw4	2014	15.7	348.8	8.6	13.4	206.8	22.1
166	US-Tw4	2015	5.3	324.6	8.5	13.4	224.8	21.9
167	US-Tw4	2016	2.7	347.6	7.6	14.1	201.0	21.6
168	US-Tw4	2017	30.8	337.8	7.9	15.1	208.0	23.0
169	US-Tw4	2018	44.5	331.6	8.3	13.1	213.0	21.3
170	US-Tw5	2018	76.3	338.5	9.2	12.6	208.5	21.8
171	US-Twt	2009	NaN	NaN	NaN	NaN	NaN	NaN
172	US-Twt	2010	NaN	NaN	NaN	NaN	NaN	NaN
173	US-Twt	2011	NaN	NaN	NaN	NaN	NaN	NaN
174	US-Twt	2012	NaN	NaN	NaN	NaN	NaN	NaN
175	US-Twt	2013	NaN	NaN	NaN	NaN	NaN	NaN
176	US-Twt	2014	NaN	NaN	NaN	NaN	NaN	NaN
177	US-Twt	2015	NaN	NaN	NaN	NaN	NaN	NaN
178	US-Twt	2016	NaN	NaN	NaN	NaN	NaN	NaN
179	US-Uaf	2011	59.0	330.8	−23.4	38.5	191.9	15.0

Table B5. Continued.

	SITE_ID	Year	Start_TA_(DOY)	End_TA_(DOY)	Base_value_TA_(C)	Ampl_TA_(C)	Peak_TA_(DOY)	Peak_value_TA_(C)
180	US-Uaf	2012	43.1	317.7	−23.9	38.6	192.3	14.6
181	US-Uaf	2013	64.4	344.1	−22.1	39.6	195.9	17.5
182	US-Uaf	2014	49.9	343.0	−20.6	34.2	190.0	13.7
183	US-Uaf	2015	51.3	346.7	−19.5	34.9	182.0	15.4
184	US-Uaf	2016	27.3	325.5	−20.8	36.1	193.0	15.3
185	US-Uaf	2017	59.2	357.6	−22.1	38.3	191.0	16.2
186	US-Uaf	2018	35.4	354.6	−21.6	36.7	196.0	15.2
187	US-WPT	2011	62.3	362.6	−1.1	26.3	199.1	25.2
188	US-WPT	2012	34.9	355.2	−0.4	25.5	198.4	25.1
189	US-WPT	2013	64.2	341.1	−1.9	24.5	205.0	22.6

Earth Syst. Sci. Data, 13, 3607–3689, 2021

https://doi.org/10.5194/essd-13-3607-2021

Column	Description
SITE_ID	Site identification code as assigned by regional flux data network
Year	Data year
Start_FCH4_(DOY)	Season start for elevated methane fluxes (DOY), point "f" in Fig. 1
End_FCH4_(DOY)	Season end for elevated methane fluxes (DOY), point "h" in Fig. 1
Base_value_FCH4_(nmolCH4/m2/s)	Baseline methane flux during non-elevated season (nmol CH_4 m^{-2} s^{-1}), average of points "a" and "b" in Fig. 1
Ampl_FCH4_(nmolCH4/m2/s)	Amplitude of methane flux during elevated flux season (nmol CH_4 m^{-2} s^{-1}), difference between point "e" in Fig. 1 and Base_value_FCH4
Peak_FCH4_(DOY)	Day of maximum elevated methane flux (DOY), point "g" in Fig. 1
Peak_value_FCH4_(nmolCH4/m2/s)	Maximum value of methane flux (nmol CH_4 m^{-2} s^{-1}), point "e" in Fig. 1
Start_GPP_DT_(DOY)	Season start for elevated GPP_DT (DOY), point "f" in Fig. 1
End_GPP_DT_(DOY)	Season end for elevated GPP_DT fluxes (DOY), point "h" in Fig. 1
Base_value_GPP_DT_(µmolCO2/m2/s)	Baseline GPP_DT flux during non-elevated season (µmol CO_2 m^{-2} s^{-1}), average of points "a" and "b" in Fig. 1
Ampl_GPP_DT_(µmolCO2/m2/s)	Amplitude of GPP_DT flux during elevated flux season (µmol CO_2 m^{-2} s^{-1}), difference between point "e" in Fig. 1 and Base_value_GPP_DT
Peak_GPP_DT_(DOY)	Day of maximum elevated GPP_DT flux (DOY), point "g" in Fig. 1
Peak_value_GPP_DT_(µmolCO2/m2/s)	Maximum value of GPP_DT flux (µmol CO_2 m^{-2} s^{-1}), point "e" in Fig. 1
Probe_name	Temperature probe name as given in data files
Soil_temp_depth_m	Depth of soil temperature probe (m), with negative values being under the surface
Start_TS_(DOY)	Season start for elevated TS (DOY), point "f" in Fig. 1
End_TS_(DOY)	Season end for elevated TS (DOY), point "h" in Fig. 1
Base_value_TS_(C)	Baseline TS during non-elevated season (C), average of points "a" and "b" in Fig. 1
Ampl_TS_(C)	Amplitude of TS during elevated temperature season (C), difference between point "e" in Fig. 1 and Base_value_TS
Peak_TS_(DOY)	Day of maximum elevated TS (DOY), point "g" in Fig. 1
Peak_value_TS_(C)	Maximum value of TS (C), point "e" in Fig. 1
Start_TA_(DOY)	Season start for elevated TA (DOY), point "f" in Fig. 1
End_TA_(DOY)	Season end for elevated TA (DOY), point "h" in Fig. 1
Base_value_TA_(C)	Baseline TA during non-elevated season (C), average of points "a" and "b" in Fig. 1
Ampl_TA_(C)	Amplitude of TA during elevated temperature season (C), difference between point "e" in Fig. 1 and Base_value_TA
Peak_TA_(DOY)	Day of maximum elevated TA (DOY), point "g" in Fig. 1
Peak_value_TA_(C)	Maximum value of TA (C), point "e" in Fig. 1

Table B6. Seasonality parameters estimated using TIMESAT software for soil temperature (TS, from every probe).

	SITE _ID	Year	Probe _name	Soil_temp _depth_m	Start_TS _(DOY)	End_TS _(DOY)	Base_value _TS_(C)	Ampl_TS _(C)	Peak_TS) _(DOY)	Peak_value _TS_(C)
1	AT-Neu	2010	TS_1	−0.05	61.3	339.4	0.15	17.54	200.9	17.7
2	AT-Neu	2011	TS_1	−0.05	51.0	328.8	0.40	16.37	201	16.77
3	AT-Neu	2012	TS_1	−0.05	61.1	341.9	0.73	17.57	202.9	18.3
4	BR-Npw	2016	TS_1	NaN	18.4	343.2	22.41	5.982	188	28.4
5	CA-SCB	2014	TS_1	0	105.9	292.2	−0.63	20.62	196.6	19.99
6	CA-SCB	2014	TS_2	−0.02	105.1	294.1	−0.74	20.42	197.5	19.68
7	CA-SCB	2014	TS_3	−0.04	112.0	294.4	0.05	19.07	199.6	19.11
8	CA-SCB	2014	TS_5	−0.16	123.2	317.7	−1.38	18.6	205.3	17.23
9	CA-SCB	2015	TS_1	0	106.9	287.1	−0.39	17.23	186.8	16.84
10	CA-SCB	2015	TS_2	−0.02	107.1	287.4	−0.42	17.08	187.4	16.66
11	CA-SCB	2015	TS_3	−0.04	107.4	289.8	−0.51	16.81	188.9	16.3
12	CA-SCB	2015	TS_5	−0.16	114.9	305.5	−0.39	15.84	195.7	15.45
13	CA-SCB	2016	TS_1	0	101.6	284.1	−0.31	19.07	193.2	18.77
14	CA-SCB	2016	TS_2	−0.02	101.8	284.1	−0.30	18.96	193.5	18.66
15	CA-SCB	2016	TS_3	−0.04	102.2	285.2	−0.30	18.6	194.3	18.3
16	CA-SCB	2016	TS_5	−0.16	101.2	299.0	−0.24	16.99	201.1	16.74
17	CA-SCB	2017	TS_1	0	107.4	289.7	−0.25	17.67	198	17.42
18	CA-SCB	2017	TS_2	−0.02	107.2	288.9	−0.25	17.59	198	17.33
19	CA-SCB	2017	TS_3	−0.04	108.6	289.3	−0.26	17.28	199	17.02
20	CA-SCB	2017	TS_5	−0.16	116.3	300.3	−0.24	14.95	214	14.71
21	CA-SCC	2014	TS_1	−0.1	123.4	287.1	−0.55	15.64	203	15.09
22	CA-SCC	2014	TS_2	−0.15	114.9	287.7	−0.83	14.49	200.8	13.66
23	CA-SCC	2014	TS_3	−0.2	111.4	288.6	−0.69	11.52	194.9	10.84
24	CA-SCC	2014	TS_4	−0.25	129.5	287.2	−0.22	8.612	207.4	8.391
25	CA-SCC	2014	TS_5	−0.3	142.4	288.0	−0.10	6.329	212.1	6.225
26	CA-SCC	2015	TS_1	−0.1	113.9	285.2	−0.28	16.26	189.2	15.98
27	CA-SCC	2015	TS_2	−0.15	113.1	284.2	−0.24	14.56	192.8	14.32
28	CA-SCC	2015	TS_3	−0.2	111.8	285.4	−0.22	12.71	199.1	12.48
29	CA-SCC	2015	TS_4	−0.25	120.8	287.1	−0.16	10.08	204.8	9.922
30	CA-SCC	2015	TS_5	−0.3	131.9	285.4	−0.09	7.705	209.2	7.616
31	CA-SCC	2016	TS_1	−0.1	108.1	260.1	−0.33	18.37	190.9	18.04
32	CA-SCC	2016	TS_2	−0.15	109.0	260.2	−0.30	17.31	192.1	17.01
33	CA-SCC	2016	TS_3	−0.2	110.5	260.4	−0.26	15.4	194.1	15.14
34	CA-SCC	2016	TS_4	−0.25	119.2	260.3	−0.20	13.38	200.2	13.18
35	CA-SCC	2016	TS_5	−0.3	130.8	261.7	−0.12	10.03	202.2	9.906
36	DE-Hte	2012	TS_3	−0.2	77.0	344.0	4.98	12.26	215.5	17.23
37	DE-Hte	2013	TS_3	−0.2	60.9	378.0	3.96	11.99	207.9	15.95
38	DE-Hte	2014	TS_1	0	NaN	327.8	8.52	8.342	205.6	16.87
39	DE-Hte	2015	TS_1	0	62.9	360.6	5.17	11.67	187.4	16.84
40	DE-Hte	2016	TS_1	0	71.9	NaN	4.94	12.36	175.6	17.3
41	DE-Hte	2017	TS_1	0	61.6	343.3	4.50	11.76	186	16.26
42	DE-SfN	2012	TS_1	−0.02	NaN	372.6	0.00	23.55	206.5	15.29
43	DE-SfN	2012	TS_3	−0.1	NaN	366.7	1.64	12.91	219.7	14.55
44	DE-SfN	2012	TS_4	−0.2	NaN	367.4	4.86	7.276	242.7	12.14
45	DE-SfN	2012	TS_5	−0.5	NaN	367.4	4.86	7.276	242.7	12.14
46	DE-SfN	2013	TS_1	−0.02	55.8	381.5	0.92	13.62	216.4	14.54
47	DE-SfN	2013	TS_3	−0.1	60.4	384.8	1.56	12.5	221.1	14.06
48	DE-SfN	2013	TS_4	−0.2	83.6	394.5	3.62	8.417	243.4	12.04
49	DE-SfN	2013	TS_5	−0.5	83.6	394.5	3.62	8.417	243.4	12.04
50	DE-Zrk	2014	TS_1	−0.05	54.8	361.6	4.36	13.93	202.3	18.29
51	DE-Zrk	2014	TS_2	−0.1	59.3	366.5	4.87	12.65	207.3	17.52
52	DE-Zrk	2014	TS_3	−0.2	62.9	371.3	5.53	11.5	211.7	17.03
53	DE-Zrk	2014	TS_4	−0.3	67.4	375.1	6.05	10.4	216.5	16.45
54	DE-Zrk	2014	TS_5	−0.5	72.5	379.0	6.57	9.359	221	15.93
55	DE-Zrk	2015	TS_1	−0.05	58.3	359.3	4.28	13.24	215.5	17.52

Table B6. Continued.

	SITE _ID	Year	Probe _name	Soil_temp _depth_m	Start_TS _(DOY)	End_TS _(DOY)	Base_value _TS_(C)	Ampl_TS _(C)	Peak_TS) _(DOY)	Peak_value _TS_(C)
56	DE-Zrk	2015	TS_2	−0.1	62.6	365.0	4.79	12	219.8	16.8
57	DE-Zrk	2015	TS_3	−0.2	66.0	369.8	5.42	10.87	223.7	16.29
58	DE-Zrk	2015	TS_4	−0.3	70.5	374.4	5.93	9.771	228	15.7
59	DE-Zrk	2015	TS_5	−0.5	74.7	378.8	6.43	8.751	232.2	15.19
60	DE-Zrk	2016	TS_1	−0.05	72.8	332.0	4.28	14.93	200.4	19.2
61	DE-Zrk	2016	TS_2	−0.1	76.3	337.4	4.79	13.6	204.4	18.39
62	DE-Zrk	2016	TS_3	−0.2	79.7	343.2	5.43	12.33	208.1	17.77
63	DE-Zrk	2016	TS_4	−0.3	83.6	347.6	5.94	11.14	212	17.09
64	DE-Zrk	2016	TS_5	−0.5	87.1	354.2	6.40	10.07	216	16.47
65	DE-Zrk	2017	TS_1	−0.05	69.1	351.4	4.40	14.72	199	19.12
66	DE-Zrk	2017	TS_2	−0.1	73.3	356.5	4.91	13.33	204	18.23
67	DE-Zrk	2017	TS_3	−0.2	77.2	362.4	5.56	12.02	208	17.58
68	DE-Zrk	2017	TS_4	−0.3	82.2	367.2	6.04	10.8	212	16.84
69	DE-Zrk	2017	TS_5	−0.5	86.2	373.0	6.48	9.675	217	16.15
70	DE-Zrk	2018	TS_1	−0.05	84.5	336.1	4.83	12.32	203	17.14
71	DE-Zrk	2018	TS_2	−0.1	86.6	342.6	5.30	11.27	208	16.57
72	DE-Zrk	2018	TS_3	−0.2	87.7	348.1	5.89	10.25	212	16.14
73	DE-Zrk	2018	TS_4	−0.3	89.8	354.8	6.31	9.308	217	15.61
74	DE-Zrk	2018	TS_5	−0.5	92.0	360.5	6.69	8.412	222	15.11
75	FI-Lom	2006	TS_1	−0.07	114.1	290.8	−0.11	13.42	204.8	13.31
76	FI-Lom	2006	TS_2	−0.3	117.2	307.9	0.27	12.01	214.1	12.28
77	FI-Lom	2006	TS_3	−0.5	128.8	329.0	1.06	9.071	225.8	10.13
78	FI-Lom	2007	TS_1	−0.07	126.8	302.0	0.11	13.05	200	13.16
79	FI-Lom	2007	TS_2	−0.3	134.0	321.0	0.42	11.5	207.5	11.92
80	FI-Lom	2007	TS_3	−0.5	138.4	348.0	1.06	8.873	221.1	9.936
81	FI-Lom	2008	TS_1	−0.07	135.6	296.7	0.16	12.73	202.9	12.88
82	FI-Lom	2008	TS_2	−0.3	141.5	318.7	0.58	10.62	209.6	11.2
83	FI-Lom	2008	TS_3	−0.5	146.7	349.2	1.17	8.214	221.2	9.382
84	FI-Lom	2009	TS_1	−0.07	117.2	291.9	0.14	11.73	214	11.87
85	FI-Lom	2009	TS_2	−0.3	123.5	314.5	0.67	9.692	221	10.36
86	FI-Lom	2009	TS_3	−0.5	133.7	336.6	1.30	7.896	233	9.193
87	FI-Lom	2010	TS_1	−0.07	129.9	318.5	0.05	12.13	208	12.18
88	FI-Lom	2010	TS_2	−0.3	138.1	338.2	0.52	9.962	218	10.48
89	FI-Lom	2010	TS_3	−0.5	147.3	359.9	1.19	7.344	231	8.532
90	FI-Si2	2012	TS_1	−0.05	NaN	323.5	0.00	19.85	204.6	16.02
91	FI-Si2	2012	TS_2	−0.2	103.6	333.5	−0.04	15.75	217.5	15.71
92	FI-Si2	2012	TS_3	−0.35	105.6	NaN	0.00	19.38	230.6	15.09
93	FI-Si2	2012	TS_4	−0.5	110.9	NaN	0.00	17.26	237.5	14.66
94	FI-Si2	2013	TS_1	−0.05	106.9	341.0	−0.05	16.04	199.4	15.98
95	FI-Si2	2013	TS_2	−0.2	102.6	356.1	0.23	14.91	207.3	15.14
96	FI-Si2	2013	TS_3	−0.35	NaN	376.5	0.00	18.26	209.6	14.23
97	FI-Si2	2013	TS_4	−0.5	NaN	392.4	0.00	16.71	216.4	13.48
98	FI-Si2	2014	TS_1	−0.05	104.6	331.1	−0.04	17.07	208.5	17.03
99	FI-Si2	2014	TS_2	−0.2	107.8	359.8	0.59	15.33	215.3	15.92
100	FI-Si2	2014	TS_3	−0.35	112.0	385.9	0.99	13.61	222.2	14.61
101	FI-Si2	2014	TS_4	−0.5	118.2	400.1	1.59	12.01	229.1	13.59
102	FI-Si2	2015	TS_1	−0.05	76.5	352.3	−0.87	16.31	211	15.44
103	FI-Si2	2015	TS_2	−0.2	80.1	364.7	−0.41	14.83	218	14.42
104	FI-Si2	2015	TS_3	−0.35	82.0	374.8	0.12	13.27	225	13.39
105	FI-Si2	2015	TS_4	−0.5	88.2	382.4	0.84	11.7	233	12.53
106	FI-Si2	2016	TS_1	−0.05	102.6	329.4	−0.88	16.48	206	15.6
107	FI-Si2	2016	TS_2	−0.2	102.2	361.0	−0.77	16.02	212	15.25
108	FI-Si2	2016	TS_3	−0.35	103.1	383.8	−0.63	14.7	219	14.07
109	FI-Si2	2016	TS_4	−0.5	104.8	399.0	−0.20	13.36	227	13.16
110	HK-MPM	2016	TS_2	NaN	NaN	566.9	0.00	7.789	219.8	28.92
111	HK-MPM	2016	TS_3	NaN	NaN	373.1	20.56	7.386	227.3	27.95
112	HK-MPM	2017	TS_2	NaN	NaN	NaN	0.00	8.726	218.5	29.13
113	HK-MPM	2017	TS_3	NaN	69.6	364.5	19.53	8.572	233.6	28.1

Table B6. Continued.

	SITE _ID	Year	Probe _name	Soil_temp _depth_m	Start_TS _(DOY)	End_TS _(DOY)	Base_value _TS_(C)	Ampl_TS _(C)	Peak_TS) _(DOY)	Peak_value _TS_(C)
114	HK-MPM	2018	TS_2	NaN	NaN	NaN	0.00	7.231	204.9	28.66
115	HK-MPM	2018	TS_3	NaN	64.8	383.4	19.17	8.406	221.4	27.58
116	JP-BBY	2015	TS_1	−0.183	87.8	340.8	0.94	21.59	218.1	22.53
117	JP-BBY	2015	TS_2	−0.233	90.6	341.0	1.34	20.9	219.9	22.25
118	JP-BBY	2015	TS_3	−0.283	90.3	341.6	1.58	20.42	221.4	22
119	JP-BBY	2015	TS_4	−0.383	96.0	341.3	2.39	19.09	225.1	21.48
120	JP-BBY	2015	TS_5	−0.483	95.8	341.5	2.91	18.09	228.9	21
121	JP-BBY	2016	TS_1	−0.183	80.8	330.6	0.36	22.19	217.8	22.55
122	JP-BBY	2016	TS_2	−0.233	82.3	335.4	0.67	21.64	220.8	22.3
123	JP-BBY	2016	TS_3	−0.283	84.3	332.6	0.99	21.1	222	22.09
124	JP-BBY	2016	TS_4	−0.383	89.0	332.4	1.76	19.92	225.6	21.68
125	JP-BBY	2016	TS_5	−0.483	94.3	331.9	2.44	18.83	228.9	21.27
126	JP-BBY	2017	TS_1	−0.183	80.4	347.8	0.20	21.75	213.8	21.95
127	JP-BBY	2017	TS_2	−0.233	84.5	347.8	0.82	21.02	214.6	21.83
128	JP-BBY	2017	TS_3	−0.283	86.2	347.1	1.06	20.56	216.3	21.62
129	JP-BBY	2017	TS_4	−0.383	92.2	346.0	1.97	19.34	218.5	21.31
130	JP-BBY	2017	TS_5	−0.483	98.2	345.2	2.70	18.34	221	21.03
131	JP-BBY	2018	TS_1	−0.183	78.3	355.4	0.50	20.38	222	20.88
132	JP-BBY	2018	TS_2	−0.233	83.5	357.6	1.48	19.23	224	20.7
133	JP-BBY	2018	TS_3	−0.283	85.9	355.9	1.69	18.78	225	20.47
134	JP-BBY	2018	TS_4	−0.383	95.9	351.3	2.81	17.25	229	20.07
135	JP-BBY	2018	TS_5	−0.483	103.8	349.4	3.63	16.1	232	19.73
136	JP-Mse	2012	TS_1	−0.01	60.4	348.9	2.15	23.76	211.8	25.91
137	MY-MLM	2014	TS	NaN	NaN	358.4	25.06	3.968	194.5	29.03
138	MY-MLM	2015	TS	NaN	27.3	NaN	25.57	1.973	172.7	27.55
139	NZ-Kop	2012	TS_1	−0.5	62.5	360.3	8.30	8.394	219.8	16.7
140	NZ-Kop	2012	TS_2	−0.1	65.5	362.4	8.45	8.093	222.1	16.54
141	NZ-Kop	2012	TS_3	−0.2	68.8	365.6	8.73	7.243	228.2	15.98
142	NZ-Kop	2013	TS_1	−0.5	45.6	367.0	8.41	7.635	210.5	16.04
143	NZ-Kop	2013	TS_2	−0.1	47.6	371.0	8.54	7.486	212.3	16.03
144	NZ-Kop	2013	TS_3	−0.2	52.7	377.2	8.82	6.87	217.8	15.69
145	NZ-Kop	2014	TS_1	−0.5	56.9	365.7	8.16	8.79	219	16.95
146	NZ-Kop	2014	TS_2	−0.1	59.4	367.5	8.29	8.512	221	16.8
147	NZ-Kop	2014	TS_3	−0.2	62.9	372.5	8.55	7.792	226	16.34
148	NZ-Kop	2015	TS_1	−0.5	56.5	371.8	7.73	9.355	214	17.09
149	NZ-Kop	2015	TS_2	−0.1	58.3	374.7	7.87	9.063	217	16.93
150	NZ-Kop	2015	TS_3	−0.2	62.7	378.4	8.19	8.217	222	16.4
151	RU-Ch2	2014	TS_1	−0.04	138.8	263.8	−0.13	14.42	206.6	14.29
152	RU-Ch2	2014	TS_2	−0.08	146.1	262.1	−0.14	13.03	206.5	12.9
153	RU-Ch2	2014	TS_3	−0.16	155.9	264.5	−0.05	4.581	210.5	4.535
154	RU-Ch2	2015	TS_1	−0.04	143.9	269.6	−0.14	13.97	193.3	13.83
155	RU-Ch2	2015	TS_2	−0.08	147.3	265.7	−0.10	12.3	195.7	12.2
156	RU-Ch2	2015	TS_3	−0.16	159.9	266.6	−0.04	3.995	205.2	3.96
157	RU-Ch2	2016	TS_1	−0.04	127.0	273.5	−0.16	11.64	200.2	11.48
158	RU-Ch2	2016	TS_2	−0.08	133.9	272.6	−0.10	10.06	203.2	9.964
159	RU-Ch2	2016	TS_3	−0.16	148.0	275.5	−0.04	4.042	217.7	4.001
160	RU-Che	2014	TS_1	−0.04	138.0	267.6	−0.12	15.04	208	14.92
161	RU-Che	2014	TS_2	−0.08	149.7	263.7	−0.09	8.959	206.6	8.873
162	RU-Che	2014	TS_3	−0.16	155.0	265.5	−0.07	7.006	210.3	6.938
163	RU-Che	2015	TS_1	−0.04	143.8	274.7	−0.17	14.81	193.7	14.64
164	RU-Che	2015	TS_2	−0.08	149.5	267.1	−0.06	8.336	197.9	8.273
165	RU-Che	2015	TS_3	−0.16	154.5	271.0	−0.04	5.942	202.4	5.9
166	RU-Che	2016	TS_1	−0.04	126.7	274.0	−0.19	12.95	200.4	12.76
167	RU-Che	2016	TS_2	−0.08	137.0	273.7	−0.07	7.076	205.4	7.01
168	RU-Che	2016	TS_3	−0.16	142.5	275.6	−0.05	5.498	211.8	5.451
169	SE-Deg	2014	TS_1	−0.02	111.8	303.6	−0.53	17.22	201.6	16.69

Table B6. Continued.

	SITE _ID	Year	Probe _name	Soil_temp _depth_m	Start_TS _(DOY)	End_TS _(DOY)	Base_value _TS_(C)	Ampl_TS _(C)	Peak_TS) _(DOY)	Peak_value _TS_(C)
170	SE-Deg	2014	TS_2	−0.05	119.1	308.1	−0.31	13.23	207.4	12.93
171	SE-Deg	2014	TS_3	−0.1	125.5	315.6	−0.10	12.54	212	12.44
172	SE-Deg	2014	TS_4	−0.15	134.6	321.2	0.29	11.63	215.6	11.93
173	SE-Deg	2014	TS_5	−0.3	126.7	330.9	0.52	11.61	220	12.13
174	SE-Deg	2014	TS_6	−0.5	130.6	341.7	0.89	11.33	223.1	12.21
175	SE-Deg	2015	TS_1	−0.02	104.2	310.6	−0.28	15.2	207.2	14.91
176	SE-Deg	2015	TS_2	−0.05	110.6	312.6	0.09	13.86	209.5	13.95
177	SE-Deg	2015	TS_3	−0.1	112.9	321.4	0.41	12.94	212.9	13.36
178	SE-Deg	2015	TS_4	−0.15	115.7	329.2	0.60	11.94	216.6	12.54
179	SE-Deg	2015	TS_5	−0.3	118.3	339.2	0.90	11.08	220.5	11.98
180	SE-Deg	2015	TS_6	−0.5	121.8	348.0	1.30	10.19	224.6	11.48
181	SE-Deg	2016	TS_1	−0.02	108.1	306.4	−0.19	14.88	200.3	14.68
182	SE-Deg	2017	TS_1	−0.02	133.4	326.9	−0.20	12.35	215	12.15
183	SE-Deg	2018	TS_1	−0.02	111.7	310.2	−0.17	14.7	198	14.52
184	US-Atq	2014	TS_1	NaN	10.7	139.5	−0.20	8.068	61	7.864
185	US-Atq	2014	TS_2	NaN	18.0	137.3	−0.08	4.191	74.3	4.109
186	US-Atq	2014	TS_3	NaN	28.5	138.5	−0.03	2.366	83.5	2.334
187	US-Beo	2014	TS_1	NaN	155.1	270.1	−0.04	4.874	211.1	4.829
188	US-Beo	2014	TS_2	NaN	168.6	270.6	−0.02	2.94	219.6	2.922
189	US-Beo	2014	TS_3	NaN	170.5	269.5	−0.02	3.128	219.9	3.104
190	US-Bes	2013	TS_1	NaN	143.2	262.0	−0.05	5.649	201.3	5.602
191	US-Bes	2013	TS_2	NaN	150.6	267.5	−0.04	6.744	205.7	6.706
192	US-Bes	2013	TS_3	NaN	146.0	267.3	−0.06	8.248	202.3	8.187
193	US-Bes	2014	TS_1	NaN	151.8	282.3	−0.10	3.924	198.5	3.822
194	US-Bes	2015	TS_1	NaN	140.4	271.0	−0.11	4.763	195.3	4.65
195	US-Bes	2015	TS_2	NaN	148.8	269.6	−0.11	5.512	202.8	5.401
196	US-Bes	2015	TS_3	NaN	146.8	271.7	−0.16	7.182	197.8	7.027
197	US-BZB	2014	TS_1	−0.075	123.1	298.4	−0.44	15.35	215.8	14.91
198	US-BZB	2014	TS_2	−0.05	115.2	292.1	−0.59	15.49	209.9	14.9
199	US-BZB	2015	TS_1	−0.075	107.8	295.6	−0.38	14.04	210.2	13.67
200	US-BZB	2015	TS_2	−0.05	98.6	293.2	−0.67	14.56	203.5	13.9
201	US-BZB	2016	TS_1	−0.075	125.1	292.4	−0.33	16.39	214.3	16.06
202	US-BZB	2016	TS_2	−0.05	109.9	290.9	−0.74	16.89	211.7	16.15
203	US-BZF	2014	TS_1	−0.075	96.1	322.8	−1.56	16.12	205.4	14.56
204	US-BZF	2014	TS_2	−0.05	112.7	322.8	−1.22	15.9	208.3	14.68
205	US-BZF	2015	TS_1	−0.075	108.4	331.1	−1.20	14.88	197.5	13.68
206	US-BZF	2015	TS_2	−0.05	111.5	336.1	−1.12	14.83	200.2	13.72
207	US-BZF	2016	TS_1	−0.075	95.5	315.9	−1.03	17.18	205.1	16.15
208	US-BZF	2016	TS_2	−0.05	100.1	317.6	−0.90	17.72	206	16.81
209	US-BZS	2015	TS_1	NaN	116.5	275.2	−0.07	4.866	202.9	4.792
210	US-BZS	2015	TS_2	NaN	97.3	283.7	−0.27	8.135	187.7	7.862
211	US-BZS	2015	TS_3	NaN	105.9	272.5	−0.13	10.61	193.1	10.47
212	US-BZS	2016	TS_1	NaN	119.1	278.9	−0.05	5.584	208.4	5.535
213	US-BZS	2016	TS_2	NaN	87.6	279.0	−0.25	12.09	203.1	11.84
214	US-BZS	2016	TS_3	NaN	98.3	277.9	−0.16	11.67	198.8	11.51
215	US-ICs	2014	TS_1	−0.075	147.3	263.1	−0.08	5.467	205.6	5.39
216	US-ICs	2014	TS_2	−0.05	147.1	262.7	−0.01	6.41	205.1	6.402
217	US-ICs	2015	TS_1	−0.075	141.6	255.7	−0.02	6.12	195.2	6.098
218	US-ICs	2015	TS_2	−0.05	140.4	256.9	−0.02	7.07	193.1	7.047
219	US-ICs	2016	TS_1	−0.075	146.7	265.9	−0.05	5.67	206.2	5.623
220	US-ICs	2016	TS_2	−0.05	146.8	265.7	−0.05	6.654	206.1	6.599
221	US-Ivo	2014	TS_1	−0.05	136.9	264.3	−0.20	10.84	195.7	10.64
222	US-Ivo	2014	TS_1	−0.4	136.9	264.3	−0.20	10.84	195.7	10.64
223	US-Ivo	2014	TS_2	−0.1	142.5	266.5	−0.16	9.908	195.5	9.744
224	US-Ivo	2014	TS_3	−0.15	145.0	262.7	−0.19	6.761	204.8	6.574
225	US-Ivo	2014	TS_4	−0.3	166.6	262.1	−0.03	4.068	214.3	4.034
226	US-Ivo	2015	TS_1	−0.05	139.4	257.1	−0.14	14.86	185.6	14.72

Table B6. Continued.

	SITE _ID	Year	Probe _name	Soil_temp _depth_m	Start_TS _(DOY)	End_TS _(DOY)	Base_value _TS_(C)	Ampl_TS _(C)	Peak_TS) _(DOY)	Peak_value _TS_(C)
227	US-Ivo	2015	TS_1	−0.4	139.4	257.1	−0.14	14.86	185.6	14.72
228	US-Ivo	2015	TS_2	−0.1	141.2	256.7	−0.09	11.99	189.1	11.9
229	US-Ivo	2015	TS_3	−0.15	145.8	261.0	−0.07	6.85	199.1	6.785
230	US-Ivo	2015	TS_4	−0.3	158.9	259.6	−0.03	4.032	208.2	3.997
231	US-Ivo	2016	TS_1	−0.05	133.6	262.4	−0.10	8.895	197.3	8.796
232	US-Ivo	2016	TS_1	−0.4	133.6	262.4	−0.10	8.895	197.3	8.796
233	US-Ivo	2016	TS_2	−0.1	139.7	264.2	−0.04	6.76	202.2	6.719
234	US-Ivo	2016	TS_3	−0.15	153.8	269.5	−0.05	4.305	211.5	4.253
235	US-Ivo	2016	TS_4	−0.3	171.2	271.0	−0.01	2.644	221.2	2.631
236	US-LA1	2012	TS_1	−0.1	29.1	331.4	15.59	13.5	197.2	29.08
237	US-LA2	2012	TS_1	−0.1	36.6	336.1	15.04	14.35	193.2	29.39
238	US-LA2	2013	TS_1	−0.1	65.8	377.9	14.70	16.06	201.5	30.76
239	US-Los	2014	TS_1	0	136.2	417.4	1.95	8.263	244.3	10.22
240	US-Los	2015	TS_1	0	148.2	422.3	2.43	7.761	258.7	10.19
241	US-Los	2016	TS_1	0	135.2	415.7	2.47	8.083	255.1	10.56
242	US-Los	2017	TS_1	0	141.1	414.6	1.89	7.451	256	9.343
243	US-Los	2018	TS_1	0	169.8	421.8	1.46	7.419	260	8.883
244	US-Myb	2011	TS_3	−0.08	NaN	329.5	12.12	8.859	231.7	20.98
245	US-Myb	2011	TS_4	−0.16	NaN	333.9	12.36	8.288	235.8	20.65
246	US-Myb	2011	TS_5	−0.32	NaN	339.0	12.72	7.56	241.4	20.28
247	US-Myb	2011	TS_1	−0.02	NaN	326.6	11.96	9.156	229.3	21.12
248	US-Myb	2012	TS_3	−0.08	35.6	372.2	9.39	10.96	216.1	20.36
249	US-Myb	2012	TS_4	−0.16	40.4	375.5	9.90	10.23	220.7	20.13
250	US-Myb	2012	TS_5	−0.32	47.4	379.3	10.56	9.212	227.2	19.78
251	US-Myb	2012	TS_1	−0.02	29.9	372.1	8.98	11.77	214.4	20.74
252	US-Myb	2013	TS_3	−0.08	34.4	354.7	9.25	11.28	210.9	20.52
253	US-Myb	2013	TS_4	−0.16	40.1	359.0	9.87	10.41	215	20.28
254	US-Myb	2013	TS_5	−0.32	45.1	363.8	10.53	9.441	221.9	19.97
255	US-Myb	2013	TS_1	−0.02	NaN	355.1	8.47	12.24	208.2	20.7
256	US-Myb	2014	TS_3	−0.08	26.0	365.9	9.64	12.28	210	21.93
257	US-Myb	2014	TS_4	−0.16	38.1	364.2	10.74	11.23	211	21.97
258	US-Myb	2014	TS_5	−0.32	44.3	366.1	11.25	10.25	218	21.5
259	US-Myb	2015	TS_3	−0.08	17.3	340.7	9.77	11.85	212	21.62
260	US-Myb	2015	TS_4	−0.16	12.8	339.0	10.79	10.84	221	21.63
261	US-Myb	2015	TS_5	−0.32	18.8	343.9	11.35	9.93	226	21.28
262	US-Myb	2016	TS_3	−0.08	5.1	357.8	9.61	11.19	201	20.8
263	US-Myb	2016	TS_4	−0.16	3.4	356.2	9.84	10.87	208	20.72
264	US-Myb	2016	TS_5	−0.32	12.0	360.5	10.73	9.627	214	20.36
265	US-Myb	2017	TS_3	−0.08	27.3	352.9	9.86	13.1	214	22.96
266	US-Myb	2017	TS_4	−0.16	28.3	357.4	9.92	12.74	215	22.66
267	US-Myb	2017	TS_5	−0.32	36.8	360.4	10.85	11.23	223	22.08
268	US-Myb	2017	TS_1	−0.02	62.8	325.7	12.70	10.71	216.8	23.41
269	US-Myb	2018	TS_3	−0.08	36.3	326.1	10.20	10.72	207	20.92
270	US-Myb	2018	TS_4	−0.16	41.3	332.8	10.47	10.35	209	20.82
271	US-Myb	2018	TS_5	−0.32	48.4	336.1	11.18	9.293	215	20.47
272	US-Myb	2018	TS_1	−0.02	38.4	344.9	10.05	11.93	200.3	21.98
273	US-NC4	2012	TS_1	−0.05	42.4	336.0	7.87	15.75	215.4	23.62
274	US-NC4	2013	TS_1	−0.05	60.0	368.8	6.92	16.83	210.5	23.74
275	US-NC4	2014	TS_1	−0.05	54.4	362.3	6.73	16.81	208.5	23.54
276	US-NC4	2015	TS_1	−0.05	68.1	387.3	8.27	16.06	205	24.33
277	US-NC4	2016	TS_1	−0.05	53.0	351.4	9.41	15.04	220	24.45
278	US-ORv	2012	TS	NaN	57.4	352.6	4.36	20.61	203.9	24.97
279	US-ORv	2013	TS	NaN	63.7	356.7	2.93	19.98	210.8	22.9
280	US-ORv	2014	TS	NaN	68.1	365.0	2.11	20.17	205.3	22.28
281	US-ORv	2015	TS	NaN	68.8	387.8	1.77	21.26	206	23.04
282	US-OWC	2016	TS_1	−0.05	0.0	0.0	0.00	0	211.2	23.91
283	US-Sne	2017	TS_1	−0.01	46.1	337.9	10.33	13.14	212.7	23.47
284	US-Sne	2017	TS_2	−0.02	41.1	341.8	10.76	12.66	205.7	23.41
285	US-Sne	2017	TS_3	−0.08	42.9	343.8	11.04	12.17	208.5	23.22

Table B6. Continued.

	SITE _ID	Year	Probe _name	Soil_temp _depth_m	Start_TS _(DOY)	End_TS _(DOY)	Base_value _TS_(C)	Ampl_TS _(C)	Peak_TS) _(DOY)	Peak_value _TS_(C)
286	US-Sne	2017	TS_4	−0.16	46.4	346.2	11.39	11.79	211	23.18
287	US-Sne	2017	TS_5	−0.32	50.6	350.5	11.98	10.7	216	22.67
288	US-Sne	2018	TS_1	−0.01	48.4	325.1	10.28	12.15	217.3	22.43
289	US-Sne	2018	TS_2	−0.02	33.9	331.0	10.55	11.34	210.2	21.89
290	US-Sne	2018	TS_3	−0.08	36.8	331.5	10.87	10.63	212.1	21.5
291	US-Sne	2018	TS_4	−0.16	35.6	335.4	11.23	10.09	220.1	21.32
292	US-Sne	2018	TS_5	−0.32	49.1	335.9	11.88	9.045	218	20.92
293	US-Srr	2016	TS_1	NaN	NaN	326.3	10.03	10.71	200.5	20.74
294	US-Srr	2017	TS_1	NaN	11.3	346.8	7.22	13.71	199.5	20.93
295	US-StJ	2016	TS_2	−0.05	68.4	347.4	4.05	16.22	213.7	20.27
296	US-StJ	2016	TS_3	−0.1	68.4	347.4	5.84	14.1	213.7	19.94
297	US-Tw1	2012	TS_1	−0.02	50.5	360.0	5.99	11.52	225.2	17.51
298	US-Tw1	2012	TS_2	−0.04	48.0	358.8	6.14	11.32	227	17.46
299	US-Tw1	2012	TS_3	−0.08	50.1	367.9	5.18	12.31	222.1	17.49
300	US-Tw1	2012	TS_4	−0.16	49.0	367.5	5.31	12.19	224.5	17.5
301	US-Tw1	2012	TS_5	−0.32	−79.1	347.2	7.89	9.513	225.3	17.4
302	US-Tw1	2013	TS_1	−0.02	35.8	337.6	4.39	14.59	206.6	18.97
303	US-Tw1	2013	TS_2	−0.04	36.1	337.7	4.39	14.57	206.8	18.96
304	US-Tw1	2013	TS_3	−0.08	36.8	338.1	4.40	14.54	207.5	18.94
305	US-Tw1	2013	TS_4	−0.16	37.6	338.8	4.41	14.59	208.4	19.01
306	US-Tw1	2013	TS_5	−0.32	38.6	340.1	4.46	14.62	209.6	19.07
307	US-Tw1	2014	TS_1	−0.02	41.2	395.4	6.67	10.89	208.3	17.56
308	US-Tw1	2014	TS_2	−0.04	41.9	397.1	6.70	10.85	208.6	17.55
309	US-Tw1	2014	TS_3	−0.08	43.5	400.0	6.78	10.72	209.8	17.49
310	US-Tw1	2014	TS_4	−0.16	45.6	404.8	6.88	10.56	211.3	17.44
311	US-Tw1	2014	TS_5	−0.32	49.6	416.3	7.09	10.24	213.9	17.33
312	US-Tw1	2015	TS_1	−0.02	50.7	342.5	9.02	7.831	235	16.85
313	US-Tw1	2015	TS_2	−0.04	52.0	342.4	9.09	7.706	235	16.8
314	US-Tw1	2015	TS_3	−0.08	55.6	342.0	9.26	7.385	238	16.64
315	US-Tw1	2015	TS_4	−0.16	59.6	343.0	9.51	6.972	240	16.48
316	US-Tw1	2015	TS_5	−0.32	69.4	345.2	10.00	6.208	246	16.21
317	US-Tw1	2016	TS_1	−0.02	34.6	361.1	8.78	7.943	218	16.72
318	US-Tw1	2016	TS_2	−0.04	35.5	362.2	8.86	7.837	219	16.69
319	US-Tw1	2016	TS_3	−0.08	38.6	363.1	9.04	7.546	221	16.59
320	US-Tw1	2016	TS_4	−0.16	44.7	365.9	9.33	7.14	223	16.47
321	US-Tw1	2016	TS_5	−0.32	56.2	370.5	9.86	6.35	229	16.21
322	US-Tw1	2017	TS_1	−0.02	41.2	343.7	7.55	10.22	228	17.77
323	US-Tw1	2017	TS_2	−0.04	41.7	344.6	7.61	10.11	229	17.72
324	US-Tw1	2017	TS_3	−0.08	42.6	345.0	7.75	9.803	231	17.55
325	US-Tw1	2017	TS_4	−0.16	45.0	347.2	7.97	9.368	234	17.34
326	US-Tw1	2017	TS_5	−0.32	48.8	349.2	8.38	8.5	240	16.88
327	US-Tw1	2018	TS_1	−0.02	60.5	327.4	6.70	10.42	222	17.12
328	US-Tw1	2018	TS_2	−0.04	61.5	327.4	6.75	10.36	223	17.1
329	US-Tw1	2018	TS_3	−0.08	64.6	328.4	6.85	10.18	225	17.03
330	US-Tw1	2018	TS_4	−0.16	67.7	329.4	7.01	9.925	227	16.93
331	US-Tw1	2018	TS_5	−0.32	75.1	331.4	7.31	9.459	230	16.77
332	US-Tw4	2015	TS_1	−0.02	15.9	327.2	10.04	11.56	199.4	21.6
333	US-Tw4	2015	TS_3	−0.08	20.2	329.8	10.48	10.96	202.3	21.44
334	US-Tw4	2015	TS_4	−0.16	23.9	332.5	10.86	10.42	205.7	21.28
335	US-Tw4	2015	TS_5	−0.32	29.2	338.6	11.49	9.449	212.4	20.94
336	US-Tw4	2016	TS_1	−0.02	9.6	358.7	8.16	11.29	201.7	19.45
337	US-Tw4	2016	TS_3	−0.08	13.2	360.1	8.67	10.58	205.7	19.25
338	US-Tw4	2016	TS_4	−0.16	15.9	362.6	9.11	9.991	209.2	19.11
339	US-Tw4	2016	TS_5	−0.32	21.0	367.6	9.91	8.876	216.2	18.78
340	US-Tw4	2017	TS_1	−0.02	38.3	347.3	8.07	11.52	211.9	19.59
341	US-Tw4	2017	TS_3	−0.08	42.1	351.8	8.45	10.91	215.3	19.36
342	US-Tw4	2017	TS_4	−0.16	46.0	354.7	8.83	10.35	218.6	19.18
343	US-Tw4	2017	TS_5	−0.32	53.5	361.4	9.52	9.275	224.9	18.79

Table B6. Continued.

	SITE _ID	Year	Probe _name	Soil_temp _depth_m	Start_TS _(DOY)	End_TS _(DOY)	Base_value _TS_(C)	Ampl_TS _(C)	Peak_TS) _(DOY)	Peak_value _TS_(C)
344	US-Tw4	2018	TS_1	−0.02	58.1	344.9	8.00	10.93	218	18.93
345	US-Tw4	2018	TS_3	−0.08	63.9	349.1	8.38	10.41	222	18.79
346	US-Tw4	2018	TS_4	−0.16	68.0	352.1	8.71	9.862	225	18.57
347	US-Tw4	2018	TS_5	−0.32	75.3	357.9	9.33	8.8	231	18.13
348	US-Tw5	2018	TS_1	−0.02	NaN	414.8	0.00	8.894	222.2	18.37
349	US-Tw5	2018	TS_2	−0.1	NaN	401.0	0.00	12.32	204.4	22.24
350	US-Tw5	2018	TS_3	−0.02	NaN	414.8	0.00	8.894	222.2	18.37
351	US-Tw5	2018	TS_4	−0.08	NaN	423.4	0.00	7.898	227.3	18.14
352	US-Tw5	2018	TS_5	−0.16	NaN	430.2	0.00	7.531	230	17.94
353	US-Uaf	2011	TS_1	−0.09	86.2	372.5	−12.29	21.95	199.6	9.667
354	US-Uaf	2012	TS_1	−0.09	73.8	338.5	−11.83	20.86	202.4	9.028
355	US-Uaf	2013	TS_1	−0.09	109.6	395.5	−10.08	20.52	200.4	10.44
356	US-Uaf	2014	TS_1	−0.09	76.1	365.4	−10.94	19.94	206	8.999
357	US-Uaf	2015	TS_1	−0.09	81.0	423.2	−9.77	19.76	190	9.998
358	US-Uaf	2016	TS_1	−0.09	77.4	315.8	−7.74	19.13	198	11.39
359	US-Uaf	2017	TS_1	−0.09	84.9	380.2	−7.39	19.08	196	11.69
360	US-Uaf	2018	TS_1	−0.09	96.0	333.3	−5.60	17.72	199	12.11
361	US-WPT	2011	TS_1	−0.1	81.0	342.2	5.27	19.27	202.6	24.54
362	US-WPT	2011	TS_2	−0.3	NaN	347.0	6.38	16.62	209.7	23.01
363	US-WPT	2012	TS_1	−0.1	40.3	345.6	3.70	21.6	197.4	25.3
364	US-WPT	2012	TS_2	−0.3	44.9	355.0	4.52	19.21	203.8	23.72
365	US-WPT	2013	TS_1	−0.1	74.6	340.5	3.73	18.23	207.2	21.96
366	US-WPT	2013	TS_2	−0.3	77.6	352.3	4.32	16.69	211.7	21.01

Column	Description
SITE_ID	Site identification code as assigned by regional flux data network
Year	Data year
Probe_name	Temperature probe name as given in data files
Soil_temp_depth_m	Depth of soil temperature probe (m), with negative values being under the surface
Start_TS_(DOY)	Season start for elevated TS (DOY), point "f" in Fig. 1
End_TS_(DOY)	Season end for elevated TS (DOY), point "h" in Fig. 1
Base_value_TS_(C)	Baseline TS during non-elevated season (C), average of points "a" and "b" in Fig. 1
Ampl_TS_(C)	Amplitude of TS during elevated temperature season (C), difference between point "e" in Fig. 1 and Base_value_TS
Peak_TS_(DOY)	Day of maximum elevated TS (DOY), point "g" in Fig. 1
Peak_value_TS_(C)	Maximum value of TS (C), point "e" in Fig. 1

Table B7. Installation depths for soil temperature probes.

	SITE_ID	Year	Probe name	Soil_temp_depth_m	Additional_notes
1	AT-NEU		TS_1	−0.05	
2	AT-NEU		TS_2	−0.1	
3	AT-NEU		TS_3	−0.2	
4	BR-NPW		TS_1		
5	BR-NPW		TS_2		
6	BW-GUM		No data		
7	BW-NXR		No data		
8	CA-SCB		TS_1	0	
9	CA-SCB		TS_2	−0.02	
10	CA-SCB		TS_3	−0.04	
11	CA-SCB		TS_4	−0.08	
12	CA-SCB		TS_5	−0.16	
13	CA-SCB		TS_6	−0.32	
14	CA-SCB		TS_7	−0.64	
15	CA-SCB		TS_8	−1.28	
16	CA-SCC		TS_1	−0.1	
17	CA-SCC		TS_2	−0.15	
18	CA-SCC		TS_3	−0.2	
19	CA-SCC		TS_4	−0.25	
20	CA-SCC		TS_5	−0.3	
21	CA-SCC		TS_6	−0.5	
22	CA-SCC		TS_7	−0.6	
23	CA-SCC		TS_8	−0.7	
24	CH-CHA		TS_1	−0.01	
25	CH-CHA		TS_2	−0.02	
26	CH-CHA		TS_3	−0.04	
27	CH-CHA		TS_4	−0.07	
28	CH-CHA		TS_5	−0.1	
29	CH-CHA		TS_6	−0.15	
30	CH-CHA		TS_7	−0.25	
31	CH-CHA		TS_8	−0.4	
32	CH-CHA		TS_9	−0.95	
33	CH-DAV		TS_1	−0.05	
34	CH-DAV		TS_2	−0.15	
35	CH-DAV		TS_3	−0.5	
36	CH-DAV		TS_4	–	
37	CH-DAV		TS_5	–	
38	CH-DAV		TS_6	–	
39	CH-OE2		TS_1	−0.05	
40	CH-OE2		TS_2	−0.1	
41	CH-OE2		TS_3	−0.15	
42	CH-OE2		TS_4	–	
43	CH-OE2		TS_5	−0.3	
44	CH-OE2		TS_6	−0.5	
45	CH-OE2		TS_7	–	
46	CN-HGU		TS		
47	DE-DGW		No data		
48	DE-HTE		TS_1	0	
49	DE-HTE		TS_2	−0.1	
50	DE-HTE		TS_3	−0.2	
51	DE-SFN		TS_1	−0.02	
52	DE-SFN		TS_3	−0.1	
53	DE-SFN		TS_4	−0.2	
54	DE-SFN		TS_5	−0.5	
55	DE-ZRK		TS_1	−0.05	

Table B7. Continued.

	SITE_ID	Year	Probe name	Soil_temp_depth_m	Additional_notes
56	DE-ZRK		TS_2	−0.1	
57	DE-ZRK		TS_3	−0.2	
58	DE-ZRK		TS_4	−0.3	
59	DE-ZRK		TS_5	−0.5	
60	FI-HYY		TS_1	−0.02	
61	FI-HYY		TS_2	−0.04	
62	FI-HYY		TS_3	−0.12	
63	FI-HYY		TS_4	−0.25	
64	FI-HYY		TS_5	−0.5	
65	FI-LOM		TS_1	−0.07	
66	FI-LOM		TS_2	−0.3	
67	FI-LOM		TS_3	−0.5	
68	FI-SI2		TS_1	−0.05	
69	FI-SI2		TS_2	−0.2	
70	FI-SI2		TS_3	−0.35	
71	FI-SI2		TS_4	−0.5	
72	FI-SII	Pre−2016	TS_1	−0.05	
73	FI-SII	Pre−2016	TS_2	−0.2	
74	FI-SII	Pre−2016	TS_3	−0.35	
75	FI-SII	Pre−2016	TS_4	−0.5	
76	FI-SII	After 2017	TS_1	0	
77	FI-SII	After 2017	TS_2	−0.5	
78	FI-SII	After 2017	TS_3	−0.1	
79	FI-SII	After 2017	TS_4	−0.15	
80	FI-SII	After 2017	TS_5	−0.25	
81	FI-SII	After 2017	TS_6	−0.45	
82	FI-SII	After 2017	TS_7	−0.95	
83	FR-LGT		TS_1	−0.02	
84	FR-LGT		TS_2	−0.05	
85	FR-LGT		TS_3	−0.1	
86	FR-LGT		TS_4	−0.2	
87	FR-LGT		TS_5	−0.4	
88	HK-MPM		TS_1		
89	HK-MPM		TS_2		
90	HK-MPM		TS_3		
91	ID-PAG		TS_1	−0.05	
92	IT-BCI		TS_1	−0.05	
93	IT-BCI		TS_2	−0.1	
94	IT-BCI		TS_3	−0.3	
95	IT-BCI		TS_4	−0.5	
96	IT-BCI		TS_5	−1	
97	IT-CAS		TS_1	−0.035	
98	IT-CAS		TS_2	−0.075	
99	IT-CAS		TS_3	−0.15	
100	JP-BBY		TS_1	−0.183	
101	JP-BBY		TS_2	−0.233	
102	JP-BBY		TS_3	−0.283	
103	JP-BBY		TS_4	−0.383	
104	JP-BBY		TS_5	−0.483	
105	JP-MSE		TS_1	−0.01	
106	JP-MSE		TS_2	−0.025	
107	JP-MSE		TS_3	−0.05	
108	JP-MSE		TS_4	−0.1	
109	JP-MSE		TS_5	−0.2	
110	JP-MSE		TS_6	−0.4	
111	JP-SWL		no data		

Table B7. Continued.

	SITE_ID	Year	Probe name	Soil_temp_depth_m	Additional_notes
112	KR-CRK		TS_1	−0.05	
113	KR-CRK		TS_2	−0.15	
114	MAERC		TS		
115	MY-MLM		TS_1	−0.05	
116	NL-HOR		TS_1	−0.01	
117	NL-HOR		TS_2	−0.02	
118	NL-HOR		TS_3	−0.04	
119	NL-HOR		TS_4	−0.05	
120	NL-HOR		TS_5	−0.1	
121	NL-HOR		TS_6	−0.15	
122	NL-HOR		TS_7	−0.25	
123	NL-HOR		TS_8	−0.4	
124	NL-HOR		TS_9	−0.6	
125	NZ-KOP		TS_1	−0.5	
126	NZ-KOP		TS_2	−0.1	
127	NZ-KOP		TS_3	−0.2	
128	PH-RIF		TS_1		
129	RU-CH2		TS_1	−0.04	
130	RU-CH2		TS_2	−0.08	
131	RU-CH2		TS_3	−0.16	
132	RU-CHE		TS_1	−0.04	
133	RU-CHE		TS_2	−0.08	
134	RU-CHE		TS_3	−0.16	
135	RU-COK		No data		
136	RU-FY2		TS_1		
137	RU-FY2		TS_2		
138	RU-FY2		TS_3		
139	RU-FY2		TS_4		
140	RU-FY2		TS_5		
141	SE-DEG		TS_1	−0.02	
142	SE-DEG		TS_2	−0.05	
143	SE-DEG		TS_3	−0.1	
144	SE-DEG		TS_4	−0.15	
145	SE-DEG		TS_5	−0.3	
146	SE-DEG		TS_6	−0.5	
147	UK-LBT		No data		
148	US-A03		TS_1	−0.025	
149	US-A03		TS_2	−0.1	
150	US-A03		TS_3	−0.3	
151	US-A10		TS_1	−0.025	
152	US-A10		TS_2	−0.1	
153	US-A10		TS_3	−0.3	
154	US-ATQ		TS_1		
155	US-ATQ		TS_2		
156	US-ATQ		TS_3		
157	US-BEO		TS_1		
158	US-BEO		TS_2		
159	US-BEO		TS_3		
160	US-BES		TS_1		
161	US-BES		TS_2		
162	US-BES		TS_3		
163	US-BI1		TS_1	−0.02	
164	US-BI1		TS_2	−0.04	
165	US-BI1		TS_3	−0.08	
166	US-BI1		TS_4	−0.16	
167	US-BI1		TS_5	−0.32	

Table B7. Continued.

	SITE_ID	Year	Probe name	Soil_temp_depth_m	Additional_notes
168	US-BI2		TS_1	−0.02	
169	US-BI2		TS_2	−0.04	
170	US-BI2		TS_3	−0.08	
171	US-BI2		TS_4	−0.16	
172	US-BI2		TS_5	−0.32	
173	US-BRW				
174	US-BZB		TS_1	−0.075	
175	US-BZB		TS_2	−0.05	
176	US-BZF		TS_1	−0.075	
177	US-BZF		TS_2	−0.05	
178	US-BZS		TS_1		
179	US-BZS		TS_2		
180	US-BZS		TS_3		
181	US-CRT		TS_1		
182	US-DPW		No data		
183	US-EDN		TS_1	−0.25	
184	US-EDN		TS_2	−0.15	
185	US-EDN		TS_3	−0.05	
186	US-EDN		TS_4	0	
187	US-EDN		TS_5	0.05	
188	US-EDN		TS_6	0.1	
189	US-EDN		TS_7	0.2	
190	US-EDN		TS_8	0.3	
191	US-EML		TS_1	−0.05	
192	US-EML		TS_2	−0.1	
193	US-EML		TS_3	−0.2	
194	US-EML		TS_4	−0.4	
195	US-HO1		TS_1	−0.05	
196	US-HO1		TS_2	−0.1	
197	US-HRA		No data	−0.02	
198	US-HRC		No data	−0.02	
199	US-ICS		TS_1	−0.075	
200	US-ICS		TS_2	−0.05	
201	US-IVO		TS_1	−0.05	
202	US-IVO		TS_2	−0.1	
203	US-IVO		TS_3	−0.15	
204	US-IVO		TS_4	−0.3	
205	US-IVO		TS_5	−0.4	
206	US-LA1		TS	−0.1	
207	US-LA2		TS	−0.1	
208	US-LOS		TS_1	0	
209	US-LOS		TS_2	−0.05	
210	US-LOS		TS_3	−0.1	
211	US-LOS		TS_4	−0.2	
212	US-LOS		TS_5	−0.5	
213	US-MRM		TS_1		
214	US-MRM		TS_2		
215	US-MYB		TS_1	−0.02	
216	US-MYB		TS_2	−0.04	
217	US-MYB		TS_3	−0.08	
218	US-MYB		TS_4	−0.16	
219	US-MYB		TS_5	−0.32	
220	US-NC4		TS_1	−0.05	
221	US-NC4		TS_2	−0.2	
222	US-NGB		No data		
223	US-NGC		No data		
224	US-ORV		TS_1	−0.08	

Table B7. Continued.

	SITE_ID	Year	Probe name	Soil_temp_depth_m	Additional_notes
225	US-OWC		TS_1	−0.05	
226	US-OWC		TS_2	−0.3	
227	US-PFA				
228	US-SND		TS_1	−0.08	
229	US-SND		TS_2	−0.16	
230	US-SND		TS_3		
231	US-SND		TS_4		
232	US-SND		TS_5		
233	US-SND		TS_6		
234	US-SNE		TS_1	−0.01	
235	US-SNE		TS_2	−0.02	
236	US-SNE		TS_3	−0.08	
237	US-SNE		TS_4	−0.16	
238	US-SNE		TS_5	−0.32	
239	US-SRR		TS_1		
240	US-SRR		TS_2		
241	US-SRR		TS_3		
242	US-SRR		TS_4		
243	US-SRR		TS_5		
244	US-STJ		TS_2	−0.05	
245	US-STJ		TS_3	−0.1	
246	US-TW1		TS_1	−0.02	
247	US-TW1		TS_2	−0.04	
248	US-TW1		TS_3	−0.08	
249	US-TW1		TS_4	−0.16	
250	US-TW1		TS_5	−0.32	
251	US-TW3		TS_1	−0.02	
252	US-TW3		TS_2	−0.04	
253	US-TW3		TS_3	−0.08	
254	US-TW3		TS_4	−0.16	
255	US-TW3		TS_5	−0.32	
256	US-TW4		TS_1	−0.02	
257	US-TW4		TS_2	−0.04	
258	US-TW4		TS_3	−0.08	
259	US-TW4		TS_4	−0.16	
260	US-TW4		TS_5	−0.32	
261	US-TW5		TS_1	−0.02	
262	US-TW5		TS_2	−0.1	
263	US-TW5		TS_3	−0.02	
264	US-TW5		TS_4	−0.08	
265	US-TW5		TS_5	−0.16	
266	US-TWT		TS_1	−0.02	
267	US-TWT		TS_2	−0.04	
268	US-TWT		TS_3	−0.08	
269	US-TWT		TS_4	−0.16	
270	US-TWT		TS_5	−0.32	
271	US-UAF		TS_1	−0.09	average of 3 depths: −0.15, −0.02, −0.1
272	US-UAF		TS_2	−0.18333	average of 3 depths: −0.3, −0.05, −0.2
273	US-UAF		TS_3	−0.28333	average of 3 depths: −0.3, −0.05, −0.2
274	US-UAF		TS_4	−0.36667	average of 3 depths: −0.5, −0.2, −0.4
275	US-UAF		TS_5	−0.5	average of 2 depths: −0.7, −0.3
276	US-UAF		TS_6	−0.6	average of 2 depths: −0.8, −0.4
277	US-UAF		TS_7	−0.75	average of 2 depths: −1, −0.5
278	US-UAF		TS_8	−0.925	average of 2 depths: −1.25, 0.6,
279	US-UAF		TS_9	−1	
280	US-WPT		TS_1	−0.1	
281	US-WPT		TS_2	−0.3	

Column	Description
SITE_ID	Site identification code as assigned by regional flux data network
Year	When relevant, information about time span of probe location; if blank, assume constant probe depth
Probe_name	Temperature probe name as given in data files
Soil_temp_depth_m	Depth of soil temperature probe (m), with negative values being under the surface
Additional_notes	When relevant, additional information about site

Author contributions. KBD oversaw the data release, performed the seasonality analysis, gathered metadata, and prepared the manuscript with contributions from all co-authors. SHK gathered and standardized the data, and gap-filled the CH_4 flux data. AM prepared the manuscript and gathered metadata. EFC did the representativeness analysis and prepared the manuscript. GM gathered data and prepared the manuscript. RBJ oversaw the data collection, processing, analysis, and release. DC and YWC oversaw the FLUXNET-CH_4 dataset release on https://fluxnet.org (last access: 6 July 2021). DP, EC, and CT did the data collection, curation, and pre-processing for all of the sites outside North and South America. The remaining co-authors contributed eddy-covariance data to FLUXNET-CH_4 dataset and/or participated in editing the manuscript.

Competing interests. The authors declare that they have no conflict of interest.

Disclaimer. Publisher's note: Copernicus Publications remains neutral with regard to jurisdictional claims in published maps and institutional affiliations.

Acknowledgements. We acknowledge primary support from the Gordon and Betty Moore Foundation (grant GBMF5439, "Advancing Understanding of the Global Methane Cycle"; Stanford University) and from the John Wesley Powell Center for Analysis and Synthesis of the US Geological Survey ("Wetland FLUXNET Synthesis for Methane" working group). Benjamin R. K. Runkle was supported by the US National Science Foundation CBET CAREER Award 1752083. Ankur R. Desai acknowledges support of the DOE AmeriFlux Network Management Project. Masahito Ueyama was supported by ArCS II (JPMXD1420318865) and JSPS KAKENHI (20K21849). Dario Papale and Nina Buchmann acknowledge the support of the RINGO (GA 730944) H2020 EU project. Nina Buchmann and Kathrin Fuchs acknowledge the SNF project M4P (40FA40_154245/1) and InnoFarm (407340_172433). Nina Buchmann acknowledges support from the SNF for ICOS-CH phases 1 and 2 (20FI21_148992, 20FI20_173691). Carlo Trotta acknowledges the support of the E-SHAPE (GA 820852) H2020 EU project. William J. Riley was supported by the US Department of Energy, BER, RGCM, RUBISCO project under contract no. DEAC02−05CH11231. Jessica Turner acknowledges support from NSF GRFP (DGE−1747503) and NTL LTER (DEB−1440297). Minseok Kang was supported by the National Research Foundation of Korea (NRF−2018 R1C1B6002917). Carole Helfter acknowledges the support of the UK Natural Environment Research Council (the Global Methane Budget project, grant number NE/N015746/1). Rodrigo Vargas acknowledges support from the National Science Foundation (1652594). Dennis Baldocchi acknowledges the California Department of Water Resources for a funding contract from the California Department of Fish and Wildlife and the United States Department of Agriculture (NIFA grant #2011-67003-30371), as well as the US Department of Energy's Office of Science (AmeriFlux contract #7079856) for funding the AmeriFlux core sites. US-A03 and US-A10 are operated by the Atmospheric Radiation Measurement (ARM) user facility, a US Department of Energy's Office of Science user facility managed by the Biological and Environmental Research Program. Work at ANL was supported by the US Department of Energy's Office of Science and Office of Biological and Environmental Research under contract DE-AC02−06CH11357. Any use of trade, firm, or product names is for descriptive purposes only and does not imply endorsement by the US government. The CH-Dav, DE-SfN, FI-Hyy, FI-Lom, FI-Sii, FR-LGt, IT-BCi, SE-Deg, and SE-Sto sites are part of the ICOS European Research Infrastructure. Oliver Sonnentag acknowledges funding by the Canada Research Chairs, Canada Foundation for Innovation Leaders Opportunity Fund, and Natural Sciences and Engineering Research Council Discovery Grant programs for work at CA-SCC and CA-SCB. Benjamin Poulter acknowledges support from the NASA Carbon Cycle and Ecosystems program. Derrick Lai acknowledges the support of the Research Grants Council of the Hong Kong Special Administrative Region, China (project no. CUHK 458913). We thank Nathaniel Goenawan for his help with the representativeness analysis.

Financial support. This research has been supported by the Gordon and Betty Moore Foundation (grant no. GBMF5439), the John Wesley Powell Center for Analysis and Synthesis of the US Geological Survey, the National Science Foundation (grant nos. 1752083, DGE−1747503, and 1652594), the ArCS II (grant no. JPMXD1420318865), the JSPS KAKENHI (grant no. 20K21849), the RINGO (grant no. GA 730944), the SNF (grant nos. 40FA40_154245/1, 20FI21_148992, and 20FI20_173691), the InnoFarm (grant no. 407340_172433), the E-SHAPE (grant no. GA 820852), the US Department of Energy (grant nos. DEAC02−05CH11231, 7079856, and DE-AC02−06CH11357), the NTL LTER (grant no. DEB−1440297), the National Research Foundation of Korea (grant no. NRF−2018 R1C1B6002917), the UK Natural Environment Research Council (grant no. NE/N015746/1), the California Department of Fish and Wildlife (grant no. 2011-67003-30371), the Canada Research Chairs, the Canada Foundation for Innovation Leaders Opportunity Fund, the Natural Sciences and Engineering Research Council Discovery Grant programs, and the NASA Carbon Cycle and Ecosystems program.

Review statement. This paper was edited by David Carlson and reviewed by two anonymous referees.

References

Abdalla, M., Hastings, A., Truu, J., Espenberg, M., Mander, Ü, and Smith, P.: Emissions of methane from northern peatlands: a review of management impacts and implications for future management options, Ecol. Evol., 6, 7080–7102, https://doi.org/10.1002/ece3.2469, 2016.

Alberto, M. and Wassmann, R.: FLUXNET-CH_4 PHRiF Philippines Rice Institute flooded, Philippines, FLUXNET-CH4 Community Product [data set], https://doi.org/10.18140/FLX/1669653, 2020.

Alberto, M. C. R., Wassmann, R., Gummert, M., Buresh, R. J., Quilty, J. R., Correa, T. Q., Centeno, C. A. R., and Oca, G.

M.: Straw incorporated after mechanized harvesting of irrigated rice affects net emissions of CH_4 and CO_2 based on eddy covariance measurements, Field Crop. Res., 184, 162–175, https://doi.org/10.1016/j.fcr.2015.10.004, 2015.

Anderson, D. E., Verma, S. B., and Rosenberg, N. J.: Eddy correlation measurements of CO_2, latent heat, and sensible heat fluxes over a crop surface, Bound.-Lay. Meteorol., 29, 263–272, https://doi.org/10.1007/bf00119792, 1984.

Anderson, F. E., Bergamaschi, B., Sturtevant, C., Knox, S., Hastings, L., Windham-Myers, L., Detto, M., Hestir, E. L., Drexler, J., Miller, R. L., Matthes, J. H., Verfaillie, J., Baldocchi, D., Snyder, R. L., and Fujii, R.: Variation of energy and carbon fluxes from a restored temperate freshwater wetland and implications for carbon market verification protocols, J. Geophys. Res.-Biogeo., 121, 777–795, https://doi.org/10.1002/2015JG003083, 2016.

Angle, J. C., Morin, T. H., Solden, L. M., Narrowe, A. B., Smith, G. J., Borton, M. A., Rey-Sanchez, C., Daly, R. A., Mirfenderesgi, G., Hoyt, D. W., Riley, W. J., Miller, C. S., Bohrer, G., and Wrighton, K. C.: Methanogenesis in oxygenated soils is a substantial fraction of wetland methane emissions, Nat. Commun., 8, 1567, https://doi.org/10.1038/s41467-017-01753-4, 2017.

Bartlett, K. B., Bartlett, D. S., Harriss, R. C., and Sebacher, D. I.: Methane emissions along a salt marsh salinity gradient, Biogeochemistry, 4, 183–202, https://doi.org/10.1007/bf02187365, 1987.

Bastviken, D., Tranvik, L. J., Downing, J. A., Crill, P. M., and Enrich-Prast, A.: Freshwater methane emissions offset the continental carbon sink, Science, 331, 6013, https://doi.org/10.1126/science.1196808, 2011.

Billesbach, D. and Sullivan, R.: FLUXNET-CH_4 US-A03 ARM-AMF3-Oliktok, United States, FLUXNET-CH4 Community Product [data set], https://doi.org/10.18140/FLX/1669661, 2020a.

Billesbach, D. and Sullivan, R.: FLUXNET-CH_4 US-A10 ARM-NSA-Barrow, United States, FLUXNET-CH4 Community Product [data set], https://doi.org/10.18140/FLX/1669662, 2020b.

Bloom, A. A., Bowman, K. W., Lee, M., Turner, A. J., Schroeder, R., Worden, J. R., Weidner, R., McDonald, K. C., and Jacob, D. J.: A global wetland methane emissions and uncertainty dataset for atmospheric chemical transport models (WetCHARTs version 1.0), Geosci. Model Dev., 10, 2141–2156, https://doi.org/10.5194/gmd-10-2141-2017, 2017.

Bridgham, S. D., Cadillo-Quiroz, H., Keller, J. K., and Zhuang, Q.: Methane emissions from wetlands: biogeochemical, microbial, and modeling perspectives from local to global scales, Glob. Change Biol., 19, 1325–1346, https://doi.org/10.1111/gcb.12131, 2013.

Bohrer, G. and Morin, T. H.: FLUXNET-CH_4 US-ORv Olentangy River Wetland Research Park, United States, FLUXNET-CH4 Community Product [data set], https://doi.org/10.18140/FLX/1669689, 2020.

Bohrer, G., Kerns, J., Morin, T. H., Rey-Sanchez, A. C., Villa, J., and Ju, Y.: FLUXNET-CH_4 US-OWC Old Woman Creek, United States, FLUXNET-CH4 Community Product [data set], https://doi.org/10.18140/FLX/1669690. 2020.

Campbell, D. and Goodrich, J.: FLUXNET-CH_4 NZ-Kop Kopuatai, New Zealand, FLUXNET-CH4 Community Product [data set], https://doi.org/10.18140/FLX/1669652, 2020.

Castro-Morales, K., Kleinen, T., Kaiser, S., Zaehle, S., Kittler, F., Kwon, M. J., Beer, C., and Göckede, M.: Year-round simulated methane emissions from a permafrost ecosystem in Northeast Siberia, Biogeosciences, 15, 2691–2722, https://doi.org/10.5194/bg-15-2691-2018, 2018.

Chadburn, S. E., Aalto, T., Aurela, M., Baldocchi, D., Biasi, C., Boike, J., Burke, E. J., Comyn-Platt, E., Dolman, A. J., Duran-Rojas, C., Fan, Y., Friborg, T., Gao, Y., Gedney, N., Göckede, M., Hayman, G. D., Holl, D., Hugelius, G., Kutzbach, L., Lee, H., Lohila, A., Parmentier, F. W., Sachs, T., Shurpali, N. J., and Westermann, S.: Modeled microbial dynamics explain the apparent temperature sensitivity of wetland methane emissions, Global Biogeochem. Cy., 34, e2020GB006678, https://doi.org/10.1029/2020gb006678, 2020.

Chamberlain, S. D., Oikawa, P., Sturtevant, C., Szutu, D., Verfaillie, J., and Baldocchi, D.: FLUXNET-CH_4 US-Tw3 Twitchell Alfalfa, United States, FLUXNET-CH4 Community Product [data set], https://doi.org/10.18140/FLX/1669697, 2020.

Chambers, L. G., Ramesh Reddy, K., and Osborne, T. Z.: Short-Term Response of Carbon Cycling to Salinity Pulses in a Freshwater Wetland, Soil Sci. Soc. Am. J., 75, 2000–2007, https://doi.org/10.2136/sssaj2011.0026, 2011.

Chang, K. Y., Riley, W. J., Knox, S. H., Jackson, R. B., McNicol, G., Poulter, B., Aurela, M., Baldocchi, D., Bansal, S., Bohrer, G., Campbell, D. I., Cescatti, A., Chu, H., Delwiche, K. B., Desai, A., Euskirchen, E., Friborg, T., Goeckede, M., Holm, G., Kang, M., Keenan, T., Krauss, K. W., Lohila, A., Mammarella, I., Miyata, A., Nilsson, M. B., Noormets, A., Papale, D., Runkle, B. R. K., Ryu, Y., Sachs, T., Schäfer, K. V. R., Schmid, H. P., Shurpali, N., Sonnentag, O., Tang, A. C. I., Torn, M. S., Trotta, C., Ueyama, M., Vargas, R., Vesala, T., Windham-Myers, L., Zhang, Z., and Zona, D.: Global wetland methane emissions have hysteretic responses to seasonal temperature, Nat. Commun., 12, 2266, https://doi.org/10.1038/s41467-021-22452-1, 2021.

Chanton, J. P., Glaser, P. H., Chasar, L. S., Burdige, D. J., Hines, M. E., Siegel, D. I., Tremblay, L. B., and Cooper, W. T.: Radiocarbon evidence for the importance of surface vegetation on fermentation and methanogenesis in contrasting types of boreal peatlands, Global Biogeochem. Cy., 22, GB4022, https://doi.org/10.1029/2008gb003274, 2008.

Chen, J. and Chu, H.: FLUXNET-CH_4 US-CRT Curtice Walter-Berger cropland, United States, FLUXNET-CH4 Community Product [data set], https://doi.org/10.18140/FLX/1669671, 2020a.

Chen, J. and Chu, H.: FLUXNET-CH_4 US-WPT Winous Point North Marsh, United States, FLUXNET-CH4 Community Product [data set], https://doi.org/10.18140/FLX/1669702, 2020b.

Chu, H., Chen, J., Gottgens, J. F., Ouyang, Z., John, R., Czajkowski, K., and Becker, R.: Net ecosystem methane and carbon dioxide exchanges in a Lake Erie coastal marsh and a nearby cropland, J. Geophys. Res.-Biogeo., 119, 722–740, https://doi.org/10.1002/2013JG002520, 2014.

Chu, H., Baldocchi, D. D., John, R., Wolf, S., and Reichstein, M.: Fluxes all of the time? A primer on the temporal representativeness of FLUXNET, J. Geophys. Res.-Biogeo., 122, 289–307, https://doi.org/10.1002/2016JG003576, 2017.

Chu, H., Luo, X., Ouyang, Z., Chan, W. S., Dengel, S., Biraud, S. C., Torn, M. S., Metzger, S., Kumar, J., Arain, M. A., Arkebauer, T. J., Baldocchi, D., Bernacchi, C., Billesbach, D., Black,

T. A., Blanken, P. D., Bohrer, G., Bracho, R., Brown, S., Brunsell, N. A., Chen, J., Chen, X., Clark, K., Desai, A.R., Duman, T., Durden, D., Fares, S., Forbrich, I., Gammon, J. A., Gough, C. M., Griffis, T., Helbig, M., Hollinger, D., Humphreys, E., Ikawa, H., Iwata, H., Ju, Y., Knowles, J. F., Knox, S. H., Kobayashi, H., Kolb, T., Law, B., Lee, X., Litvak, M., Liu, H., Munger, J. W., Noormets, A., Novick, K., Oberbauer, S. F., Oechel, W., Oikawa, P., Papuga, S. A., Pendall, E., Prajapati, P., Prueger, J., Quinton, W. L., Richardson, A. D., Russel, E. S., Scott, R. L., Starr, G., Staebler, R., Stoy, P., Stuart-Haentjens, E., Sonnentag, O., Sullivan, R. C., Suyker, A., Ueyama, M., Vargas, R., Wood, J. D., and Zona, D.: Representativeness of Eddy-Covariance flux footprints for areas surrounding AmeriFlux sites, Agr. Forest Meteorol., 301-302, 108350, https://doi.org/10.1016/j.agrformet.2021.108350, 2021.

Dalcin Martins, P., Hoyt, D. W., Bansal, S., Mills, C. T., Tfaily, M., Tangen, B. A., Finocchiaro, R. G., Johnston, M. D., McAdams, B. C., Solensky, M. J., Smith, G. J., Chin, Y.-P., and Wilkins, M. J.: Abundant carbon substrates drive extremely high sulfate reduction rates and methane fluxes in Prairie Pothole Wetlands, Glob. Change Biol., 23, 3107–3120, https://doi.org/10.1111/gcb.13633, 2017.

Dean, J. F., Middelburg, J. J., Röckmann, T., Aerts, R., Blauw, L. G., Egger, M., Jetten, M. S. M., de Jong, A. E. E., Meisel, O. H., Rasigraf, O., Slomp, C. P., in't Zandt, M. H., and Dolman, A. J.: Methane Feedbacks to the Global Climate System in a Warmer World, Rev. Geophys., 56, 207–250, https://doi.org/10.1002/2017rg000559, 2018.

Deemer, B. R., Harrison, J. A., Li, S., Beaulieu, J. J., DelSontro, T., Barros, N., Bezerra-Neto, J. F., Powers, S. M., Dos Santos, M. A., and Vonk, J. A.: Greenhouse Gas Emissions from Reservoir Water Surfaces: A New Global Synthesis, Bioscience, 66, 949–964, https://doi.org/10.1093/biosci/biw117, 2016.

Dengel, S., Zona, D., Sachs, T., Aurela, M., Jammet, M., Parmentier, F. J. W., Oechel, W., and Vesala, T.: Testing the applicability of neural networks as a gap-filling method using CH_4 flux data from high latitude wetlands, Biogeosciences, 10, 8185–8200, https://doi.org/10.5194/bg-10-8185-2013, 2013.

Delwiche, K. B., Knox, S. H., Malhotra, A., Fluet-Chouinard, E., McNicol, G., Feron, S., Ouyang, Z., Papale, D., Trotta, C., Canfora, E., Cheah, Y.-W., Christianson, D., Alberto, M. C. R., Alekseychik, P., Aurela, M., Baldocchi, D., Bansal, S., Billesbach, D. P., Bohrer, G., Bracho, R., Buchmann, N., Campbell, D. I., Celis, G., Chen, J., Chen, W., Chu, H., Dalmagro, H.J., Dengel, S., Desai, A. R., Detto, M., Dolman, H., Eichelmann, E., Euskirchen, E., Famulari, D., Friborg, T., Fuchs, K., Goeckede, M., Gogo, S., Gondwe, M. J., Goodrich, J. P., Gottschalk, P., Graham, S. L., Heimann, M., Helbig, M., Helfter, C., Hemes, K. S., Hirano, T., Hollinger, D., Hörtnagl, L., Iwata, H., Jacotot, A., Jansen, J., Jurasinski, G., Kang, M., Kasak, K., King, J., Klatt, J., Koebsch, F., Krauss, K. W., Lai, D. Y. F., Mammarella, I., Manca, G., Marchesini, L. B., Matthes, J. H., Maximon, T., Merbold, L., Mitra, B., Morin, T. H., Nemitz, E., Nilsson, M. B., Niu, S., Oechel, W.C., Oikawa, P. Y., Ono, K., Peichl, M., Peltola, O., Reba, M. L., Richardson, A. D., Riley, W., Runkle, B. R. K., Ryu, Y., Sachs, T., Sakabe, A., Sanchez, C. R., Schuur, E. A., Schäfer, K. V. R., Sonnentag, O., Sparks, J. P., Stuart- Haëntjens, E., Sturtevant, C., Sullivan, R. C., Szutu, D. J., Thom, J. E., Torn, M. S., Tuittila, E.-S., Turner, J., Ueyama, M., Valach, A. C., Vargas, R., Varlagin, A., Vazquez-Lule, A., Verfaillie, J. G., Vesala, T., Vourlitis, G. L., Ward, E. J., Wille, C., Wohlfahrt, G., Wong, G. X., Zhang, Z., Zona, D., Windham-Myers, L., Poulter, B., and Jackson, R. B.: FLUXNET-CH_4: A global, multi-ecosystem dataset and analysis of methane seasonality from freshwater wetlands (Appendix B and Figure 3), Zenodo [data set], https://doi.org/10.5281/zenodo.4672601, 2021.

Deshmukh, C. S., Julius, D., Evans, C. D., Nardi, Susanto, A. P., Page, S. E., Gauci, V., Laurén, A., Sabiham, S., Agus, F., Asyhari, A., Kurnianto, S., Suardiwerianto, Y., and Desai, A. R.: Impact of forest plantation on methane emissions from tropical peatland, Glob. Change Biol., 26, 2477–2495, https://doi.org/10.1111/gcb.15019, 2020.

Desai, A. R.: FLUXNET-CH_4 US-Los Lost Creek, United States, FLUXNET-CH4 Community Product [data set], https://doi.org/10.18140/FLX/1669682, 2020a.

Desai, A. R.: FLUXNET-CH_4 US-PFa Park Falls/WLEF, United States, FLUXNET-CH4 Community Product [data set], https://doi.org/10.18140/FLX/1669691, 2020b.

Desjardins, R. L.: A technique to measure CO_2 exchange under field conditions, Int. J. Biometeorol., 18, 76–83, https://doi.org/10.1007/bf01450667, 1974.

Detto, M., Sturtevant, C., Oikawa, P., Verfaillie, J., and Baldocchi, D.: FLUXNET-CH_4 US-Snd Sherman Island, United States, FLUXNET-CH4 Community Product [data set], https://doi.org/10.18140/FLX/1669692, 2020.

Didan, K.: MOD13A3 MODIS/Terra vegetation Indices Monthly L3 Global 1km SIN Grid V006, NASA EOSDIS Land Processes DAAC [data set], https://doi.org/10.5067/MODIS/MOD13A3.006, 2015.

Dise, N.: Winter fluxes of methane from Minnesota peatlands, Biogeochemistry, 17, 17–83, https://doi.org/10.1007/bf00002641, 1992.

Dolman, H., Hendriks, D., van Huissteden, K., and Belelli, L.: FLUXNET-CH_4 NL-Hor Horstermeer, Netherlands, FLUXNET-CH4 Community Product [data set], https://doi.org/10.18140/FLX/1669651, 2020a.

Dolman, H., Maximov, T., Parmentier, F., Budishev, A., and Marchesini, L. B.: FLUXNET-CH_4 RU-Cok Chokurdakh, Russian Federation, FLUXNET-CH4 Community Product [data set], https://doi.org/10.18140/FLX/1669656, 2020b.

Eichelmann, E., Knox, S., Rey Sanchez, C., Valach, A., Sturtevant, C., Szutu, D., Verfaillie, J., and Baldocchi, D.: FLUXNET-CH_4 US-Tw4 Twitchell East End Wetland, United States, FLUXNET-CH4 Community Product [data set], https://doi.org/10.18140/FLX/1669698, 2020.

Eklundh, L. and Jönsson, P.: TIMESAT: A Software Package for Time-Series Processing and Assessment of Vegetation Dynamics, Remote Sensing Time Series, Springer International Publishing, 141–158, https://doi.org/10.1007/978-3-319-15967-6_7. 2015.

Etheridge, D. M., Steele, L. P., Francey, R. J., and Langenfelds, R. L.: Atmospheric methane between 1000 A.D. and present: Evidence of anthropogenic emissions and climatic variability, J. Geophys. Res.-Atmos., 103, 15979–15993, https://doi.org/10.1029/98jd00923, 1998.

Etminan, M., Myhre, G., Highwood, E. J., and Shine, K. P.: Radiative forcing of carbon dioxide, methane, and nitrous oxide: A significant revision of the methane radiative forcing, Geophys. Res.

Lett., 43, 12614–12623, https://doi.org/10.1002/2016gl071930, 2016.

Euskirchen, E. and Edgar, C.: FLUXNET-CH_4 US-BZB Bonanza Creek Thermokarst Bog, United States, FLUXNET-CH4 Community Product [data set], https://doi.org/10.18140/FLX/1669668, 2020a.

Euskirchen, E. and Edgar, C.: FLUXNET-CH_4 US-BZF Bonanza Creek Rich Fen, United States, FLUXNET-CH4 Community Product [data set], https://doi.org/10.18140/FLX/1669669, 2020b.

Euskirchen, E. and Edgar, C.: FLUXNET-CH_4 US-BZS Bonanza Creek Black Spruce, United States, FLUXNET-CH4 Community Product [data set], https://doi.org/10.18140/FLX/1669670, 2020c.

Euskirchen, E., Bret-Harte, M., and Edgar, C.: FLUXNET-CH_4 US-ICs Imnavait Creek Watershed Wet Sedge Tundra, United States, FLUXNET-CH4 Community Product [data set], https://doi.org/10.18140/FLX/1669678, 2020.

Famulari, D.: FLUXNET-CH_4 IT-BCi Borgo Cioffi, Italy, FLUXNET-CH4 Community Product [data set], https://doi.org/10.18140/FLX/1669644, 2020.

Fick, S. E. and Hijmans, R. J.: WorldClim: 2: new 1km spatial resolution climate surfaces for global land areas, Int. J. Climatol., 37, 4302–4315, 2017.

Friborg, T., Christensen, T. R., and Søgaard, H.: Rapid response of greenhouse gas emission to early spring thaw in a subarctic mire as shown by micrometeorological techniques, Geophys. Res. Lett., 24, 3061–3064, https://doi.org/10.1029/97gl03024, 1997.

Gallant, A.: The Challenges of Remote Monitoring of Wetlands, Remote Sensing, 7, 10938–10950, https://doi.org/10.3390/rs70810938, 2015.

Göckede, M., Kittler, F., and Schaller, C.: Quantifying the impact of emission outbursts and non-stationary flow on eddy-covariance CH_4 flux measurements using wavelet techniques, Biogeosciences, 16, 3113–3131, https://doi.org/10.5194/bg-16-3113-2019, 2019.

Goeckede, M.: FLUXNET-CH_4 RU-Ch2 Chersky reference, Russian Federation, FLUXNET-CH4 Community Product [data set], https://doi.org/10.18140/FLX/1669654, 2020.

Gu, L., Post, W. M., Baldocchi, D. D., Andrew Black, T., Suyker, A. E., Verma, S. B., Vesala, T., and Wofsy, S. C.: Characterizing the Seasonal Dynamics of Plant Community Photosynthesis Across a Range of Vegetation Types, in: Phenology of Ecosystem Processes, edited by: Noormets, A., Springer, New York, NY, 35–58, https://doi.org/10.1007/978-1-4419-0026-5_2, 2009.

Hargreaves, K. J., Fowler, D., Pitcairn, C. E. R., and Aurela, M.: Annual methane emission from Finnish mires estimated from eddy covariance campaign measurements, Theor. Appl. Climatol., 70, 203–213, https://doi.org/10.1007/s007040170015, 2001.

Hargrove, W. W., Hoffman, F. M., and Law, B. E.: New analysis reveals representativeness of the AmeriFlux network, Eos T. Am. Geophys., 84, 529, https://doi.org/10.1029/2003EO480001, 2003.

Hatala, J. A., Detto, M., and Baldocchi, D. D.: Gross ecosystem photosynthesis causes a diurnal pattern in methane emission from rice, Geophys. Res. Lett., 39, L06409m https://doi.org/10.1029/2012gl051303, 2012.

Helbig, M., Quinton, W. L., and Sonnentag, O.: Warmer spring conditions increase annual methane emissions from a boreal peat landscape with sporadic permafrost, Environ. Res. Lett., 12, 115009, https://doi.org/10.1088/1748-9326/aa8c85, 2017.

Helfter, C.: FLUXNET-CH_4 BW-Gum Guma, Botswana, FLUXNET-CH4 Community Product [data set], https://doi.org/10.18140/FLX/1669370, 2020a.

Helfter, C.: FLUXNET-CH_4 BW-Nxr Nxaraga, Botswana, FLUXNET-CH4 Community Product [data set], https://doi.org/10.18140/FLX/1669518, 2020b.

Helfter, C.: FLUXNET-CH_4 UK-LBT London_BT, United Kingdom, FLUXNET-CH4 Community Product [data set], https://doi.org/10.18140/FLX/1670207, 2020c.

Helfter, C., Tremper, A. H., Halios, C. H., Kotthaus, S., Bjorkegren, A., Grimmond, C. S. B., Barlow, J. F., and Nemitz, E.: Spatial and temporal variability of urban fluxes of methane, carbon monoxide and carbon dioxide above London, UK, Atmos. Chem. Phys., 16, 10543–10557, https://doi.org/10.5194/acp-16-10543-2016, 2016.

Hinkle, C. R. and Bracho, R.: FLUXNET-CH_4 US-DPW Disney Wilderness Preserve Wetland, United States, FLUXNET-CH4 Community Product [data set], https://doi.org/10.18140/FLX/1669672, 2020.

Hoffman, F. M., Kumar, J., Mills, R. T., and Hargrove, W. W.: Representativeness-based sampling network design for the State of Alaska, Landscape Ecol., 28, 1567–1586, https://doi.org/10.1007/s10980-013-9902-0, 2013.

Hollinger, D. Y. and Richardson, A. D.: Uncertainty in Eddy Covariance Measurements and Its Application to Physiological Models, Tree Physiol., 25, 873–885, https://doi.org/10.1093/treephys/25.7.873, 2005.

Holm, G. O., Perez, B. C., McWhorter, D. E., Krauss, K. W., Raynie, R. C., and Killebrew, C. J.: FLUXNET-CH_4 US-LA1 Pointe-aux-Chenes Brackish Marsh, United States, FLUXNET-CH4 Community Product [data set], https://doi.org/10.18140/FLX/1669680, 2020a.

Holm, G. O., Perez, B. C., McWhorter, D. E., Krauss, K. W., Raynie, R. C., and Killebrew, C. J.: FLUXNET-CH_4 US-LA2 Salvador WMA Freshwater Marsh, United States, FLUXNET-CH4 Community Product [data set], https://doi.org/10.18140/FLX/1669681, 2020b.

Hwang, Y., Ryu, Y., Huang, Y., Kim, J., Iwata, H., and Kang, M.: Comprehensive assessments of carbon dynamics in an intermittently-irrigated rice paddy, Agr. Forest Meteorol., 285–286, 107933, https://doi.org/10.1016/j.agrformet.2020.107933, 2020.

Iwata, H.: FLUXNET-CH_4 JP-Mse Mase rice paddy field, Japan, FLUXNET-CH4 Community Product [data set], https://doi.org/10.18140/FLX/1669647, 2020a.

Iwata, H.: FLUXNET-CH_4 JP-SwL Suwa Lake, Japan, FLUXNET-CH4 Community Product [data set], https://doi.org/10.18140/FLX/1669648, 2020b.

Iwata, H., Mano, M., Ono, K., Tokida, T., Kawazoe, T., Kosugi, Y., Sakabe, A., Takahashi, K., and Miyata, A.: Exploring sub-daily to seasonal variations in methane exchange in a single-crop rice paddy in central Japan, Atmos. Environ., 179, 156–165, https://doi.org/10.1016/j.atmosenv.2018.02.015, 2018.

Iwata, H., Ueyama, M., and Harazono, Y.: FLUXNET-CH_4 US-Uaf University of Alaska, Fairbanks, United States, FLUXNET-CH4 Community Product [data set], https://doi.org/10.18140/FLX/1669701, 2020.

Jacotot, A., Gogo, S., and Laggoun-Défarge, F.: FLUXNET-CH_4 FR-LGt La Guette, France, FLUXNET-CH4 Community Product [data set], https://doi.org/10.18140/FLX/1669641, 2020.

Jönsson, P. and Eklundh, L.: Seasonality extraction by function fitting to time-series of satellite sensor data, IEEE T. Geosci. Remote, 40, 1824–1832, https://doi.org/10.1109/tgrs.2002.802519, 2002.

Jönsson, P. and Eklundh, L.: TIMESAT – a program for analyzing time-series of satellite sensor data. Comput. Geosci., 30, 833–845, https://doi.org/10.1016/j.cageo.2004.05.006, 2004.

Jung, M., Reichstein, M., and Bondeau, A.: Towards global empirical upscaling of FLUXNET eddy covariance observations: validation of a model tree ensemble approach using a biosphere model, Biogeosciences, 6, 2001–2013, https://doi.org/10.5194/bg-6-2001-2009, 2009.

Jung, M., Schwalm, C., Migliavacca, M., Walther, S., Camps-Valls, G., Koirala, S., Anthoni, P., Besnard, S., Bodesheim, P., Carvalhais, N., Chevallier, F., Gans, F., Goll, D. S., Haverd, V., Köhler, P., Ichii, K., Jain, A. K., Liu, J., Lombardozzi, D., Nabel, J. E. M. S., Nelson, J. A., O'Sullivan, M., Pallandt, M., Papale, D., Peters, W., Pongratz, J., Rödenbeck, C., Sitch, S., Tramontana, G., Walker, A., Weber, U., and Reichstein, M.: Scaling carbon fluxes from eddy covariance sites to globe: synthesis and evaluation of the FLUXCOM approach, Biogeosciences, 17, 1343–1365, https://doi.org/10.5194/bg-17-1343-2020, 2020.

Kim, Y., Johnson, M. S., Knox, S. H., Andrew Black, T., Dalmagro, H. J., Kang, M., Kim, J., and Baldocchi, D.: Gap-filling approaches for eddy covariance methane fluxes: A comparison of three machine learning algorithms and a traditional method with principal component analysis, Glob. Change Biol., 26, 1499–1518, https://doi.org/10.1111/gcb.14845, 2020.

Kittler, F., Heimann, M., Kolle, O., Zimov, N., Zimov, S., and Göckede, M.: Long-Term Drainage Reduces CO_2 Uptake and CH_4 Emissions in a Siberian Permafrost Ecosystem: Drainage impact on Arctic carbon cycle, Global Biogeochem. Cy., 31, 1704–1717, https://doi.org/10.1002/2017GB005774, 2017.

Knox, S., Matthes, J. H., Verfaillie, J., and Baldocchi, D.: FLUXNET-CH_4 US-Twt Twitchell Island, United States, FLUXNET-CH4 Community Product [data set], https://doi.org/10.18140/FLX/1669700, 2020.

Knox, S. H., Sturtevant, C., Matthes, J. H., Koteen, L., Verfaillie, J., and Baldocchi, D.: Agricultural peatland restoration: effects of land-use change on greenhouse gas (CO_2 and CH_4) fluxes in the Sacramento-San Joaquin Delta, Glob. Change Biol., 21, 750–765, https://doi.org/10.1111/gcb.12745, 2015.

Knox, S. H., Matthes, J. H., Sturtevant, C., Oikawa, P. Y., Verfaillie, J., and Baldocchi, D.: Biophysical controls on interannual variability in ecosystem-scale CO_2 and CH_4 exchange in a California rice paddy, J. Geophys. Res.-Biogeo., 121, 978–1001, https://doi.org/10.1002/2015jg003247, 2016.

Knox, S. H., Jackson, R. B., Poulter, B., McNicol, G., Fluet-Chouinard, E., Zhang, Z., Hugelius, G., Bousquet, P., Canadell, J. G., Saunois, M., Papale, D., Chu, H., Keenan, T. F., Baldocchi, D., Torn, M. S., Mammarella, I., Trotta, C., Aurela, M., Bohrer, G., Campbell, D.I., Cescatti, A., Chamberlain, S., Chen, J., Chen, W., Dengel, S., Desai, A. R., Euskirchen, E., Friborg, T., Gasbarra, D., Goded, I., Goeckede, M., Heimann, M., Helbig, M., Hirano, T., Hollinger, D. Y., Iwata, H., Jurasinski, G., Kang, M., Koebsch, F., Mammarella, I., Nilsson, M. B., Ono, K., Peichl, M., Peltola, O., Ryu, Y., Sachs, T., Sakabe, A., Sparks, J., Tuittila, E.-S., Vourlitis, G. L., Wong, G. X., Windham-Myers, L., Poulter, B., and Jackson, R. B.: FLUXNET-CH_4 Synthesis Activity: Objectives, Observations, and Future Directions, B. Am. Meterol. Soc., 100, 2607–2632, https://doi.org/10.1175/bams-d-18-0268.1, 2019.

Koebsch, F. and Jurasinski, G.: FLUXNET-CH_4 DE-Hte Huetelmoor, Germany, FLUXNET-CH4 Community Product [data set], https://doi.org/10.18140/FLX/1669634, 2020.

Koebsch, F., Jurasinski, G., Koch, M., Hofmann, J., and Glatzel, S.: Controls for multi-scale temporal variation in ecosystem methane exchange during the growing season of a permanently inundated fen, Agr. Forest Meteorol., 204, 94–105, https://doi.org/10.1016/j.agrformet.2015.02.002, 2015.

Koebsch, F., Winkel, M., Liebner, S., Liu, B., Westphal, J., Schmiedinger, I., Spitzy, A., Gehre, M., Jurasinski, G., Köhler, S., Unger, V., Koch, M., Sachs, T., and Böttcher, M. E.: Sulfate deprivation triggers high methane production in a disturbed and rewetted coastal peatland, Biogeosciences, 16, 1937–1953, https://doi.org/10.5194/bg-16-1937-2019, 2019.

Kuznetsova, A., Brockhoff, P. B., and Christensen, R. H. B.: lmerTest Package: Tests in Linear Mixed Effects Models, J. Stat. Softw., 82, 1–26, https://doi.org/10.18637/jss.v082.i13, 2017.

Kwon, M. J., Beulig, F., Ilie, I., Wildner, M., Küsel, K., Merbold, L., Mahecha, M. D., Zimov, N., Zimov, S. A., Heimann, M., Schuur, E. A. G., Kostka, J. E., Kolle, O., Hilke, I., and Göckede, M.: Plants, microorganisms, and soil temperatures contribute to a decrease in methane fluxes on a drained Arctic floodplain, Glob. Change Biol., 23, 2396–2412, https://doi.org/10.1111/gcb.13558, 2017.

Lai, D. Y. F.: Methane Dynamics in Northern Peatlands: A Review, Pedosphere, 19, 409–421, https://doi.org/10.1016/s1002-0160(09)00003-4, 2009.

Lai, D. Y. F., Roulet, N. T., and Moore, T. R.: The spatial and temporal relationships between CO_2 and CH_4 exchange in a temperate ombrotrophic bog, Atmos. Environ, 89, 249–259, https://doi.org/10.1016/j.atmosenv.2014.02.034, 2014.

Lai, D. Y. F.: FLUXNET-CH_4 HK-MPM Mai Po Mangrove, Hong Kong, FLUXNET-CH4 Community Product [data set], https://doi.org/10.18140/FLX/1669642, 2020.

Lasslop, G., Reichstein, M., Papale, D., Richardson, A. D., Arneth, A., Barr, A., Stoy, P., and Wohlfahrt, G.: Separation of net ecosystem exchange into assimilation and respiration using a light response curve approach: critical issues and global evaluation, Glob. Change Biol., 16, 187–208, https://doi.org/10.1111/j.1365-2486.2009.02041.x, 2010.

Liu, J., Zhou, Y., Valach, A., Shortt, R., Kasak, K., Rey-Sanchez, C., Hemes, K. S., Baldocchi, D., and Lai, D. Y. F.: Methane emissions reduce the radiative cooling effect of a subtropical estuarine mangrove wetland by half, Glob. Change Biol., 26, 4998–5016, https://doi.org/10.1111/gcb.15247, 2020.

Lohila, A., Aurela, M., Tuovinen, J.-P., Laurila, T., Hatakka, J., Rainne, J., and Mäkelä, T.: FLUXNET-CH_4 FI-Lom Lompolojankka, Finland, FLUXNET-CH4 Community Product [data set], https://doi.org/10.18140/FLX/1669638, 2020.

Madsen, K., Nielsen, H. B., and Tingleff, O.: Methods for non-linear least squares problems, Informatics and Mathematical Modelling, Technical Univeristy of Denmark, 2nd Edn., 2004.

Maier, R., Hörtnagl, L., and Buchmann, N.: FLUXNET-CH_4 CH-Oe2 Oensingen crop, FLUXNET-CH4 Community Product [data set], Switzerland, https://doi.org/10.18140/FLX/1669631, 2020.

Mahecha, M. D., Gans, F., Sippel, S., Donges, J. F., Kaminski, T., Metzger, S., Migliavacca, M., Papale, D., Rammig, A., and Zscheischler, J.: Detecting impacts of extreme events with ecological in situ monitoring networks, Biogeosciences, 14, 4255–4277, https://doi.org/10.5194/bg-14-4255-2017, 2017.

Malhotra, A. and Roulet, N. T.: Environmental correlates of peatland carbon fluxes in a thawing landscape: do transitional thaw stages matter?, Biogeosciences, 12, 3119–3130, https://doi.org/10.5194/bg-12-3119-2015, 2015.

Mammarella, I, Rannik, Ü., Kolari, P., Levula, J., and Vesala, T.: FLUXNET-CH_4 FI-Hyy Hyytiala, Finland, FLUXNET-CH4 Community Product [data set], https://doi.org/10.18140/FLX/1669637, 2020.

Manca, G. and Goded, I. FLUXNET-CH_4 IT-Cas Castellaro, Italy, FLUXNET-CH4 Community Product [data set], https://doi.org/10.18140/FLX/1669645, 2020.

Mastepanov, M., Sigsgaard, C., Tagesson, T., Ström, L., Tamstorf, M. P., Lund, M., and Christensen, T. R.: Revisiting factors controlling methane emissions from high-Arctic tundra, Biogeosciences, 10, 5139–5158, https://doi.org/10.5194/bg-10-5139-2013, 2013.

Matthes, J. H., Sturtevant, C., Oikawa, P., Chamberlain, S. D., Szutu, D., Ortiz, A. A., Verfaillie, J., and Baldocchi, D.: FLUXNET-CH_4 US-Myb Mayberry Wetland, United States, FLUXNET-CH4 Community Product [data set], https://doi.org/10.18140/FLX/1669685, 2020.

Matthews, E., Johnson, M. S., Genovese, V., Du, J., and Bastviken, D.: Methane emission from high latitude lakes: methane-centric lake classification and satellite-driven annual cycle of emissions. Sci. Rep.-UK, 10, 12465, https://doi.org/10.1038/s41598-020-68246-1, 2020.

Megonigal, J. P., Whalen, S. C., Tissue, D. T., Bovard, B. D., Allen, A. S., and Albert, D. B.: A Plant-Soil-Atmosphere Microcosm for Tracing Radiocarbon from Photosynthesis through Methanogenesis, Soil Sci. Soc. Am. J., 63, 665–671, https://doi.org/10.2136/sssaj1999.03615995006300030033x, 1999.

Meijide, A., Manca, G., Goded, I., Magliulo, V., di Tommasi, P., Seufert, G., and Cescatti, A.: Seasonal trends and environmental controls of methane emissions in a rice paddy field in Northern Italy, Biogeosciences, 8, 3809–3821, https://doi.org/10.5194/bg-8-3809-2011, 2011.

Melloh, R. A. and Crill, P. M.: Winter methane dynamics in a temperate peatland, Global Biogeochem. Cy., 10, 247–254, https://doi.org/10.1029/96gb00365, 1996.

Melton, J. R., Wania, R., Hodson, E. L., Poulter, B., Ringeval, B., Spahni, R., Bohn, T., Avis, C. A., Beerling, D. J., Chen, G., Eliseev, A. V., Denisov, S. N., Hopcroft, P. O., Lettenmaier, D. P., Riley, W. J., Singarayer, J. S., Subin, Z. M., Tian, H., Zürcher, S., Brovkin, V., van Bodegom, P. M., Kleinen, T., Yu, Z. C., and Kaplan, J. O.: Present state of global wetland extent and wetland methane modelling: conclusions from a model intercomparison project (WETCHIMP), Biogeosciences, 10, 753–788, https://doi.org/10.5194/bg-10-753-2013, 2013.

Merbold, L.: FLUXNET-CH_4 RU-Che Cherski, Russian Federation, FLUXNET-CH4 Community Product [data set], https://doi.org/10.18140/FLX/1669655, 2020.

Merbold, L., Fuchs, K., Buchmann, N., and Hörtnagl, L.: FLUXNET-CH_4 CH-Cha Chamau, Switzerland, FLUXNET-CH4 Community Product [data set], https://doi.org/10.18140/FLX/1669629, 2020a.

Merbold, L., Hörtnagl, L., and Buchmann, N.: FLUXNET-CH_4 CH-Dav Davos, Switzerland, FLUXNET-CH4 Community Product [data set], https://doi.org/10.18140/FLX/1669630, 2020b.

Meyer, H. and Pebesma, E.: Predicting into unknown space? Estimating the area of applicability of spatial prediction models, arXiv [preprint], arXiv:2005.07939, 2020.

Mishra, S. R., Pattnaik, P., Sethunathan, N., and Adhya, T. K.: Anion-Mediated Salinity Affecting Methane Production in a Flooded Alluvial Soil. Geomicrobiol. J., 20, 579–586, https://doi.org/10.1080/713851167, 2003.

Moffat, A. M., Papale, D., Reichstein, M., Hollinger, D. Y., Richardson, A. D., Barr, A. G., Beckstein, C., Braswell, B. H., Churkina, G., Desai, A. R., Falge, E., Gove, J. H., Heimann, M., Hui, D., Jarvis, A. J., Kattge, J., Noormets, A., and Stauch, V. J.: Comprehensive comparison of gap-filling techniques for eddy covariance net carbon fluxes, Agr. Forest Meteorol., 147, 209–232, https://doi.org/10.1016/j.agrformet.2007.08.011, 2007.

Myhre, G., Shindell, D., Bréon, F.-M., Collins, W., Fuglestvedt, J., Huang, J., Koch, D., Lamarque, J.-F., Lee, D., Mendoza, B., Nakajima, T., Robock, A., Stephens, G., Takemura, T., and Zhang, H.: Anthropogenic and Natural Radiative Forcing Supplementary Material, in: Climate Change 2013: The Physical Science Basis, Contribution of Working Group I to the Fifth Assessment Report of the Intergovernmental Panel on Climate Change, edited by: Stocker, T. F., Qin, D., Plattner, G.-K., Tignor, M., Allen, S. K., Boschung, J., Nauels, A., Xia, Y., Bex, V., and Midgley, P. M., 2013.

Nemitz, E., Mammarella, I., Ibrom, A., Aurela, M., Burba, G. G., Dengel, S., Gielen, B., Grelle, A., Heinesch, B., Herbst, M., Hörtnagl, L., Klemedtsson, L., Lindroth, A., Lohila, A., McDermitt, D. K., Meier, P., Merbold, L., Nelson, D., Nicolini, G., Nilsson, M. B., Peltola, O., Rinne, J., and Zahniser, M.: Standardisation of eddy-covariance flux measurements of methane and nitrous oxide, Int. Agrophy., 32, 517–549, https://doi.org/10.1515/intag-2017-0042, 2018.

Nielsen, H. B.: Damping parameter in Marquardt's method, Department of Mathematical Modeling, IMM, Technical University of Denmark, Technical Report, IMM-REP-1999-05, 1999.

Nilsson, M. B. and Peichl, M.: FLUXNET-CH_4 SE-Deg Degero, Sweden, FLUXNET-CH4 Community Product [data set], https://doi.org/10.18140/FLX/1669659, 2020.

Niu, S. and Chen, W.: FLUXNET-CH_4 CN-Hgu Hongyuan, China, FLUXNET-CH4 Community Product [data set], https://doi.org/10.18140/FLX/1669632, 2020.

Noormets, A., King, J., Mitra, B., Miao, G., Aguilos, W., Minick, W., Prajapati, P., and Domec, J.-C.: FLUXNET-CH_4 US-NC4 NC_AlligatorRiver, United States, FLUXNET-CH4 Community Product [data set], https://doi.org/10.18140/FLX/1669686, 2020.

Oikawa, P. Y., Jenerette, G. D., Knox, S. H., Sturtevant, C., Verfaillie, J., Dronova, I., Poindexter, C. M., Eichelmann, E., and Baldocchi, D. D.: Evaluation of a hierarchy of models reveals

importance of substrate limitation for predicting carbon dioxide and methane exchange in restored wetlands, J. Geophys. Res.-Biogeo., 122, 145–167, https://doi.org/10.1002/2016JG003438, 2017.

Oikawa, P.: FLUXNET-CH_4 US-EDN Eden Landing Ecological Reserve, United States, FLUXNET-CH4 Community Product [data set], https://doi.org/10.18140/FLX/1669673, 2020.

Olefeldt, D., Turetsky, M. R., Crill, P. M., and McGuire, A. D.: Environmental and physical controls on northern terrestrial methane emissions across permafrost zones, Glob. Change Biol., 19, 589–603, https://doi.org/10.1111/gcb.12071, 2013.

Papale, D., Andrew Black, T., Carvalhais, N., Cescatti, A., Chen, J., Jung, M., Kiely, G., Lasslop, G., Mahecha, M. D., Margolis, H., Merbold, L., Montagnani, L., Moors, E., Olesen, J. E., Reichstein, M., Tramontana, G., van Gorsel, E., Wohlfahrt, G., and Ráduly, B.: Effect of spatial sampling from European flux towers for estimating carbon and water fluxes with artificial neural networks, J. Geophys. Res.-Biogeo., 120, 1941–1957, https://doi.org/10.1002/2015jg002997, 2015.

Parmentier, F. J. W., van Huissteden, J., van der Molen, M. K., Schaepman-Strub, G., Karsanaev, S. A., Maximov, T. C., and Dolman, A. J.: Spatial and temporal dynamics in eddy covariance observations of methane fluxes at a tundra site in northeastern Siberia, J. Geophys. Res., 116, 1368, https://doi.org/10.1029/2010JG001637, 2011.

Pastorello, G., Trotta, C., Canfora, E., Chu, H., Christianson, D., Cheah, Y.-W., Poindexter, C., Chen, J., Elbashandy, A., Humphrey, M., Isaac, P., Polidori, D., Ribeca, A., van Ingen, C., Zhang, L., Amiro, B., Ammann, C., Arain, M. A., Ardö, J., et al.: The FLUXNET2015 dataset and the ONEFlux processing pipeline for eddy covariance data, Sci. Data, 7, 225, https://doi.org/10.1038/s41597-020-0534-3, 2020.

Pattnaik, P., Mishra, S. R., Bharati, K., Mohanty, S. R., Sethunathan, N., and Adhya, T. K.: Influence of salinity on methanogenesis and associated microflora in tropical rice soils, Microbiol. Res., 155, 215–220, https://doi.org/10.1016/S0944-5013(00)80035-X, 2000.

Poffenbarger, H. J., Needelman, B. A., and Patrick Megonigal, J.: Salinity Influence on Methane Emissions from Tidal Marshes, Wetlands, 31, 831–842, https://doi.org/10.1007/s13157-011-0197-0, 2011.

Poulter, B., Bousquet, P., Canadell, J. G., Ciais, P., Peregon, A., Saunois, M., Arora, V. K., Beerling, D. J., Brovkin, V., Jones, C. D., Joos, F., Gedney, N., Ito, A., Kleinen, T., Koven, C. D., McDonald, K., Melton, J. R., Peng, C., Peng, S., Prigent, C., Schroeder, R., Riley, W. J., Saito, M., Spahni, R., Tian, H., Taylor, L., Viovy, N., Wilton, D., Wiltshire, A., Xu, X., Zhang, B., Zhang, Z., and Zhu, Q.: Global wetland contribution to 2000–2012 atmospheric methane growth rate dynamics, Environ. Res. Lett., 12, 094013, https://doi.org/10.1088/1748-9326/aa8391, 2017.

R Core Team: R: A Language and Environment for Statistical Computing. R Foundation for Statistical Computing, Vienna, 2018.

Reba, M., Runkle, B., and Suvocarev, K.: FLUXNET-CH_4 US-HRC Humnoke Farm Rice Field – Field C, United States, FLUXNET-CH4 Community Product [data set], https://doi.org/10.18140/FLX/1669677, 2020.

Reichstein, M., Falge, E., Baldocchi, D., Papale, D., Aubinet, M., Berbigier, P., Bernhofer, C., Buchmann, N., Gilmanov, T., Granier, A., Grunwald, T., Havrankova, K., Ilvesniemi, H., Janous, D., Knohl, A., Laurila, T., Lohila, A., Loustau, D., Matteucci, G., Meyers, T., Miglietta, F., Ourcival, J.-M., Pumpanen, J., Rambal, S., Rotenberg, E., Sanz, M., Tenhunen, J., Seufert, G., Vaccari, F., Vesala, T., Yakir, D., and Valentini, R.: On the separation of net ecosystem exchange into assimilation and ecosystem respiration: review and improved algorithm, Glob. Change Biol., 11, 1424–1439, https://doi.org/10.1111/j.1365-2486.2005.001002.x, 2005.

Rey-Sanchez, C., Szutu, D., Shortt, R., Chamberlain, S. D., Verfaillie, J., and Baldocchi, D.: FLUXNET-CH_4 US-Bi1 Bouldin Island Alfalfa, United States, FLUXNET-CH4 Community Product [data set], https://doi.org/10.18140/FLX/1669666, 2020a.

Rey-Sanchez, C., Szutu, D., Hemes, K., Verfaillie, J., and Baldocchi, D.: FLUXNET-CH_4 US-Bi2 Bouldin Island corn, United States, FLUXNET-CH4 Community Product [data set], https://doi.org/10.18140/FLX/1669667, 2020b.

Richardson, A. D. and Hollinger, D. Y.: A method to estimate the additional uncertainty in gap-filled NEE resulting from long gaps in the CO_2 flux record, Agr. Forest Meteorol., 147, 199–208, https://doi.org/10.1016/j.agrformet.2007.06.004, 2007.

Richardson, A. D. and Hollinger, D. Y.: FLUXNET-CH_4 US-Ho1 Howland Forest (main tower), United States, FLUXNET-CH4 Community Product [data set], https://doi.org/10.18140/FLX/1669675, 2020.

Richardson, A. D., Hollinger, D. Y., Burba, G. G., Davis, K. J., Flanagan, L. B., Katul, G. G., William Munger, J., Ricciuto, D. M., Stoy, P. C., Suyker, A. E., Verma, S. B., and Wofsy, S. C.: A multi-site analysis of random error in tower-based measurements of carbon and energy fluxes, Agr. Forest Meteorol., 136, 1–18, https://doi.org/10.1016/j.agrformet.2006.01.007, 2006.

Richardson, A. D., Mahecha, M. D., Falge, E., Kattge, J., Moffat, A. M., Papale, D., Reichstein, M., Stauch, V. J., Braswell, B. H., Churkina, G., Kruijt, B., and Hollinger, D. Y.: Statistical properties of random CO_2 flux measurement uncertainty inferred from model residuals, Agr. Forest Meteorol., 148, 38–50, https://doi.org/10.1016/j.agrformet.2007.09.001, 2008.

Richardson, A. D., Aubinet, M., Barr, A. G., Hollinger, D. Y., Ibrom, A., Lasslop, G., and Reichstein, M.: Uncertainty quantification, Eddy Covariance: A Practical Guide to Measurement and Data Analysis, edited by: Aubinet, M., Vesala, T., and Papale, D.: Springer Atmospheric Sciences, 2012.

Rinne, J., Riutta, T., Pihlatie, M., Aurela, M., Haapanala, S., Tuovinen, J.-P., Tuittila, E.-S., and Vesala, T.: Annual cycle of methane emission from a boreal fen measured by the eddy covariance technique, Tellus B, 59, 449–457, https://doi.org/10.1111/j.1600-0889.2007.00261.x, 2007.

Runkle, B., Reba, M., and Suvocarev, K.: FLUXNET-CH_4 US-HRA Humnoke Farm Rice Field – Field A, United States, FLUXNET-CH4 Community Product [data set], https://doi.org/10.18140/FLX/1669676, 2020.

Runkle, B. R. K., Suvočarev, K., Reba, M. L., Reavis, C. W., Smith, S. F., Chiu, Y.-L., and Fong, B.: Methane Emission Reductions from the Alternate Wetting and Drying of Rice Fields Detected Using the Eddy Covariance Method, Environ. Sci. Technol., 53, 671–681, https://doi.org/10.1021/acs.est.8b05535, 2019.

Ryu, Y., Kang, M., and Kim, J.: FLUXNET-CH_4 KR-CRK Cheorwon Rice paddy, Korea, Republic of, FLUXNET-CH4 Commu-

nity Product [data set], https://doi.org/10.18140/FLX/1669649, 2020.

Sachs, T. and Wille, C.: FLUXNET-CH_4 DE-Dgw Dagowsee, Germany, FLUXNET-CH4 Community Product [data set], https://doi.org/10.18140/FLX/1669633, 2020a.

Sachs, T. and Wille, C.: FLUXNET-CH_4 DE-Zrk Zarnekow, Germany, FLUXNET-CH4 Community Product [data set], https://doi.org/10.18140/FLX/1669636, 2020b.

Sachs, T., Giebels, M., Boike, J., and Kutzbach, L.: Environmental controls on CH_4 emission from polygonal tundra on the microsite scale in the Lena river delta, Siberia: controls on tundra CH_4 flux and scaling, Glob. Change Biol., 16, 3096–3110, https://doi.org/10.1111/j.1365-2486.2010.02232.x, 2010.

Sakabe, A., Itoh, M., Hirano, T., and Kusin, K.: FLUXNET-CH_4 ID-Pag Palangkaraya undrained forest, Indonesia, FLUXNET-CH4 Community Product [data set], https://doi.org/10.18140/FLX/1669643, 2020.

Saunois, M., Bousquet, P., Poulter, B., Peregon, A., Ciais, P., Canadell, J. G., Dlugokencky, E. J., Etiope, G., Bastviken, D., Houweling, S., Janssens-Maenhout, G., Tubiello, F. N., Castaldi, S., Jackson, R. B., Alexe, M., Arora, V. K., Beerling, D. J., Bergamaschi, P., Blake, D. R., Brailsford, G., Brovkin, V., Bruhwiler, L., Crevoisier, C., Crill, P., Covey, K., Curry, C., Frankenberg, C., Gedney, N., Höglund-Isaksson, L., Ishizawa, M., Ito, A., Joos, F., Kim, H.-S., Kleinen, T., Krummel, P., Lamarque, J.-F., Langenfelds, R., Locatelli, R., Machida, T., Maksyutov, S., McDonald, K. C., Marshall, J., Melton, J. R., Morino, I., Naik, V., O'Doherty, S., Parmentier, F.-J. W., Patra, P. K., Peng, C., Peng, S., Peters, G. P., Pison, I., Prigent, C., Prinn, R., Ramonet, M., Riley, W. J., Saito, M., Santini, M., Schroeder, R., Simpson, I. J., Spahni, R., Steele, P., Takizawa, A., Thornton, B. F., Tian, H., Tohjima, Y., Viovy, N., Voulgarakis, A., van Weele, M., van der Werf, G. R., Weiss, R., Wiedinmyer, C., Wilton, D. J., Wiltshire, A., Worthy, D., Wunch, D., Xu, X., Yoshida, Y., Zhang, B., Zhang, Z., and Zhu, Q.: The global methane budget 2000–2012, Earth Syst. Sci. Data, 8, 697–751, https://doi.org/10.5194/essd-8-697-2016, 2016.

Saunois, M., Stavert, A. R., Poulter, B., Bousquet, P., Canadell, J. G., Jackson, R. B., Raymond, P. A., Dlugokencky, E. J., Houweling, S., Patra, P. K., Ciais, P., Arora, V. K., Bastviken, D., Bergamaschi, P., Blake, D. R., Brailsford, G., Bruhwiler, L., Carlson, K. M., Carrol, M., Castaldi, S., Chandra, N., Crevoisier, C., Crill, P. M., Covey, K., Curry, C. L., Etiope, G., Frankenberg, C., Gedney, N., Hegglin, M. I., Höglund-Isaksson, L., Hugelius, G., Ishizawa, M., Ito, A., Janssens-Maenhout, G., Jensen, K. M., Joos, F., Kleinen, T., Krummel, P. B., Langenfelds, R. L., Laruelle, G. G., Liu, L., Machida, T., Maksyutov, S., McDonald, K. C., McNorton, J., Miller, P. A., Melton, J. R., Morino, I., Müller, J., Murguia-Flores, F., Naik, V., Niwa, Y., Noce, S., O'Doherty, S., Parker, R. J., Peng, C., Peng, S., Peters, G. P., Prigent, C., Prinn, R., Ramonet, M., Regnier, P., Riley, W. J., Rosentreter, J. A., Segers, A., Simpson, I. J., Shi, H., Smith, S. J., Steele, L. P., Thornton, B. F., Tian, H., Tohjima, Y., Tubiello, F. N., Tsuruta, A., Viovy, N., Voulgarakis, A., Weber, T. S., van Weele, M., van der Werf, G. R., Weiss, R. F., Worthy, D., Wunch, D., Yin, Y., Yoshida, Y., Zhang, W., Zhang, Z., Zhao, Y., Zheng, B., Zhu, Q., Zhu, Q., and Zhuang, Q.: The Global Methane Budget 2000–2017, Earth Syst. Sci. Data, 12, 1561–1623, https://doi.org/10.5194/essd-12-1561-2020, 2020.

Schäfer, K.: FLUXNET-CH_4 US-MRM Marsh Resource Meadowlands Mitigation Bank, United States, FLUXNET-CH4 Community Product [data set], https://doi.org/10.18140/FLX/1669684, 2020.

Schmid, H. P. and Klatt, J.: FLUXNET-CH_4 DE-SfN Schechenfilz Nord, Germany, FLUXNET-CH4 Community Product [data set], https://doi.org/10.18140/FLX/1669635, 2020.

Schuur, E. A.: FLUXNET-CH_4 US-EML Eight Mile Lake Permafrost thaw gradient, Healy Alaska, United States, FLUXNET-CH4 Community Product [data set], https://doi.org/10.18140/FLX/1669674, 2020.

Seyfferth, A. L., Bothfeld, F., Vargas, R., Stuckey, J. W., Wang, J., Kearns, K., Michael, H. A., Guimond, J., Yu, X., and Sparks, D. L.: Spatial and temporal heterogeneity of geochemical controls on carbon cycling in a tidal salt marsh, Geochim. Cosmochim. Ac., 282, 1–18, https://doi.org/10.1016/j.gca.2020.05.013, 2020.

Shortt, R., Hemes, K., Szutu, D., Verfaillie, J., and Baldocchi, D.: FLUXNET-CH_4 US-Sne Sherman Island Restored Wetland, United States, FLUXNET-CH4 Community Product [data set], https://doi.org/10.18140/FLX/1669693, 2020.

Sims, D. A., Rahman, A. F., Cordova, V. D., El-Masri, B. Z., Baldocchi, D. D., Flanagan, L. B., Goldstein, A. H., Hollinger, D. Y., Misson, L., Monson, R. K., Oechel, W. C., Schmid, H. P., Wofsy, S. C., and Xu, L.: On the use of MODIS EVI to assess gross primary productivity of North American ecosystems, J. Geophys. Res.-Biogeo., 111, G04015, https://doi.org/10.1029/2006jg000162, 2006.

Sonnentag, O. and Helbig, M.: FLUXNET-CH_4 CA-SCB Scotty Creek Bog, Canada, FLUXNET-CH4 Community Product [data set], https://doi.org/10.18140/FLX/1669613, 2020a.

Sonnentag, O. and Helbig, M.: FLUXNET-CH_4 CA-SCC Scotty Creek Landscape, Canada, FLUXNET-CH4 Community Product [data set], https://doi.org/10.18140/FLX/1669628, 2020b.

Spahni, R., Wania, R., Neef, L., van Weele, M., Pison, I., Bousquet, P., Frankenberg, C., Foster, P. N., Joos, F., Prentice, I. C., and van Velthoven, P.: Constraining global methane emissions and uptake by ecosystems, Biogeosciences, 8, 1643–1665, https://doi.org/10.5194/bg-8-1643-2011, 2011.

Sparks, J. P.: FLUXNET-CH_4 US-MAC MacArthur Agro-Ecology, United States, FLUXNET-CH4 Community Product [data set], https://doi.org/10.18140/FLX/1669683, 2020.

Sturtevant, C. S., Ruddell, B. L., Knox, S. H., Verfaillie, J. G., Matthes, J. H., Oikawa, P. Y., and Baldocchi, D. D.: Identifying scale-emergent, nonlinear, asynchronous processes of wetland methane exchange, J. Geophys. Res.-Biogeo., 121, 188–204, https://doi.org/10.1002/2015JG003054, 2016.

Tagesson, T., Mölder, M., Mastepanov, M., Sigsgaard, C., Tamstorf, M. P., Lund, M., Falk, J. M., Lindroth, A., Christensen, T. R., and Ström, L.: Land-atmosphere exchange of methane from soil thawing to soil freezing in a high-Arctic wet tundra ecosystem, Glob. Change Biol., 18, 1928–1940, https://doi.org/10.1111/j.1365-2486.2012.02647.x, 2012.

Taoka, T., Iwata, H., Hirata, R., Takahashi, Y., Miyabara, Y., and Itoh, M.: Environmental Controls on Diffusive and Ebullitive Methane Emission at a Sub-Daily Time Scale in the Littoral Zone of a Mid-Latitude Shallow Lake, J. Geophys. Res.-Biogeo., 125, e2020JG005753, https://doi.org/10.1029/2020JG005753, 2020.

Torn, M. and Dengel, S.: FLUXNET-CH_4 US-NGB NGEE Arctic Barrow, United States, FLUXNET-CH4 Community Prod-

uct [data set], https:// https://doi.org/10.18140/FLX/1669687, 2020a.

Torn, M. and Dengel, S.: FLUXNET-CH_4 US-NGC NGEE Arctic Council, United States, FLUXNET-CH4 Community Product [data set], https://doi.org/10.18140/FLX/1669688, 2020b.

Treat, C. C., Anthony Bloom, A., and Marushchak, M. E.: Nongrowing season methane emissions-a significant component of annual emissions across northern ecosystems, Glob. Change Biol., 24, 3331–3343, https://doi.org/10.1111/gcb.14137, 2018.

Turetsky, M. R., Kotowska, A., Bubier, J., Dise, N. B., Crill, P., Hornibrook, E. R. C., Minkkinen, K., Moore, T. R., Myers-Smith, I. H., Nykänen, H., Olefeldt, D., Rinne, J., Saarnio, S., Shurpali, N., Tuittila, E.-S., Waddington, J. M., White, J. R., Wickland, K. P., and Wilmking, M.: A synthesis of methane emissions from 71 northern, temperate, and subtropical wetlands, Glob. Change Biol., 20, 2183–2197, https://doi.org/10.1111/gcb.12580, 2014.

Ueyama, M., Hirano, T., and Kominami, Y.: FLUXNET-CH_4 JP-BBY Bibai bog, Japan, FLUXNET-CH4 Community Product [data set], https://doi.org/10.18140/FLX/1669646, 2020.

Valach, A., Szutu, D., Eichelmann, E., Knox, S., Verfaillie, J., and Baldocchi, D.: FLUXNET-CH_4 US-Tw1 Twitchell Wetland West Pond, United States, FLUXNET-CH4 Community Product [data set], https://doi.org/10.18140/FLX/1669696, 2020a.

Valach, A., Kasak, K., Szutu, D., Verfaillie, J., and Baldocchi, D.: FLUXNET-CH_4 US-Tw5 East Pond Wetland, United States, FLUXNET-CH4 Community Product [data set], https://doi.org/10.18140/FLX/1669699, 2020b.

Varlagin, A.: FLUXNET-CH_4 RU-Fy2 Fyodorovskoye dry spruce, Russian Federation, FLUXNET-CH4 Community Product [data set], https://doi.org/10.18140/FLX/1669657, 2020.

Vazquez-Lule, A. and Vargas, R.: FLUXNET-CH_4 US-StJ St Jones Reserve, United States, FLUXNET-CH4 Community Product [data set], https://doi.org/10.18140/FLX/1669695, 2020.

Vázquez-Lule, A. and Vargas, R.: Biophysical drivers of net ecosystem and methane exchange across phenological phases in a tidal salt marsh, Agr. Forest Meteorol., 300, 108309, https://doi.org/10.1016/j.agrformet.2020.108309, 2021.

Verma, S. B., Ullman, F. G., Billesbach, D., Clement, R. J., Kim, J., and Verry, E. S.: Eddy correlation measurements of methane flux in a northern peatland ecosystem, Bound.-Lay. Meteorol., 58, 289–304, https://doi.org/10.1007/BF02033829, 1992.

Vermote, E.: MOD09A1 MODIS Surface Reflectance 8-Day L3 Global 500m SIN Grid V006, NASA EOSDIS Land Processes DAAC [data set], https://doi.org/10.5067/MODIS/MOD09A1.006 (Terra), 2015.

Vesala, T., Tuittila, E.-S., Mammarella, I., and Alekseychik, P.: FLUXNET-CH_4 FI-Si2 Siikaneva-2 Bog, Finland, FLUXNET-CH4 Community Product [data set], https://doi.org/10.18140/FLX/1669639, 2020a.

Vesala, T., Tuittila, E.-S., Mammarella, I., and Rinne, J.: FLUXNET-CH_4 FI-Sii Siikaneva, Finland, FLUXNET-CH4 Community Product [data set], https://doi.org/10.18140/FLX/1669640, 2020b.

Villarreal, S., Guevara, M., Alcaraz-Segura, D., Brunsell, N. A., Hayes, D., Loescher, H. W., and Vargas, R.: Ecosystem functional diversity and the representativeness of environmental networks across the conterminous United States, Agr. Forest Meteorol., 262, 423–433, https://doi.org/10.1016/j.agrformet.2018.07.016, 2018.

Villarreal, S., Guevara, M., Alcaraz-Segura, D., and Vargas, R.: Optimizing an Environmental Observatory Network Design Using Publicly Available Data, J. Geophys. Res.-Biogeo., 124, 1812–1826, https://doi.org/10.1029/2018JG004714, 2019.

Vourlitis, G., Dalmagro, H., de Nogueira, J. S., Johnson, M., and Arruda, P. FLUXNET-CH_4 BR-Npw Northern Pantanal Wetland, Brazil, FLUXNET-CH4 Community Product [data set], https://doi.org/10.18140/FLX/1669368, 2020.

Vuichard, N. and Papale, D.: Filling the gaps in meteorological continuous data measured at FLUXNET sites with ERA-Interim reanalysis, Earth Syst. Sci. Data, 7, 157–171, https://doi.org/10.5194/essd-7-157-2015, 2015.

Weston, N. B., Dixon, R. E., and Joye, S. B.: Ramifications of increased salinity in tidal freshwater sediments: Geochemistry and microbial pathways of organic matter mineralization, J. Geophys. Res., 111, G01009, https://doi.org/10.1029/2005jg000071, 2006.

Weston, N. B., Vile, M. A., Neubauer, S. C., and Velinsky, D. J.: Accelerated microbial organic matter mineralization following saltwater intrusion into tidal freshwater marsh soils, Biogeochemistry, 102, 135–151, https://doi.org/10.1007/s10533-010-9427-4, 2011.

Wik, M., Crill, P. M., Varner, R. K., and Bastviken, D.: Multiyear measurements of ebullitive methane flux from three subarctic lakes, J. Geophys. Res.-Biogeo., 118, 1307–1321, https://doi.org/10.1002/jgrg.20103, 2013.

Windham-Myers, L., Stuart-Haëntjens, E., Bergamaschi, B., and Knox, S.: FLUXNET-CH_4 US-Srr Suisun marsh – Rush Ranch, United States, FLUXNET-CH4 Community Product [data set], https://doi.org/10.18140/FLX/1669694, 2020.

Windsor, J., Moore, T. R., and Roulet, N. T.: Episodic fluxes of methane from subarctic fens, Can. J. Soil Sci., 72, 441–452, https://doi.org/10.4141/cjss92-037, 1992.

Wohlfahrt, G.: FLUXNET-CH_4 AT-Neu Neustift, Austria, FLUXNET-CH4 Community Product [data set], https://doi.org/10.18140/FLX/1669365, 2020.

Wong, G. X., Melling, L., Tang, A. C. I. Aeries, E. B., Waili, J. W., Musin, K. K., Lo, K. S., and Kiew, F.: FLUXNET-CH_4 MY-MLM Maludam National Park, Malaysia, FLUXNET-CH4 Community Product [data set], https://doi.org/10.18140/FLX/1669650, 2020.

Wutzler, T., Lucas-Moffat, A., Migliavacca, M., Knauer, J., Sickel, K., Šigut, L., Menzer, O., and Reichstein, M.: Basic and extensible post-processing of eddy covariance flux data with REddyProc, Biogeosciences, 15, 5015–5030, https://doi.org/10.5194/bg-15-5015-2018, 2018.

Xu, X., Riley, W. J., Koven, C. D., Billesbach, D. P., Chang, R. Y.-W., Commane, R., Euskirchen, E. S., Hartery, S., Harazono, Y., Iwata, H., McDonald, K. C., Miller, C. E., Oechel, W. C., Poulter, B., Raz-Yaseef, N., Sweeney, C., Torn, M., Wofsy, S. C., Zhang, Z., and Zona, D.: A multi-scale comparison of modeled and observed seasonal methane emissions in northern wetlands, Biogeosciences, 13, 5043–5056, https://doi.org/10.5194/bg-13-5043-2016, 2016.

Yvon-Durocher, G., Allen, A. P., Bastviken, D., Conrad, R., Gudasz, C., St-Pierre, A., Thanh-Duc, N., and del Giorgio, P. A.: Methane fluxes show consistent temperature dependence

across microbial to ecosystem scales, Nature, 507, 488–491, https://doi.org/10.1038/nature13164, 2014.

Zhang, Z., Fluet-Choinard, E., Jensen, K., McDonald, K., Hugelius, G., Gumbricht, T., Carrol, M., Prigent, C., Bartsch, A., and Poulter, B.: Development of a global dataset of Wetland Area and Dynamics for Methane Modeling (WAD2M), Zenodo [data set], https://doi.org/10.5281/zenodo.3998454, 2020.

Zhang, Z., Fluet-Chouinard, E., Jensen, K., McDonald, K., Hugelius, G., Gumbricht, T., Carroll, M., Prigent, C., Bartsch, A., and Poulter, B.: Development of the global dataset of Wetland Area and Dynamics for Methane Modeling (WAD2M), Earth Syst. Sci. Data, 13, 2001–2023, https://doi.org/10.5194/essd-13-2001-2021, 2021.

Zona, D. and Oechel, W. C.: FLUXNET-CH_4 US-Atq Atqasuk, United States, FLUXNET-CH4 Community Product [data set], https://doi.org/10.18140/FLX/1669663, 2020a.

Zona, D. and Oechel, W. C.: FLUXNET-CH_4 US-Beo Barrow Environmental Observatory (BEO) tower, United States, FLUXNET-CH4 Community Product [data set], https://doi.org/10.18140/FLX/1669664, 2020b.

Zona, D. and Oechel, W. C.: FLUXNET-CH_4 US-Bes Barrow-Bes (Biocomplexity Experiment South tower), United States, FLUXNET-CH4 Community Product [data set], https://doi.org/10.18140/FLX/1669665, 2020c.

Zona, D. and Oechel, W. C.: FLUXNET-CH_4 US-Ivo Ivotuk, United States, FLUXNET-CH4 Community Product [data set], https://doi.org/10.18140/FLX/1669679, 2020d.

Zona, D., Gioli, B., Commane, R., Lindaas, J., Wofsy, S. C., Miller, C. E., Dinardo, S. J., Dengel, S., Sweeney, C., Karion, A., Chang, R. Y.-W., Henderson, J. M., Murphy, P. C., Goodrich, J. P., Moreaux, V., Liljedahl, A., Watts, J. D., Kimball, J. S., Lipson, D. A., and Oechel, W. C.: Cold season emissions dominate the Arctic tundra methane budget, P. Natl. Acad. Sci. USA, 113, 40–45, https://doi.org/10.1073/pnas.1516017113, 2016.